

CO-CURRENT TURBULENT-TURBULENT FLOW OF AIR AND WATER-CLAY SUSPENSIONS IN
HORIZONTAL PIPES

A THESIS

Presented to
the Faculty of the Graduate Division

by

Henderson Crawford Ward

In Partial Fulfillment
of the Requirements for the Degree
Doctor of Philosophy
in the School of Chemical Engineering

Georgia Institute of Technology

September 1952

CO-CURRENT TURBULENT-TURBULENT FLOW OF AIR AND WATER-CLAY SUSPENSIONS IN
HORIZONTAL PIPES

Approved: _____



Date Approved by Chairman: Sept. 10, 1952

To my wife

Rebekah Candler Ward

whose love, patience and understanding

have made this work possible

ACKNOWLEDGEMENTS

The author wishes to make the following acknowledgements: to Doctor J. M. DallaValle for his invaluable aid and assistance, to Doctor Paul Weber for his interest and assistance, to Mr. Harold G. Blocker for making the specific gravity, particle-size distribution, and capillary instrument (viscosity) measurements, to Professor LeRoy A. Woodward for making the electron-microscope photographs, to Mr. P.T. Bankston for his assistance in the preparation of the preliminary manuscript, to Dr. Karl M. Murphy for carefully editing the final manuscript, and to the Georgia Kaolin Company of Dry Branch, Georgia for kindly donating the clay used in this study.

The author also wishes to express his appreciation to the Shell Oil Company for making this work possible through the award of the Shell Fellowship in Chemical Engineering during the academic years of 1949-50 and 1950-51.

TABLE OF CONTENTS

	Page
ACKNOWLEDGEMENT	iv
SUMMARY	v
Chapter	
I INTRODUCTION.. . . .	1
II THEORETICAL BACKGROUND	5
III EXPERIMENTAL EQUIPMENT	35
IV MATERIAL	39
V EXPERIMENTAL PROCEDURE	40
VI DISCUSSION OF RESULTS.	44
VII CONCLUSIONS.	58
NOMENCLATURE.	59
REFERENCES.	66
LIST OF TABLES.	69
LIST OF FIGURES106
APPENDICES.143

CO-CURRENT TURBULENT-TURBULENT FLOW OF AIR AND WATER-CLAY SUSPENSIONS IN
HORIZONTAL PIPES

Henderson Crawford Ward

SUMMARY

Although progress has been made recently in the fields of co-current gas-Newtonian liquid flow and turbulent flow of non-Newtonian materials, relatively little is known theoretically about these complex types of flow. For this reason, results of studies in these fields cannot be applied with certainty to the co-current flow of a gas and a non-Newtonian material, a type of flow which occurs in many industrial operations and for which no data are available. An investigation of this type of flow was therefore considered advisable.

In the present study, air was used as the gas phase and four concentrations of kaolin clay in water were used as the non-Newtonian materials. Two of these suspensions behaved as pseudoplastics, while the other two exhibited Bingham plastic properties. Viscosity determinations were made with a Brookfield Synchro-lectric and a capillary tube viscometer.

Pressure-drop measurements were made in $3/4$, 1 and $1\ 1/2$ inch horizontal pipes for each of these suspensions flowing alone and co-currently with air. Suspension flow rates were varied from 0.15 to 16 pounds per second, while air flow rates were varied from 0.0015 to 0.025 pounds per second. The majority of the tests were conducted in the

turbulent flow region. The characteristics of the main centrifugal pump used to circulate the suspensions through the system were determined at each solids concentration.

From the data obtained on each of the suspensions in the capillary tube viscometer and the three test sections, the flow curves of each were determined in both the laminar and turbulent flow regions. In the turbulent flow region, the usual Newtonian friction factor-Reynolds number relationship was found to be valid, confirming the work of previous investigators in this field. However, no significance could be found for the "turbulent viscosity" which results from using this relationship.

The pressure-drop data obtained on the co-current flow of air and these suspensions in the turbulent-turbulent region was correlated within the range of ± 20 percent by the $f-X$ method of Lockhart and Martinelli.

CHAPTER I

INTRODUCTION

Although investigations of the characteristics of two fluid phases flowing with a common interface were begun a century ago, it has been only recently that progress has been made in this field. This progress has been the result of the more intensified research of the past ten years necessitated by the increasing degree in which industry is using the medium of two-phase flow for chemical reactions and for the transfer of heat or mass between the phases. That progress has been slow in this field is readily understandable when one considers that the number of variables involved is more than twice those in single-phase flow, a field itself which still presents many unanswered problems. An excellent summary of recent progress in gas-liquid flow is presented by Bergelin (1).

In all the investigations to date, air has been used as the gas phase, and Newtonian fluids such as water, benzene and hydrocarbon oils used as the liquid phase. Most of the data available (2, 3, 4, 5, 6, 7, 8) are for co-current flow of the two phases in horizontal and vertical cylindrical ducts, ranging in size from capillary tubes to 2 inch pipes, without mass exchange between the phases. However, some data are available (1) for the case when mass exchange occurs between the phases.

There are four possible combinations of viscous-turbulent conditions in gas-liquid flow, and a mobile boundary exists between the phases

which may vary, causing the flow channel of each phase to change as well as the channel roughness to vary as interfacial waves form. If gas is added in increasing amounts to a horizontal pipe running full of liquid, the five distinct types of flow which occur successively are:

- 1) bubble flow in which the gas flows along the top of the pipe in the form of bubbles at approximately the same velocity as the liquid,
- 2) stratified flow in which the gas flows along the top of the pipe and the liquid along the bottom with a smooth interface between,
- 3) wave flow which is similar to stratified flow except that the interface is disturbed by waves,
- 4) slugging flow in which occasional frothy slugs pass rapidly through the pipe, and
- 5) annular flow in which the liquid flows in a film around the pipe wall and the gas flows through the central core at a high velocity.

The transition from one type to another is not abrupt and the point of wave formation is influenced by pipe length, entrance effects and external vibrations and pulsations. At the point of wave formation, rapid periodic fluctuations in pressure occur which decrease in frequency and increase in amplitude when slugging flow begins. As the gas velocity is further increased, the slugging type of flow gradually changes to annular with the pressure fluctuations increasing in frequency and decreasing in amplitude. In the regions of slugging and annular flow, quantities of liquid are carried by the gas phase. The effect of this entrainment on the pressure drop is now under investigation at the University of Delaware.

During upward co-current motion in vertical tubes, bubble, slugging and annular flow occur while during downward flow only

slugging and annular flow are possible. Since countercurrent flow is governed by the available hydraulic gradient, the types of flow in this case are rather limited and few data are available.

The only general correlation available at the present time for the determination of the pressure drop during co-current two-phase flow is that of Lockhart and Martinelli (8), the accuracy being within the range of ± 40 per cent. However, Bergelin and Gazely (9) have shown that this correlation is not applicable to stratified flow and that it predicts pressure drops up to 100 per cent above the experimentally determined ones.

In many cases of industrial importance, particularly in chemical reactors, the co-current flow of a gas and a non-Newtonian material occurs, and at the present time no data are available for such a system. Most non-Newtonian materials are generally made up of two or more phases and their flow properties are therefore influenced by a number of factors such as particle shape, size, weight, distribution, and surface properties of the different phases. Much progress has been made recently in the study of non-Newtonians and excellent reviews of this progress are presented by Alves (10) and Alves, Boucher and Pigford (11).

Investigations by Babbitt and Caldwell on clay and sewage suspensions (12), by Wilhelm, Wroughton and Loeffel on cement rock-water suspensions (13), by Alves, Boucher and Pigford on lime-water and titanium dioxide-water slurries (11), by Binder and Busher on grain-water suspensions (14), by Winding, Baumann and Kranich on GR-S latices (15), and others have indicated that in general non-Newtonians in

the turbulent flow region behave as Newtonians, that is they exhibit a relatively constant viscosity.

Thus, one might suspect that in the turbulent flow region, the correlation of Lockhart and Martinelli would apply to the co-current flow of a gas and a non-Newtonian material, unless the introduction of a gas phase would so alter the flow properties of the non-Newtonian material that its viscosity would no longer remain constant or would cause other changes not accounted for in the correlation. Since the theories of neither field are far enough developed to provide a quantitative answer, the only recourse is to experiment. Therefore, it was felt that an investigation of the flow properties of a gas and non-Newtonian material in the turbulent flow region would not only extend the range of Lockhart and Martinelli's correlation, if applicable to this case, but would also provide additional information on the turbulent flow of a non-Newtonian material.

For these reasons, the present investigation was undertaken on the system air and water-clay suspensions, the latter being a typical non-Newtonian material and readily available. The experimental work consisted of the pressure-drop measurements in three different size pipes of air and water-clay suspensions of various concentrations and the determination of the viscosity and various physical properties of the suspensions. A centrifugal pump was chosen to circulate the material through the system and tests were conducted on its performance to determine the effect of solids concentration on its characteristics.

CHAPTER II

THEORETICAL BACKGROUND

I Viscosity

Flow curves.---The basis for the determination of the flow properties of a given material is its behavior when subjected to various shearing rates and shearing stresses in the laminar region. A plot of this behavior is termed the flow curve, and the type of flow curve exhibited serves as the criterion for classifying the material as a Newtonian or a non-Newtonian. The flow curve of a Newtonian material is a straight line passing through the origin, as illustrated by curve I in figure 1a, and the inverse slope of this line multiplied by the conversion factor g_c is defined as the coefficient of viscosity by the following rheological equation:

$$\mu = g_c \frac{S}{\dot{R}_s} \quad (1)$$

where S is the shearing stress and \dot{R}_s is the shearing rate, the dot denoting differentiation with respect to time. The conversion factor g_c appears since engineering units (pounds-foot-seconds) are used throughout this discussion. It should be noted that in this case the viscosity is independent of the shearing rate and shearing stress and is therefore a constant, this discussion being limited to constant temperature and pressure conditions.

The flow curves of non-Newtonian materials, limited in this discussion to solid-liquid suspensions and to soft plastic solids, neither exhibiting elastic properties, are not straight lines passing through the origin. Of the infinite number of types of curves remaining, only that of a straight line with a positive slope and a positive intercept on the shearing stress axis has been found by rheologists to characterize in true rheological properties an ideal material which some actual materials closely approximate. Such an ideal material is called a Bingham body (after its founder E. C. Bingham) or plastic and is represented by curve II in figure 1a. The intercept on the shearing stress axis is termed the yield value, ζ , since the material will not start to flow until the applied stress exceeds this value. The product of g_c and the inverse slope of the line is defined as the coefficient of rigidity by the following rheological equation:

$$\eta = g_c \frac{S - \zeta}{R_s} . \quad (2)$$

At this point it should be emphasized that equations (1) and (2) are true rheological equations and, in order to convert them to instrumental equations, appropriate substitutions must be made for the shearing rate and stress. Since, as will be shown later, many materials are neither Newtonians or Bingham plastics, our definition of a flow curve must be generalized so that the laboratory data of all materials may be compared on a similar basis when obtained in the same sort of apparatus. Naturally it would be desirable to be able to reduce the data obtained in all different sorts of apparatuses to the same basis.

However, as this is not possible at the present time, it is necessary to accept the former procedure and introduce the concept of consistency which is, quoting Reiner (16), "that property of a material by which it resists a permanent change of shape and is defined by the complete force-flow relation." This force-flow relation is given by the consistency curve of the material under consideration and is determined by plotting the laboratory data in such a way that the dimensions of the apparatus are not a factor. The quantities M and N will be termed "consistency variables" and the consistency curve will be referred to as the "flow curve" in the following discussion.

In addition to Bingham plastics, the following general types of non-Newtonian suspensions are known to exist: (1) pseudoplastic, (2) generalized Bingham plastic, (3) dilatant and (4) thixotropic. A brief description of each type follows:

(1) A typical flow curve of a pseudoplastic material is given by curve I in figure 1b, and curve II of the same figure represents what Reiner (16) calls a generalized Newtonian liquid. Both curves begin at the origin and are identical up to the point (x, y) where curve I approaches an asymptote having a positive slope and intercept on the x axis while curve II, after passing through a point of inflection, approaches an asymptote which commences at the origin. Both curves have a tangent line at the origin whose inverse slope multiplied by the conversion factor g_c represents the viscosity at zero rate of shear, μ_0 , and gives the lower boundary of the apparent viscosity. The product of g_c and the inverse slope of the asymptote of curve I has been called by Alves (10, 11), Williamson (17) and Winding, Baumann,

and Kranich (15) the limiting viscosity at infinite rate of shear, μ'_{∞} , although it would seem more in keeping with the assumed analogy to a Bingham plastic to use the term "rigidity" instead of "viscosity." The product of g_c and the inverse slope of the asymptote to curve II is truly the limiting viscosity at infinite rate of shear, μ_{∞} . Whether curves I and II are identical, with curve I not determined at high enough rates of shear, is not certain, but this appears to be the case for surely the apparent viscosity cannot decrease below that of the dispersion liquid or become zero.

(2) Curve II in figure 2a, typical of a generalized Bingham plastic material, begins at some point on the x axis, denoted by δ and called the yield value, increases monotonically and approaches an asymptote of positive slope and intercept on the x axis. The inverse slope of this asymptote multiplied by g_c gives the coefficient of rigidity at infinite rate of shear.

(3) Referring to curve I in figure 2a, typical of a dilatant material, it can be observed that the apparent viscosity increases with increasing rates of shear.

(4) The curves in figure 2b are typical of a thixotropic material as obtained in a rotational type viscometer. The curve AB is the "upcurve" and the curve CA is the "downcurve" and the area of the loop ABC, termed the "hysteresis" loop, indicates the amount of thixotropy.

As Alves, Boucher and Pigford (11) point out, most solutions and suspensions behave as Newtonians at low concentrations but change to one of the non-Newtonian types when the concentration reaches a certain critical value. Further increases in concentration may cause

additional changes in the type of non-Newtonian properties exhibited.

Nature of viscosity.--Viscosity has long been recognized as one of the most fundamental properties of a fluid, being that property by which the layers of the fluid resist motion either relative to themselves or to the walls of a containing vessel. Although none of the many theories and explanations (16--22) advanced for viscosity have been completely successful, the following factors are known to have an effect: particle size, shape, density, distribution, surface properties of the phases, temperature, and pressure. In the case of a simple liquid, the particles are the molecules themselves and the following simplified picture (22) offers an explanation of the viscosity. Due to the short mean free paths between molecules in a liquid, the frequency of collisions is high as the molecules move with their translational energy of $3/2 RT$. As these collisions occur between molecules in neighboring filaments of flow in streamline motion, there is a net dissipation of directed energy into undirected energy which is the friction of viscous flow. If strong interlocking fields of force exist between the molecules, that is they are polar, there is a tendency toward "sticking" on collision and consequently a greater slipping frictional loss between the filaments.

With increase in molecular weight occurs a corresponding increase in molecular surface and attractive forces, the intensity of the surface forces per unit area being approximately constant, and thus an increase in viscosity results. However, since the attractive forces are not great enough to produce a connected structure, the layers of the liquid are able to move relative to each other without

causing any internal rupture in the system and, as the molecules are not elongated enough to become orientated or aligned during flow, it is reasonable to assume that the rate of shear is proportional to the stress. Thus all simple liquids should be Newtonians which, according to Reiner (16), is the case. This picture, if correct, offers a simple explanation for the change of viscosity with temperature at constant pressure. As the temperature is increased at constant pressure, the slight increase in the volume of the liquid greatly reduces its internal pressure because of the influence of molecular distance on the attractive forces and this effect being greater than the effect of increased translational energy thereby produces a decrease in viscosity. By the same reasoning one would expect the viscosity to increase with increase in pressure although more slowly than with temperature. Of the many empirical equations developed to relate the variation of the viscosity of pure liquids with temperature and pressure, Lewis, Squires and Broughton (22) recommend the following equation proposed by Andrade as probably being the best available:

$$\mu (v)^{1/3} = Be^{C/vT} \quad (3)$$

where v is the specific volume at the absolute temperature T ; B and C are constants characteristic of each liquid, and μ is the viscosity in poise.

When suspensions of either solid or liquid particles in a simple liquid are considered, it is found that by picturing the particles as being arranged in various kinds of aggregates and thereby giving to the system a structure, many of the various types of behavior of these

materials can be explained. At low concentrations of suspended matter, one would expect approximate Newtonian behavior since the particles or flocculates (particles held together by surface forces) are separated by relatively large distances and shear can take place mainly in the clear Newtonian spaces. However, unless the particles are spherical, some departure from Newtonian behavior would be expected since the particles disturb the streamlines of flow, the effect being greater at low rates of shear. In practice many dilute suspensions do exhibit approximate Newtonian behavior and their viscosity can be determined by Einstein's equation derived for spherical particles:

$$\mu_{\text{soln.}} = \mu_{\text{solv.}} (1 + 2.5 C_v) \quad (4)$$

where C_v is the volume concentration of the dispersed phase. Defining the terms "relative viscosity," "specific viscosity" and "intrinsic viscosity" as did Reiner, Staudinger and Kraemer respectively (16):

$$\mu_{\text{rel.}} = \frac{\mu_{\text{soln.}}}{\mu_{\text{solv.}}} \quad (5)$$

$$\mu_{\text{spec.}} = \frac{\mu_{\text{soln.}} - \mu_{\text{solv.}}}{\mu_{\text{solv.}}} = \mu_{\text{rel.}} - 1 \quad (6)$$

$$\mu_I = \frac{\mu_{\text{spec.}}}{C_v}, \quad (7)$$

a second approximation is given by Mark's equation

$$\mu_I = 2.5 + 14.1 C_v. \quad (8)$$

At higher concentrations of suspended matter, the system may behave as any one of the types of non-Newtonians discussed earlier.

Pseudoplastics are usually composed of particles of submicroscopic size which may be flocculated to some extent and which undergo Brownian motion. At increasing shearing rates, the particles tend to become orientated in the direction of flow causing, if the particles are not spherical, a decrease in viscosity. However, this orientation is lessened or possibly exceeded by the Brownian motion in which case the viscosity remains constant, although in general an equilibrium is set up between these actions with a decrease in viscosity resulting. Stresses are set up in the particles through reaction forces occurring because of their interference with the deformation of the liquid which may tend to break up the flocculates, elongate the particles, actually break the particles and set the particles in vibration if they are elastic, effects which, except the last, tend to decrease the viscosity. If the particles are such that adsorption of the liquid has occurred, this layer may become progressively sheared off at increasing rates of shear causing the viscosity to decrease. Another factor of importance is that of steric immobilization as discussed by Kraemer and Williamson (16), who picture the particles as forming either large molecules with the liquid immobilized in its branches and rings, micelles, ordered groups of micelles, or aggregates of particles. These may become deformed or ruptured at increasing rates of shear thereby reducing the viscosity by releasing the entrapped liquid and permitting orientation of the particles in the line of flow. As pointed out earlier, there are conflicting ideas about what happens at very high rates of shear. Of course if the particles actually break or steric immobilization occurs, the flow curve up and flow curve down will be different.

Dilatant materials were first observed and explained by Reynolds (16, 19) in 1885 and are loose suspensions which, on standing, settle into a minimum of voids. As the shearing rate is increased, the volume of voids begins to dilate or expand and the result is that, due to an insufficiency of liquid to fill them, the viscosity increases. As soon as the shearing action is stopped, the material reverts to its original state.

Bingham plastics are usually composed of microscopically visible particles suspended in a liquid medium, the particles being highly flocculated and giving a continuous structure to the system. The material undergoes an elastic deformation under increasing stress until the yield value is exceeded and then begins to flow with a solid plug, whose radius depends on factors to be discussed later, at the center of the tube. If the structure is such that it is not broken down or orientated during flow, the material is a true Bingham plastic, whereas if these effects as well as some of those mentioned in the discussion of pseudoplastics occur, the material exhibits a changing coefficient of rigidity and is a generalized Bingham plastic.

The term "thixotropy" is unfortunately interpreted in many different ways. To avoid any possible confusion it will be defined according to Green (19) as being the property possessed by some materials of becoming fluid when agitated but returning reversibly to their original state on standing. Thixotropic materials possess flocculated structures whose breakdown is a function of time as well as rate of shear, and the rotational type of viscometer is ideal for studying this type of material. When up and down curves of these materials are

obtained from this type of instrument, an indication of the amount of thixotropy is given by the area of the "hysteresis" loop, no loop indicating no thixotropy and a large loop indicating a considerable amount.

The limited data available on the effect of temperature and pressure on the viscosity of non-Newtonians appear to indicate that their effect is qualitatively the same as on the viscosity of the dispersing phase.

Methods of Measurement

Tube instrument.--One type of apparatus used to determine the flow curves of Newtonian and non-Newtonian materials is the pipe-line viscometer, which consists of a known length of pipe, ranging in size from capillaries to plant-scale pipes, over which the pressure drop is determined at various flow rates. Common means of forcing the material through the system are constant liquid heads, pumps, and controlled gas pressures. The rate of shear, in this case, is given by the velocity gradient

$$\dot{r}_s = -\left(\frac{du}{dr}\right). \quad (9)$$

The steady laminar flow of Newtonian fluids in this type of apparatus was first investigated by Hagen (1839) and Poiseuille (1840) and the results of their work are given by this equation, known as the Hagen-Poiseuille law:

$$\Delta P_F = \frac{128\mu QL}{g_c \pi D^4} \quad (10)$$

If

$$y = \frac{32Q}{\pi D^3} \quad (11)$$

is plotted against

$$x = \frac{D\Delta P_F}{4L} \quad (12)$$

the dimensions of the apparatus do not enter and the inverse slope of the resulting straight line passing through the origin is numerically equal to the coefficient of viscosity divided by the conversion factor g_c . As mentioned earlier, for this reason the variables x and y are called consistency variables. Thus, data obtained on the same fluid in tubes of different length and diameter will fall on the same line.

In this case, y and x represent the shearing rate and stress respectively at the tube wall.

For the steady laminar flow of Bingham plastics in cylindrical tubes, the following equation derived by Buckingham (1921) and independently by Reiner (1926) and known as the Buckingham-Reiner equation is applicable if no slippage occurs at the tube wall

$$Q = \frac{\pi D^4 \Delta P_F g_c}{128L \eta} \left[1 - \frac{4}{3} \left(\frac{\delta 4L}{D\Delta P_F} \right) + \frac{1}{3} \left(\frac{\delta 4L}{D\Delta P_F} \right)^4 \right], \quad \frac{D\Delta P_F}{4L} \geq \delta \quad (13)$$

This becomes, in the same consistency variables y and x of equations (11) and (12),

$$y = \frac{g_c x}{\eta} \left[1 - \frac{4}{3} \left(\frac{\delta}{x} \right) + \frac{1}{3} \left(\frac{\delta}{x} \right)^4 \right], \quad x \geq \delta \quad (14)$$

The radius b and the velocity U_b of the central "plug" are respectively

$$b = \frac{2L\delta}{\Delta P_F} \quad (15)$$

and

$$U_b = \frac{\Delta P_F g_c}{4L\eta} (R - b)^2. \quad (16)$$

In this case x represents the shearing stress at the tube wall and y , though not representing the rate of shear at any point in the tube, is often referred to as "the rate of shear" or the "mean rate of shear" in analogy to its significance in Newtonian flow. A plot of equation (14) is shown in figure 3a where it is graphically illustrated that the curve has no truly linear portion. However, for large values of δ/x , the curve may be approximated by its asymptote

$$y = \frac{g_c}{\eta} \left(x - \frac{4}{3} \delta \right) \quad (17)$$

which has a slope of g_c/η and a x intercept of $4/3 \delta$. Babbitt and Caldwell (23) have shown that the resulting error is 5.9 percent when $\delta/x = 0.5$ and 1.8 percent when $\delta/x = 0.4$. For cases where an approximation is not desirable, recourse must be made to equation (14). By introducing several dimensionless quantities, McMillen (24) in his very thorough analysis of this equation has shown how the calculations may be greatly simplified. He presents these dimensionless quantities in graphical form, and has demonstrated by experiment that entrance and contraction losses for plastic materials are much greater than for

ordinary liquids. Hedström (25) has presented some of McMillen's dimensionless quantities in nomogram form for increased accuracy in computations.

For the steady laminar flow of pseudoplastics in cylindrical tubes, no true rheological equation exists at present, although many have been proposed. Reiner (16), assuming that

$$\phi = F(S^2) \quad (18)$$

where ϕ is the coefficient of fluidity as defined by

$$\phi = \frac{\dot{R}_s}{g_c S} \quad (19)$$

has, by a power series development, arrived at

$$\phi = \phi_0 + \sum_{n=1}^{\infty} \gamma_{2n} S^{2n} \quad (20)$$

where

$$\gamma_{2n} = \frac{F^{(n)}(0)}{n!} \quad (21)$$

Introducing the consistency variables y and x of equations (11) and (12), the final result is

$$\frac{y}{g_c} = \phi_0 x + \sum_{n=1}^{\infty} \frac{2}{n+2} \gamma_{2n} x^{2n+1} \quad (22)$$

Proceeding along more theoretical lines, Reiner defines a coefficient of structural stability by

$$\chi = \frac{\phi_{\infty} - \phi}{\frac{d\phi}{d(S^2)}} \quad (23)$$

which leads to the rheological equation

$$\phi = \phi_{\infty} - (\phi_{\infty} - \phi_0) e^{-\frac{S^2}{\chi}} \quad (24)$$

which upon integration and introducing y and x from equations (11) and (12) gives

$$\frac{y}{E_c} = x\phi_{\infty} - \frac{2\chi^2}{x^3} (\phi_{\infty} - \phi_0) \left[1 - \frac{x^2}{\chi} e^{-\frac{x^2}{\chi}} - e^{-\frac{x^2}{\chi}} \right]. \quad (25)$$

Williamson (17), considering part of the power as being necessary to maintain laminar flow and the remainder as deforming and disintegrating the aggregates of particles, derived an equation for flow between parallel plates. However, the form of this equation has been found to fit the consistency curves of many materials (15) flowing in cylindrical tubes and is therefore presented here as an empirical equation

$$x = \frac{\delta'}{d + y} y + \frac{\mu'_{\infty} y}{E_c} \quad (26)$$

where δ' and μ'_{∞} are the intercept and inverse slope respectively of the asymptote of curve I in figure 1b.

For the steady laminar flow of a generalized Bingham plastic in a cylindrical tube, Reiner (16) assumes that the coefficient of rigidity η as defined by

$$\eta = g_c \frac{(S - \delta)}{R_s} \quad (27)$$

can be expressed as

$$\frac{1}{\eta} = F \left[(S - \delta)^2 \right]. \quad (28)$$

This equation, when developed into a power series, gives

$$\frac{1}{\eta} = \sum_{n=0}^{\infty} \gamma_{2n} (S - \delta)^{2n+1} \quad (29)$$

where

$$\gamma_{2n} = \frac{F^{(n)}(0)}{n!} \quad (30)$$

and becomes in terms of our same consistency variables

$$\frac{y}{g_c} = \sum_{n=0}^{\infty} \frac{2\gamma_{2n}}{n+1} x^{2n+1} \left(1 - \frac{\delta}{x}\right)^{3n+2} \quad (31)$$

$$\left[1 - 2 \frac{1 - \frac{\delta}{x}}{2n+3} + 2 \frac{\left(1 - \frac{\delta}{x}\right)^2}{(2n+3)(2n+4)} \right], \quad x \geq \delta .$$

Typical flow curves of a thixotropic material flowing laminarily in different size pipes of different lengths are shown in figure 3b and the effect of varying length and diameter are indicated on the figure.

Schofield and Scott Blair (26) point out that y should be a function of x only if the following conditions prevail: 1) that each particle of the material moves in a straight line, at a constant

velocity, parallel to the axis of the tube; 2) there is no slip at the wall; 3) the velocity gradient, at any point, is a function only of the shearing stress at that point. They have developed, using these conditions, the equation

$$y = \frac{8g_c}{x^3} \int_0^x S \int_S^x F(S) dS \cdot dS \quad (32)$$

This equation, then, tends to summarize the results presented thus far, for they have all been based on the above three assumptions.

That these assumptions are not always met is evidenced by the experimental facts that many soft plastic materials begin to flow in small tubes before their yield value is exceeded and many substances flow relatively faster in small tubes than in large ones, the effect becoming greater at higher rates of shear. In order to account for the first discrepancy, Buckingham (20) reasoned that the flow of a plastic material at stresses less than the yield stress was caused by a thin fluid lubricating envelope next to the tube wall which permitted the material to slide through the tube as a plug and proposed that equation (13) be modified in the following way

$$y = \frac{8 \epsilon x g_c}{\mu_w D} , \quad x \leq \delta \quad (33 a)$$

$$y = \frac{x g_c}{\eta} \left[1 - \frac{4}{3} \frac{\delta}{x} + \frac{1}{3} \left(\frac{\delta}{x} \right)^4 \right] + \frac{8 \epsilon x g_c}{\mu_w D} , \quad x \geq \delta \quad (33 b)$$

where ϵ is the mean thickness of the fluid film and μ_w is its viscosity. This type of slippage is illustrated in figure 4a. However, Scott Blair and Crowther (27) found that for clays and soil pastes it was necessary,

to explain their data over a fairly wide range, to introduce a yield value for the fluid film since it was not completely free and therefore not a true fluid. They proposed that

$$y = \frac{8 \epsilon (x - \delta') g_c}{\mu_w D}, \quad x \leq \delta \quad (34 a)$$

$$y = \frac{x g_c}{\eta} \left[1 - \frac{4}{3} \frac{\delta}{x} + \frac{1}{3} \left(\frac{\delta}{x} \right)^4 \right] + \frac{8 \epsilon (x - \delta') g_c}{\mu_w D}, \quad x \geq \delta. \quad (34 b)$$

Referring to figure 4a, it can be noted that this type of slippage would not occur until a definite stress δ' was reached, where $\delta' < \delta$.

The spread of the flow curves, as obtained in different size capillaries, at higher rates of shear has been termed the "sigma phenomenon" by Schofield and Scott Blair (26) and it is illustrated in figure 4b. Although various explanations have been offered for this phenomenon (20, 21, 26, 28, 29), how to correct for it or to what it is due is not fully understood. If slippage is the cause of the spread, several methods of correction are available. Mooney (30), by assuming slippage to occur entirely at the wall and to be a function of the shearing stress only, has shown that

$$\frac{\partial \left(\frac{8Q}{\pi D^3} \right)_x}{\partial \left(\frac{1}{R} \right)_x} = x \beta g_c = U_a \quad (35)$$

where β is the coefficient of slip as defined by the second equation of (35) and that

$$\frac{8Q\phi}{\pi D^3} = \frac{y\phi}{4} = \frac{g_c}{x^3} \int_0^x \phi S^3 dS \quad (36)$$

where Q_ϕ is the efflux due to fluidity alone, ϕ being the fluidity as defined by equation (19). Differentiation of equation (36) with respect to x yields

$$g_c x \phi_w = (\dot{R}_s)_w = \frac{3}{4} y_\phi + \frac{x}{4} \frac{dy_\phi}{dx} \quad (37)$$

Thus Mooney's method for correcting for slip in the tube instrument is to plot the data obtained in various diameter tubes as $8Q/\pi D^3$, y of equation (11) divided by 4 , against $1/R$ at constant values of x , the slopes of the resulting straight lines being, by equation (35), $x \beta g_c$ at those x values. From a plot of $x \beta g_c$ versus x , values of y_ϕ can be obtained by subtracting values of $x \beta g_c / R$ from corresponding values of $y/4$ and a plot of y_ϕ versus x constructed. From this plot, the values at the tube wall of the fluidity, ϕ_w , and rate of shear, $(\dot{R}_s)_w$, can be obtained by using equation (37).

Reiner (16) has assumed that slippage occurs due to a thin layer of fluid existing at the wall and has presented formulas for Bingham plastics, generalized Newtonians and generalized Bingham plastics with wall effects, as he terms slippage, which combine the calculation of fluidity and wall effects. Due to their length and complication in use, they are not presented here.

Rotation viscometer.--Another type of instrument commonly used to determine the various rheological properties of both Newtonian and non-Newtonian materials is the rotation viscometer. In this instrument the material is contained between two co-axial cylinders, one fixed and the other rotating, and the torque, T_o , that is required to maintain the angular velocity ω of the rotating cylinder constant against the

viscous resistance of the material is measured. Since in steady laminar flow, the material between the cylinders is in equilibrium, the couples, produced by the shearing stresses, acting on the convex and concave surfaces of each lamina of the material are of equal magnitude but act in opposite directions. As the same couples act on every lamina, they are constants, and therefore the torque

$$T_o = 2 \pi r h r^2 S = \text{constant} \quad (38)$$

where h is the height of the cylinder which is immersed in the material. The rate of shear is given by

$$\dot{R}_s = r \frac{d\dot{\phi}}{dr} \quad (39)$$

$\dot{\phi}$ being the angular velocity of the material. Equations (38) and (39) are true for all types of materials.

For the steady laminar flow of a Newtonian fluid in a rotation viscometer, the following equations apply

$$\dot{\phi} = \frac{\dot{\omega}_i R_i^2 \left(\frac{R_E^2}{r^2} - 1 \right) - \dot{\omega}_E R_E^2 \left(\frac{R_i^2}{r^2} - 1 \right)}{R_E^2 - R_i^2} \quad (40)$$

$$T_o = \frac{4 \pi h \mu R_i^2}{g_c} \frac{|\dot{\omega}_i - \dot{\omega}_E|}{1 - a} \quad (41)$$

where

$$a = \left(\frac{R_i}{R_E} \right)^2 \quad (42)$$

Consistency variables Z and W are

$$Z = \frac{2 \left| \dot{\omega}_i - \dot{\omega}_E \right|}{1 - a} \quad (43)$$

$$W = \frac{T_o}{2R_i^2 \pi h} \quad (44)$$

In this case Z and W represent, at the internal cylinder wall, the rate of shear and shearing stress respectively.

For the steady laminar flow of Bingham plastics in a rotation instrument, Reiner and Rivlin (16) have developed the following equation when slippage and end effects are absent:

$$\frac{\eta}{g_c} \dot{\omega}_i = \frac{T_o}{4\pi h R_i^2} (1 - a) + \frac{\delta}{2} \ln a, \quad T_o \geq T_1 = 2\pi h R_E^2 \delta \quad (45)$$

Expressed in the consistency variables, Z and W, this equation becomes

$$Z = \frac{g_c}{\eta} \left(W + \frac{\delta \ln a}{1 - a} \right), \quad W \geq W_1 = \frac{\delta}{a} \quad (46)$$

A plot of this equation is shown in figure 5a. It is noted that it is a straight line beginning at W_1 , whose inverse slope is η/g_c . The portion of the curve between the intercept δ on the W axis and W_1 is curved, but a knowledge of its equation is unnecessary since by extrapolating the straight line of equation (46) to the W axis and calling the intercept W_o ,

$$\delta = \frac{W_o (a - 1)}{\ln a} \quad (47)$$

Because of this linear relationship between Z and W , the rotation instrument has a decided advantage over the tube instrument in the study of Bingham plastics. It is worth noting, as Green (19) points out, that the length of the curvilinear portion of the curve can be decreased by decreasing $(R_E - R_1)$, h , or both.

In the case of the steady laminar flow of pseudoplastics and generalized Bingham plastics in rotation instruments, Reiner's proposed rheological equations (20) and (24) for pseudoplastics lead to

$$\frac{Z}{E_c} = \phi_0 W + \sum_{n=1}^{\infty} \frac{1 - a^{2n+1}}{(2n+1)(1-a)} \gamma_{2n} W^{2n+1} \quad (48)$$

and

$$\frac{Z}{E_c} = \phi_{\infty} W - \frac{(\phi_{\infty} - \phi_0)(\pi \psi)^{1/2}}{2(1-a)} \left[F\left(\frac{W}{\psi^{1/2}}\right) - F\left(\frac{Wa}{\psi^{1/2}}\right) \right] \quad (49)$$

where

$$F(t) = \frac{2}{\pi^{1/2}} \int_0^t e^{-t^2} dt \quad (\text{Gauss' error integral}) \quad (50)$$

respectively, while equation (29) for generalized Bingham plastics leads to

$$\frac{Z}{E_c} = \frac{1}{1-a} \sum_{n=0}^{\infty} \gamma_{2n} \delta^{2n+1} \left[\sum_{m=0}^{2n} \frac{1}{2n+1-m} \left(\frac{2n+1}{m} \right) \left(\frac{W}{\delta} \right)^{2n+1-m} \left(1 - a^{2n+1-m} + \ln a \right) \right] \quad (51)$$

for $W \geq \delta/a$ and

$$\frac{z}{g_c} = \frac{1}{1-a} \sum_{n=0}^{\infty} \gamma_{2n} \delta^{2n+1} \left\{ \sum_{m=0}^{2n} \frac{1}{2n+1-m} \right. \quad (52)$$

$$\left. \left(\frac{2n+1}{m} \right) \left[\left(\frac{W}{\delta} \right)^{2n+1-m} - 1 \right] - \ln \left(\frac{W}{\delta} \right) \right\}$$

for $\delta < W \leq \delta/a$.

The rotational viscometer is particularly suitable for the investigation of thixotropic materials since the up and down curves as illustrated in figure 2b can be obtained quickly. Extensive work has been done on those materials by Green and Weltman (19) and equations are available for the hysteresis loop and the effect of time.

End effects have been studied by various investigators (11, 19) and various methods and equations have been devised to correct for them. Mooney (30) and Reiner (16), proceeding along the same lines as were discussed earlier for the tube instrument, have developed methods for correcting for slippage effects.

From an engineering viewpoint in particular, it is highly desirable to be able to convert data obtained in rotational viscometers into tube flow curves and Alves, Boucher and Pigford (11) have proposed a method, applicable in many cases, for accomplishing this which is presented in Appendix III.

Turbulent flow.—Relatively little is known at present about the turbulent flow of non-Newtonian materials in terms of the basic flow curve. The limited data available indicate that the viscosity of these materials is relatively constant in this region and that the relation between the Fanning friction factor and Reynolds number given by Nikuradse's equation,

$$\frac{1}{f^{1/2}} = 2.0 \log_{10}(\text{Re } f^{1/2}) - 0.8 \quad (\text{smooth pipes}) \quad (53)$$

which is valid for Newtonians is also applicable for non-Newtonians, at least as a good approximation. The pressure drop due to friction is calculated by the usual Fanning equation

$$\left(\frac{dP}{dL}\right)_F = \frac{fU^2\rho}{2g_c D} \quad (54)$$

The curves in figure 5b are typical of a non-Newtonian material flowing in cylindrical tubes with the solid curve representing laminar flow and the dotted curves representing turbulent flow, the transition point moving down the laminar curve with increasing diameter. The turbulent viscosity, μ_T , can be obtained from a point on a turbulent flow curve by calculating the corresponding friction factor, f , then obtaining the Reynolds number, Re , from equation (53) and from this μ_T follows. If the turbulent flow curve is not available, Alves, Boucher and Pigford (11) suggest the use of the limiting viscosity, μ_{∞}' , for pseudoplastics and the coefficient of rigidity for Bingham plastics with a resulting accuracy of ± 25 percent in pressure-drop calculations. As the relationship between the transition point and the Reynolds number is unknown at present, the usual practice has been to assume that the Newtonian transition point, $\text{Re} = 2100$, is valid for these materials also. However, Hedström (25) recently has, by dimensional analysis, shown for Bingham plastics in laminar flow that

$$\left(\frac{dP}{dL}\right)_F \cdot \frac{Dg_c}{\rho U^2} = \frac{F\left(\frac{\xi Dg_c}{\eta U}\right)}{Re} = \frac{F(G)^*}{Re} \quad (55)$$

and in turbulent flow that

$$\left(\frac{dP}{dL}\right)_F \cdot \frac{Dg_c}{\rho U^2} = F_1(Re, G). \quad (56)$$

By utilizing some of the data of Wilhelm, Wroughton, and Loeffel (13) on cement rock suspensions, which he shows are Bingham plastics, he concludes that the usual f - Re relation for Newtonians, equation (53), is valid, approximately, for these materials. He then proposes that the critical Reynolds number is a function of G only and presents this relationship graphically as obtained from equations (55) and (56). This relationship is reproduced in Appendix VII, figure VII A - 3.

II Co-Current Gas-Liquid Flow in Cylindrical Conduits

The mechanics of gas-liquid flow in cylindrical conduits is far from being understood at present. All theoretical attempts to analyze this complex system have been based on the treatment of each phase separately and have involved many assumptions. For any fluid flowing in the steady state through a distance dL , the continuity equation

$$\frac{d(uA\rho)}{dL} = 0 \quad (57)$$

and the mechanical energy balance for a system containing no pump

* This relationship is presented graphically in figure VII A - 2, Appendix VII.

$$\frac{1}{\rho} \frac{dP}{dL} + \frac{u}{g_c} \frac{du}{dL} + \frac{g}{g_c} \frac{dh}{dL} + \frac{DF}{dL} = 0 \quad (58)$$

are applicable to any streamline in the fluid stream and are independent of the boundary shape. For flow channels which are not circular, the usual procedure is to replace the diameter by the hydraulic diameter defined as

$$D_H = \frac{4 \text{ Cross-sectional area}}{\text{Wetted perimeter}} = \frac{4A}{p} \quad (59)$$

However, in attempting to apply these equations to the gas and liquid phase separately, complications such as the determination of the respective flow channels, the effect of interfacial roughness, entrainment, hydraulic gradients and others arise.

Martinelli, Lockhart and co-workers at the University of California (6, 7, 8) by utilizing the following two basic assumptions: 1) that the frictional pressure drop in the liquid phase is equal to the frictional pressure drop in the gas phase and 2) that the volume of the liquid plus the volume of the gas at any instant is equal to the volume of the pipe have shown that

$$\left(\frac{\Delta P}{\Delta L} \right)_{TP} = \bar{\Phi}_L^2 \left(\frac{\Delta P}{\Delta L} \right)_{LP} = \bar{\Phi}_G^2 \left(\frac{\Delta P}{\Delta L} \right)_{GP} \quad (60)$$

$\left(\frac{\Delta P}{\Delta L} \right)_{TP}$ is the two-phase frictional pressure drop per unit length, $\left(\frac{\Delta P}{\Delta L} \right)_{LP}$ and $\left(\frac{\Delta P}{\Delta L} \right)_{GP}$ are the frictional pressure drops per unit length that would occur if the liquid and gas phases were flowing alone in the pipe respectively, and $\bar{\Phi}$ is a function of the quantity X defined as

$$X = \left[\frac{\left(\frac{\Delta P}{\Delta L} \right)_{LP}}{\left(\frac{\Delta P}{\Delta L} \right)_{GP}} \right]^{1/2} \quad (61)$$

and the flow condition, laminar or turbulent, of each phase. In addition the volume fraction of the liquid phase, R_L , and of the gas phase, R_G , are shown to be functions of X alone and tentative criteria for transition from laminar to turbulent flow are proposed as superficial Reynolds numbers of 1000 and 2000, < 1000 for viscous and > 2000 for turbulent. The four flow mechanisms possible are turbulent-turbulent, viscous-turbulent, turbulent-viscous, and viscous-viscous, the condition of the liquid phase being referred to first. This correlation was based on data obtained in vertical and horizontal pipes ranging in diameter from 0.586 inches to 1.017 inches for the co-current flow of air and the Newtonian liquids water, benzene, kerosene and various oils. The accuracy of the correlation is within the range ± 40 percent.*

Bergelin and Gazely (31), at the University of Delaware, proceeding under the same assumptions as did Martinelli and Lockhart, have derived equations similar to those of the California investigators for the cases of stratified and annular flow which predict lower pressure drops and fit their data better in the case of stratified flow. However, they pointed out that the difference in the data might be due to the type of entrance sections used and also that, since a hydraulic gradient exist in stratified flow, assumption (1) above is questionable. Jenkins (32) was able to correlate data obtained in annular flow within ± 40

* A derivation of these relations is presented in Appendix I.

percent by Lockhart and Martinelli's correlation but found that his data fell within ± 5 percent of the best line through each liquid rate thus indicating that some factor is not accounted for in the correlation. He also found Bergelin and Gazely's equation not applicable. The Delaware investigators also pointed out that the transition between each type of flow was accompanied by a change in the slope of the curve relating the pressure drop and flow rates of the phases, best shown by a plot of the gas-phase pressure drop versus the actual gas velocity at constant liquid rates.

Gazely (33), in the most fundamental study to date, has investigated interfacial shear and stability in stratified flow and has definitely shown that Lockhart and Martinelli's correlation is not applicable to such flow configurations. He outlines a stepwise method for predicting the pressure drop. However, since Lockhart and Martinelli's correlation predicts pressure drops higher than actually occur, he concludes that it is safe for design purposes. The transition point of the gas phase was shown to occur at a superficial Reynolds number of 3000 independent of the liquid rate while the liquid transition point was shown to occur at a superficial Reynolds number of 1700 to 2200 depending on the condition of the gas phase, occurring at the lower value if the gas phase is turbulent. By applying the mechanical energy balance between two sections of the tube assuming a uniform velocity distribution, incompressible flow and approximating the shearing stresses at the wall and interface, he obtained

$$\frac{U_{L1}^2 - U_{L2}^2}{2g_c \Delta L} - \frac{1}{\rho_L} \left(\frac{dP}{dL} \right)_{TP} - \left(1 - \frac{\rho_G}{\rho_L} \right) \frac{dh}{dL} = \quad (62)$$

$$\frac{f_{WL} U_L^2 P_L}{2g_c A_L} - \frac{f_{IL} \rho_G (U_G - U_L)^2 C_I}{2g_c \rho_L A_L}$$

and

$$\frac{U_{G1}^2 - U_{G2}^2}{2g_c \Delta L} - \frac{1}{\rho_G} \left(\frac{dP}{dL} \right)_{TP} = \frac{f_{WG} U_G^2 P_G}{2g_c A_G} + \frac{f_{IG} (U_G - U_L)^2 C_I}{2g_c A_G} \quad (63)$$

for the liquid and gas phases respectively. The dimensionless friction coefficients are defined by

$$f_{WL} = \frac{S_{WL} 2g_c}{\rho_L U_L^2} \quad (64)$$

$$f_{WG} = \frac{S_{WG} 2g_c}{\rho_G U_G^2} \quad (65)$$

$$f_{IL} = \frac{S_{IL} 2g_c}{\rho_G (U_G - U_L)^2} \quad (66)$$

$$f_{IG} = \frac{S_{IG} 2g_c}{\rho_G (U_G - U_L)^2} \quad (67)$$

and are indicative of the energy losses occurring at the pipe wall, subscript W, and interface, subscript I, respectively. By assuming that the liquid acted as a solid wall to the gas and that the gas flow

did not affect the liquid, he was able to approximate f_{WG} and f_{WL} by

$$\frac{1}{f_{WG}^{1/2}} = 4.0 \log_{10} (Re_G' f_{WG}^{1/2}) - 0.40 \quad (68)$$

where Re_G' is based on

$$D_G' = \frac{4A_G}{P_G + C_I} \quad (69)$$

and

$$\frac{1}{f_{WL}^{1/2}} = 4.0 \log_{10} (Re_{WL} f_{WL}^{1/2}) - 0.40 \quad (70)$$

where Re_{WL} is based on the hydraulic diameter of equation (59). He confirmed equations (68) and (70) by experiment in the case of turbulent flow and pointed out that a shape factor was apparently necessary in laminar flow.

With these assumptions, Gazely was able to obtain f_{IG} and f_{WG} from experimental data and he showed that the energy lost by the gas and gained by the liquid are equal in the case of a smooth interface but that the energy lost by the gas is greater than that gained by the liquid for a wavy interface, with the energy losses and transfer rates increasing in the latter case. The point of interfacial instability (point of rapid wave formation) was shown to occur at a relative velocity of ten to fifteen feet per second, being slightly dependent on the liquid depth, and was shown, by comparison with data on packed columns, to be the cause of "loading" in packed columns with the

"flooding" point being occasioned by the breaking of the interfacial waves.

Bergelin, Kegel, Carpenter and Gazely (3), in summarizing the work on co-current gas-liquid flow in vertical tubes at the University of Delaware, found their data to fall within a range of ± 30 percent of the results predicted by Lockhart and Martinelli's correlation. They proposed a tentative correlation, applicable to vertical tube condensers, relating the superficial friction factor and superficial Reynolds number of the gas phase, with the dimensional quantity $t_w \Gamma / t_p$ appearing as a parameter. By using this correlation, they were able to predict the pressure drops obtained by Carpenter (34) during the condensation of water, ethanol, methanol, toluene and trichloroethylene inside vertical tube condensers with an average deviation of 19 percent.

CHAPTER III

EXPERIMENTAL EQUIPMENT

The general arrangement of the experimental apparatus used in the present study is shown in the diagrammatic sketch of figure 6 and the photograph of figure 7.

As can be seen from figure 6, air from a storage tank was passed through a reducing valve and a rotameter before entering the test section. The air in the storage tank, having a capacity of approximately 8 cubic feet, was maintained at a pressure between 90 and 120 psig by a 50 CFM compressor, which furnishes these laboratories with compressed air. Before entering and leaving the storage tank, the air was passed through glass wool filters to eliminate foreign matter. The reducing valve used was a Klipfel 3/8 inch diaphragm type valve operated pneumatically. The air flow rate was controlled by means of valves located upstream from the rotameter. This instrument was a Schutte-Koerting number 6 rotameter and its calibration curve, furnished by the manufacturer, is given in Appendix V. The static temperature and pressure of the air were measured at the rotameter.

Again referring to figure 6, it can be seen that the suspensions were circulated through the system from storage tanks by two pumps. Both of these were open-impeller centrifugal pumps, the large one being an Ingersoll-Rand 1 CORVNL pump having a capacity of 75 GPM against a head of 120 feet while the recycle one was a Goulds size 1C pump

with a capacity of 50 GPM against a head of 50 feet. Each pump was fitted with a recycle line, and the rate of flow of the suspension was controlled by means of gate valves and measured gravimetrically in a 55-gallon drum. The upstream and downstream ends of the apparatus are shown photographically in figures 8 and 9 respectively. Each of the tanks used had a capacity of approximately 125 gallons and was equipped with water lines. The suction and discharge pressures of the large pump were measured and the power input to its motor was determined by a polyphase wattmeter having a range of 0-12 kilowatts with a stated accuracy of 0.5 percent of full scale reading. The temperature of the suspension was measured in the downstream tank.

In order to reduce vibrations, the pipes were insulated from the pipe rack by strips of hard rubber. The entire system was checked for leaks before using by pressurizing to 50 psig and painting all joints with a soap solution.

Entrance section.--As this investigation was concerned with turbulent flow, an entrance section was chosen that would introduce the air into the center of the liquid stream and at the same time be different from other types used in previous investigations in order to provide additional data on such devices. Consequently, the entrance section as shown in figure 10 was used.

Test section.--In order to study the effect of diameter on the pressure drop, three different size test sections were used and, as it was desirable to have a smooth surface and to prevent contamination of the fluids by rust and scale, these sections were made of copper. Pipes of 3/4, 1, and 1 1/2 inch nominal size were used and were arranged in

parallel, being connected to the remainder of the system through suitable pipe crosses and gate valves. A 5-foot glass observation section was attached to the downstream end of the 1 1/2 inch pipe. For single-phase flow, 15 pipe diameters are usually sufficient to eliminate entrance effects so that accurate pressure-drop measurements may be made, while 40 to 50 diameters are required for complete establishment of the velocity distribution. However, the number of diameters necessary to eliminate entrance effects is not known for two-phase flow, but it is certainly more than required for single-phase flow according to previous investigators in this field (32, 33). In order to have test sections of suitable length and at the same time provide adequate calming distances, pipes 20 feet in length were used and the length of each section was chosen so that 30 and 10 diameters were available on the up and downstream ends respectively for the elimination of entrance and exit effects.

Pressure taps.--All pressure tap installations were made by drilling a hole through the pipe wall the size of the inside diameter of 1/4 inch pipe, then countersinking a hole equal to the outside diameter in which 1/4 inch nipples 1 1/2 inches long were placed and brazed into position. Precaution was taken to insure that the taps were in the same horizontal plane and all burrs were removed from the inside of the pipes by a file. Smaller size pressure taps would have been preferable, of course, but were not used since they are more subject to clogging by the suspensions investigated.

Pressure measurement.--A Republic pneumatic differential pressure transmitter was used for measuring the pressure drops in the test sections.

Since over the entire range of this instrument, the displacement of the fluid in the pressure lines is negligible, the possibility of these lines becoming plugged by the suspensions is small. Water was used as the transmitting agent in the pressure lines and the output pressure of the instrument was read on a mercury filled U-tube manometer. The calibration curve for this instrument, as determined in these laboratories, is given in Appendix IV. All pressure lead lines were made of equal length to reduce pressure fluctuations caused by the centrifugal pump. Bourdon type gages, calibrated in these laboratories, were used for the static pressure measurements and were connected to the pressure taps through mud traps. The construction of these traps is shown in figure 11 and one can be seen in the photograph of figure 8.

Separating section.--The air and suspension were separated at the downstream end of the system by introducing the discharge off center of the tank, thereby producing a rotating effect. At the upstream end of the system, the recycled material was introduced below the surface of the material in that tank to prevent entrapment of air bubbles.

CHAPTER IV

MATERIAL

For the purposes of the present investigation it was desirable to have a non-Newtonian material, not exhibiting thixotropic properties, which would behave as several of the different types of these materials by suitable concentration changes and have particles of such size that rapid settling would not occur. Water-clay suspensions were chosen as meeting these requirements and a Georgia kaolin-type clay was used. This kaolin clay was mined in central Georgia (near Macon) and was kindly donated by the Georgia Kaolin Company.

Several shipments of this type of clay were received and specific gravity and particle-size distribution measurements (35) were made on representative samples of the two lots used. The specific gravity at 25° C. by ASTM procedure of lot 1 was 2.45 and that of lot 2 was 2.51.

The results of the particle-size distribution measurements are presented in figure 14. As the properties of these materials were reasonably close, they were mixed in equal proportions in making the various suspensions investigated. The average value of the specific gravities, 2.48, was used in determining the concentrations of these suspensions. The particle-size distribution may therefore be taken as the average of the curves in figure 14.

As a matter of interest, electron-microscope photographs of typical kaolin clays mined in the same location as the ones used in this investigation are shown in figures 15a and 15b.

CHAPTER V

EXPERIMENTAL PROCEDURE

The following five types of experimental tests were made in each test section:

- (1) Pressure-drop measurements for the flow of water alone. These tests were made in order to check the accuracy of the instruments and to determine whether entrance and exit effects had been eliminated by comparing the results so obtained with those predicted by the usual methods of calculation.
- (2) Pressure-drop measurements for the co-current flow of air and water. These tests were made to provide a check on the accuracy of the air system instruments, the entrance section, and the entrance and exit effects by comparing the results with those obtained by other investigators in this field.
- (3) Pressure-drop measurements for the flow of water-clay suspensions alone. These tests were made to obtain data on the flow properties of these materials.
- (4) Pressure-drop measurements for the co-current flow of air and water-clay suspensions. These tests were made in order to provide data on a type of system not previously investigated.
- (5) Suction pressure, discharge pressure and power measurements were made on the main pumping unit in order to determine the pump characteristics while handling suspensions of various concentrations.

Preparation of suspensions.--The water-clay suspensions were prepared in the two tanks at the downstream end of the apparatus shown in figure 9, each having a capacity of approximately 125 gallons. A predetermined weight of water was added to one of the tanks, which was roughly calibrated, and the mixer and recycle pump started, the lines being so adjusted that the pump was recycling only the material from this tank. The required amount of clay was added to the water slowly. Any large lumps formed were broken up by hand and open steam was added to bring the temperature of the mixture up to several degrees below that of the room. About 200 gallons of suspension were required and when the capacity of this tank was reached, the lines were adjusted so that the other tank was introduced into the system and the mixing continued until 200 gallons were obtained. This mixing process required approximately 1 1/2 hours and, to further insure complete mixing, the material was then circulated through the complete apparatus for an additional hour.

Operating procedure.--The operating procedure was practically the same in all of the various types of tests conducted and will be described in detail for the co-current flow of air and water-clay suspensions, type 4. The valving was arranged for the particular test section desired, the pressure lines were filled with water, the transmitter turned on and air bled out of the lines. The mud traps were then filled with water, and air was bled out of these lines. The main and recycle pumps were then adjusted to the desired liquid rate by means of gate valves, the pressure drop being used as indicative of this rate, and the pressure tap lines opened to the system. The pressure at the entrance section was recorded and the air bleed line opened. The air rate, as determined

by the rotameter, was set at the desired rate and pressure by means of the air control valves and the reducing valve. The air bleed line was then closed and the entrance valve opened simultaneously. Slight adjustments were usually necessary in the air control valves to produce the desired pressure and rate and to give fairly steady pressure drop readings. Naturally the liquid rate decreased slightly due to the increased head on the pump, but no changes were made in the main pump discharge valve since the liquid rate was so sensitive to small changes in this valve and the necessary change could not be predicted. In order to keep the pumps in equilibrium, adjustments were made on the recycle pump only. When equilibrium had been reached, as evidenced by the pressure-drop readings, the discharge was switched to the weighing tank and the time measured, by a Precision electric timer, for this tank to fill or the amount collected in approximately 2 minutes determined. During this time the following measurements were taken: pressure drop; rotameter pressure, reading, and temperature; air entrance pressure; pump discharge pressure, suction pressure and power; and temperature at discharge of system. At each liquid rate, three air rates were used and the liquid rate was varied from 0.15 to 16 pounds per second while the air rate was varied from 0.0015 to 0.025 pounds per second. Specific-gravity measurements were made several times during the series of these tests by a pycnometer, a calibrated gallon jug being used, and the average value of these measurements was determined. Samples of each concentration used were saved for viscosity determinations. Visual observations of the flow were made in the glass section during runs in the 1.60 inch tube.

After the series of runs was completed in each test section, the suspension was stored in the mixing tank and weighing drum, and the system was completely flushed out with water.

CHAPTER VI

DISCUSSION OF RESULTS

The data and calculated results are presented in tables I through VII and figures 16 through 33. The original data is on file in the School of Chemical Engineering of the Georgia Institute of Technology. All tests were made with the pipes in a horizontal position. The methods of calculation for the various types of tests conducted are shown in Appendix VII.

Flow of water only.--In order to check the general accuracy of the equipment and instruments, a series of runs was made in each of the test sections using water only. The results of these tests are shown in figure 16 in the form of the observed friction factor as a function of the Reynolds number and, by comparison with the accepted relationship between these variables given by equation (53), it is apparent that the agreement is good. The range of the variables in this plot indicates the limits of the experimental set-up. The temperature variation was rather large in these runs, 12 to 25° C., but it was found that this variation could be considerably reduced by preheating the water to a temperature several degrees below that of the room before the runs were started. This utilized the heat losses to the surroundings to compensate for the heat input by the pumps.

Flow of water-clay suspensions.--A series of runs was made in each of the test sections on water-clay suspensions of various concentrations in

order to determine the flow properties of these materials. These results are shown in figures 17 through 23. In figure 17 the pressure drop in the 1.60 inch tube is shown as a function of the volumetric flow rate with the solids concentration as a parameter. Here the effect of increasing amounts of solids is clearly indicated. Whereas the curves for the two lower concentrations begin at the origin, the curves for the two higher concentrations begin at a point on the pressure axis, thus indicating the presence of a yield value in these cases. It is interesting to note that the increase in pressure drop at a fixed flow rate increases approximately linearly with increasing amounts of solids up to the higher concentrations. It then increases rapidly with small increases in solids concentration. This indicates that at the higher concentrations the flow properties of the suspensions are changing rapidly and is readily noticeable when the materials are examined visually. At the lower concentrations, the particles are widely separated and tend to settle fairly rapidly but at the higher concentrations, the settling tendency disappears and the suspensions act like pastes, becoming un-pourable at a solids concentration of approximately 60 weight percent.

Due to the limitations of the experimental set-up, most of the data in the test sections on these materials was obtained in the turbulent flow region and in order to determine the types of materials being dealt with and their rheological properties, they were investigated in the laminar flow region in a rotational viscometer and a capillary tube viscometer. A Brookfield Synchro-lectric viscometer was used as the rotation instrument, the equations and dimensions being given in Appendix II, and the results obtained presented in figures 18 and 19,

where the logarithm of the angular velocity of the inner cylinder is shown as a function of the logarithm of the shearing stress at the inner cylinder wall. The data for the two lower concentrations, figure 18, give very good straight lines with positive slopes, thus indicating that in this range the data can be represented in each case by a power function. These functions were found to be

$$\dot{\omega}_1 = 2.038 \times 10^{10} (W)^{3.869}, \quad 0.00192 \leq W \leq 0.00348 \quad (71)$$

$$12.1 \text{ WT.}\%$$

$$T = 26.0^\circ \text{ C.}$$

and

$$\dot{\omega}_1 = 1.289 \times 10^{12} (W)^{6.677}, \quad 0.0143 \leq W \leq 0.0202 \quad (72)$$

$$23.6 \text{ WT.}\%$$

$$T = 26.8^\circ \text{ C.}$$

In order to predict the behavior of these materials in cylindrical tubes, these equations were converted to the consistency variables y and x of equations (11) and (12) respectively by Alves' method as discussed in Appendix III. The final results are

$$\frac{y}{4} = 2.30 \times 10^{10} (x)^{3.87}, \quad 0.00192 \leq x \leq 0.00348 \quad 12.1 \text{ WT}\% \quad (73)$$

$$0.708 \leq \frac{y}{4} \leq 7.08 \quad T = 26.0^\circ \text{ C.}$$

and

$$\frac{y}{4} = 1.78 \times 10^{12} (x)^{6.68}, \quad 0.0143 \leq x \leq 0.0202 \quad 23.6 \text{ WT}\% \quad (74)$$

$$0.865 \leq \frac{y}{4} \leq 8.65 \quad T = 26.8^\circ \text{ C.}$$

These equations indicate that these suspensions behave as pseudoplastics, but the range of the variables covered is too small to be of any use in determining the properties of these materials. The data for the higher concentrations, presented in figure 19, appear to be too complicated for analysis and yield no information on the type or properties of these suspensions.

Therefore, in order to obtain useable data on these suspensions, they were investigated in a capillary tube viscometer, shown diagrammatically in figure 13, and these results are presented in figures 20 through 23 where $y/4$ is presented as function of x . The data obtained on these materials in the three test sections is also included on these figures and they are considered to represent the flow properties of the various suspensions investigated in both the laminar and turbulent flow regions. As shown in figure 20, the 12.1 weight percent suspension behaved as a pseudoplastic and, as the data was not obtained at high enough rates of shear to indicate whether the curve approached an asymptote drawn through the origin as discussed under pseudoplastics in the Theoretical Background Chapter, the slope of the straight line section of the curve was taken as the limiting viscosity at infinite shear and was found to be 7.18×10^{-4} lb.m/ft.sec. which is 1.335 times the viscosity of water at the same temperature (30° C.). The range of the data obtained in the Brookfield viscometer, equation (73), is too small to permit a comparison between the two curves. Extrapolation of the curves for the turbulent flow region to their intersection with the viscous flow curve is too uncertain to give accurate values of the transition points.

Referring to figure 21, it is seen that the 23.6 weight percent suspension also behaved as a pseudoplastic and its limiting viscosity at infinite shear was determined in the same manner as was that of the 12.1 weight percent suspension and was found to be 10.5×10^{-4} lb.m./ft.sec. which is 1.952 times the viscosity of water at the same temperature (30° C.). Again the range of the data obtained in the Brookfield viscometer is too small to permit a comparison of the two curves. In this case also the transition points could not be determined with any degree of accuracy.

In order to obtain the viscous flow curves of the 39.9 and 47.5 weight percent suspensions, shown in figures 22 and 23 respectively, use was made of the data obtained in both the capillary instrument and in the three test sections and certain assumptions were found necessary. As can be observed in figures 22 and 23, these materials began to flow in the capillary tube at stresses less than those necessary to produce flow in the larger test sections which indicates that in the former case slippage was occurring. While slippage can occur in large tubes, it is not as likely to as in small tubes since a proportionally smaller amount of fluid is affected by the tube wall as the diameter increases. The data obtained in the test sections, then, was assumed to be valid and a slippage correction was made for the data obtained in the capillary tube in the following manner. The points at the lowest rates of shear were connected by the best straight line through the origin, as indicated in each figure, and the values of the ordinates of this assumed slippage curve were subtracted from the ordinates of the points obtained in the capillary tube at the corresponding rates of shear. The final

laminar flow curve in each case was then constructed by joining these points and those obtained in the three test sections. This assumed slippage curve is of the Buckingham type, as shown in figure 4a, and can be considered at best to be but a rough approximation. Due to the limitations of this instrument, appreciably smaller tubes could not be used and therefore the possible effect of radius could not be investigated.

In order to check the validity of the assumptions made, the yield value and asymptote to each curve were determined and, using these values, points were calculated by equation (55) for Bingham plastics. These calculated values are indicated on each figure and it is apparent that the agreement is excellent. Therefore, these suspensions behaved approximately as Bingham plastics and the assumptions made appear to be fairly accurate. However, one further point should be mentioned and that concerns kinetic energy and contraction losses. In all cases, the capillary tube data was corrected for these losses by the accepted method for Newtonians, namely

$$P_{KE} \text{ and } C = \frac{1.12U^2 \rho}{g_c} \quad (75)$$

and was found to be negligible in most cases. However, as pointed out by McMillen (24), contraction losses are much greater for Bingham plastics than for ordinary Newtonian Materials due to the necessity of reducing the plastic core upon reduction of the flow area. The data McMillen presents for these losses was not applicable in the cases of the materials investigated here, as they were determined for

materials of much higher yield values. Since the flow rates in this investigation were not too high, these corrections are probably not appreciable but until additional data are available, their effect must remain unknown. In view of the assumptions made, the laminar flow curves for the Bingham plastics must be considered approximate.

Because of the nature of the flow curves of the 39.9 and 47.5 weight percent suspensions thus obtained, it is interesting to study again the data obtained on these suspensions in the Brookfield viscometer as shown in figure 19. It is now obvious that the data resulting from that investigation were due to slippage occurring at the inner cylinder wall, as in each case all of the points were obtained at stresses below the yield stresses of the respective suspensions.

Turbulent viscosity.--In order to determine the applicability of the usual friction factor-Reynolds number relationship of Newtonians, equation (53), to the materials investigated here, the so-called turbulent viscosity of these materials was determined by plotting the calculated friction factors against the quantities $(Du\rho) \times 10^3$ of the suspensions as shown in figure 24. The best curve parallel to the curve of equation (53) was drawn through the points of each suspension and by determining the values of $(Du\rho) \times 10^3$ of each curve and the Newtonian Reynolds number at the same friction factor value, the turbulent viscosity was calculated by

$$\mu_T \times 10^3 = \frac{(Du\rho)_S \times 10^3}{Re_N} \quad (76)$$

The values thus obtained are indicated on the figure and on comparing

these with those obtained from the laminar flow curves at infinite shear (the small temperature differences being negligible in comparison to the accuracy of the determinations), it is observed that the turbulent viscosities are from 9 to 51 percent lower than those at infinite shear.

Realizing, of course, that the turbulent viscosity calculated in this manner has no recognized significance and is probably no more than a convenient method of representing data, it is still interesting to investigate the matter further since it has been widely used. In order to determine if this type of viscosity is constant or not, this quantity was calculated for each of the runs made as accurately as possible and plotted against the shearing stress at the pipe wall as shown in figures 25 and 26. These figures appear to indicate that there is some dependence on the pipe diameter as well as the rate of shear, particularly at the higher concentrations. The dependence on the diameter probably can be explained and the accuracy of the calculation method shown by comparing the data for the suspensions with the viscosity of water calculated from the water runs in the same way. While the data for the water runs was within a range of ± 5 percent of the calculated data, the range of the turbulent viscosities is within a range of ± 24 percent of the true values, since small changes in the friction factor cause large changes in the Reynolds number in the turbulent region which appear directly in the calculated viscosity. The apparent dependence of the viscosity on the diameter in the case of water is due to the deviations of the observed values from the accepted values being for the most part for each pipe on one side or the other of the accepted curve as shown in figure 16. This effect then was probably the same in the case of the various

suspensions. While the turbulent viscosity of all the suspensions except the 47.5 weight percent slurry appeared to increase with increasing shearing stresses before apparently leveling out, the turbulent viscosity of the latter appeared to decrease with increasing shearing stresses before flattening out. This decrease is probably due to these data being obtained near the transition point as shown in figure 23. In order to determine whether the difference in temperature of the different observations could account for any of the spread, this effect was approximated by calculating the ratio of the turbulent viscosity to that of water at the same temperature for each point and these results are presented in tables II A-D. They were not plotted since as can be observed, they offer no help at all. However, the data is insufficient to definitely establish whether or not the turbulent viscosity depends on the shearing stress and possibly pipe diameter. About all that can be said for the turbulent viscosity is that it indicates that the usual friction factor-Reynolds number relationship for Newtonians is applicable to non-Newtonians as an approximation when the limiting viscosity at infinite shear or the coefficient of rigidity is used in calculating the Reynolds number. Since the only way to determine the turbulent viscosity is to actually conduct tests on the material in question in turbulent flow, its use is limited to that of a convenience factor and possibly as a scale-up factor which as these data indicate is questionable.

Co-current flow of air and water.--In order to provide a general check on the air system and entrance section a series of runs was made using

air and water and the data obtained was compared with the results predicted by the correlation of Lockhart and Martinelli (8). As shown in figure 30, these data lie within a range of ± 20 percent of the correlating curve with the large majority of the data lying on the low side of the curve. However, considering the fact that the overall accuracy of the correlation is only within the range of ± 40 percent this discrepancy is probably not serious. During the runs in the 1.60 inch tube, visual observations were made in the glass section and although most of the observed flow types were rather ill-defined they could be classified roughly as either wave or semi-annular, the latter type not consisting of a true annulus through which the air was flowing but being characterized by rough waves on the water annulus and considerable entrainment of water in the air stream. These ill-defined flow types were probably due to the type of entrance section used and disturbing effects between this section and the test sections. However, considering the good agreement between the data and the correlation curve, these effects were probably not serious. At low air rates, the pressure drops were fairly steady, slight fluctuations being caused by the centrifugal pump, but as the air rate was increased the pressure fluctuations became violent as the slugging region was entered and at still higher air rates, the fluctuations decreased in amplitude and increased in frequency as the semi-annular flow region was approached. The slugging region was avoided during all runs and during the semi-annular flow, the average pressure drop was measured.

In order to illustrate the effect of the air rate on the pressure drop and to determine whether transitions in the flow types were occur-

ing, the total pressure drop in each test section was plotted against the air rate with the liquid rate as a parameter as shown in figures 27, 28, and 29. Since the liquid rate decreased slightly as the air rate increased, due to the increased head on the centrifugal pump, and since no means was available for accurately compensating for this effect, the liquid rates in each series of air runs were corrected to a constant rate in the following approximate manner by Lockhart and Martinelli's correlation (which has already been shown to be approximately valid):

$$\Delta P_{TP \text{ corrected}} = \frac{\Phi_{LTT}^2 * \left(\frac{\Delta P_{LP \text{ corr}}}{\Delta P_{GP}} \right) \Delta P_{LP \text{ corr}}}{\Phi_{LTT}^2 * \left(\frac{\Delta P_{LP \text{ uncorr}}}{\Delta P_{GP}} \right) \Delta P_{LP \text{ uncorr}}} \Delta P_{TP \text{ uncorr}} \quad (77)$$

As can be observed by reference to these figures, the pressure drop increases with increasing air rates and liquid rates, with the slopes of the lines becoming greater with decreasing pipe diameter. The only transition point noted occurs in the 0.82 inch test section, but undoubtedly each of the other curves would pass through similar inflection points at higher air rates than were used in this investigation.

Co-current flow of air and water-clay suspensions.--A series of tests was made on each of the four previously discussed water-clay suspensions and air in order to provide data on a type of system not previously investigated and to determine whether Lockhart and Martinelli's correlation was applicable to such a system. The results of these tests are presented in figure 30 and the agreement with the correlation curve is again within ± 20 percent, which is considered good. Visual observations in the glass section during runs in the 1.60 inch test section

* Functional notation: Φ_{LTT}^2 determined at indicated X^2 value.

showed that at very low air rates the air moved along the top of the pipe in the form of large bubbles which decreased in length as the air rate increased until the pipe appeared to be full of the clay suspension. At this point it was impossible to tell whether the air was dispersed throughout the suspension or whether an annular-type flow was occurring. Similar types of pressure fluctuations occurred during these runs as were encountered during the air-water runs and the slugging region was avoided. During runs in which the pressure fluctuations were rapid but of small amplitude, the average pressure drop was recorded. In order to determine whether the air was being removed from the suspensions between the runs, pressure-drop measurements were made at the same liquid rate before and after each series of air runs and specific-gravity measurements were made several times during the series of runs on each suspension.

Figures 27, 28 and 29 show the total pressure drop in each test section as a function of the air rate with the suspension rate and weight percent of solids as parameters. The liquid rates were corrected to a constant value by the approximate method of equation (77). The general trend of these curves is the same as discussed in the case of air-water runs, with the slopes of the curves becoming greater with increasing air rates, liquid rates, solids concentration and decreasing pipe diameter. Again the only transition point observed occurred in the 0.82 inch test section with similar inflection points expected to appear in the other curves at higher air rates.

It is interesting to note that, in the cases of the 39.9 and 47.5 weight percent suspensions, while the suspension was flowing laminarly

the introduction of air into the system caused a decrease in the pressure drop until very high air rates were reached. This effect can be seen by reference to tables VI C and D. The data was not further analyzed due to its very limited amount but certainly indicates a field for future study. The effect is no doubt caused by a change in viscosity and future study of it should prove interesting.

Pump characteristics

In order to determine the characteristics of the large centrifugal pump used in this investigation while handling the various suspensions studied, tests were conducted on this unit simultaneously with the other types of tests made. The results of these tests are presented in figures 32 and 33 and the manufacturer's performance curves are given in figure 31. By comparing the predicted and observed head-capacity curves for water in figures 31 and 32 respectively, it is seen that the actual performance was considerably better than predicted. This is probably due to the fact that the observed curve was obtained at a higher motor speed than the predicted one since the pump was operated by an oversize motor, rated at 3450 RPM at 15 horsepower, which had been originally attached to a larger pump, now beyond repair. As can be seen in figure 32, the head-capacity curves decrease with increase in solids concentration while the power input to the motor increases with increase in solids concentration as figure 33 shows. The expected increase in the power-capacity curves is not as rapid as expected and this discrepancy is probably due to an increased motor efficiency at the higher concentrations. However, since the efficiency of the motor was not measured,

this effect could not be quantitatively predicted and the pump efficiency could not be determined.

The results presented here are in agreement with those of other investigators (36,37) and are due mainly to the solids in the suspension instead of the increased viscosity, as comparison with the predicted performance curves of Stepanoff (38) for the effect of viscosity indicates.

Slight errors were probably made in the suction pressure determinations, as these values had to be estimated from the water performance data due to the fact that the suction pressure gage became fouled during the runs but the fouling was not detected until the runs were completed. This gage was connected directly to the suction side of the pump without the use of a mud trap since preliminary calculations indicated that at the higher flow rates, the suction pressure might be less than atmospheric. However, such was not the case for this pump as the investigations showed. Due to the small magnitude of the suction pressure in most cases, this error is believed to be small. The method of computation is shown in Appendix VI.

CHAPTER VII

CONCLUSIONS

The conclusions resulting from the present investigation may be summarized as follows:

1. The experimental pressure-drop measurements of the co-current turbulent-turbulent flow of air and water-clay suspensions in $3/4$, 1 and 1 $1/2$ inch horizontal pipes were correlated within the range of ± 20 percent of the calculated values by the correlation of Lockhart and Martinelli.
2. The usual Newtonian friction factor-Reynolds number relationship is approximately true for water-clay suspensions but the turbulent viscosity computed from this relationship has no valid significance.

NOMENCLATURE

A	cross-sectional flow area, ft. ²
A _G	cross-sectional gas flow area, ft. ²
A _L	cross-sectional liquid flow area, ft. ²
a	square of ratio of internal cylinder radius to external cylinder radius, dimensionless
B	constant used in equation (3)
b	plug radius defined by equation (15), ft.
C	constant used in equation (3)
C _I	interfacial cord length, ft.
C _G	constant in Blasius equation for friction factor for gas phase, dimensionless
C _L	constant in Blasius equation for friction factor for liquid phase, dimensionless
C _V	volume concentration, gm. mass/cm. ³
D	inside pipe diameter, ft.
D _H	hydraulic diameter, defined by equation (59), ft.
D _G	hydraulic diameter of gas cross-sectional flow area, defined by equation (I-4), ft.
D _G ⁱ	hydraulic diameter of gas cross-sectional flow area, defined by equation (69), ft.
D _L	hydraulic diameter of liquid cross-sectional flow area, defined by equation (I-3), ft.
D _P	inside pipe diameter (used for emphasis), ft.
d	constant used in equation (26), 1/sec.
F	denotes a function, or frictional energy loss, ft. lb. force/lb. mass
F ⁽ⁿ⁾	n th derivative of the function F

f	friction factor defined by equation (53), dimensionless
f_G	friction factor for gas phase calculated from Reynolds number Re_G , dimensionless
f_L	friction factor for liquid phase calculated from Reynolds number Re_L , dimensionless
f_{GP}	superficial friction factor for gas phase calculated from Reynolds number Re_{GP} , dimensionless
f_{LP}	superficial friction factor for liquid phase calculated from Reynolds number Re_{LP} , dimensionless
f_{IG}	friction factor indicative of energy lost by gas phase at interface, defined by equation (67), dimensionless
f_{IL}	friction factor indicative of energy gained by liquid phase at interface, defined by equation (66), dimensionless
f_{WG}	friction factor indicative of energy lost by gas phase at pipe wall, defined by equation (65), dimensionless
f_{WL}	friction factor indicative of energy lost by liquid phase at pipe wall, defined by equation (64), dimensionless
G	dimensionless group $SDg_c/\eta U$
g	acceleration due to gravity, ft./sec. ²
g_c	conversion factor, 32.17 ft. lb. mass/sec. ² lb. force
H	net head delivered by pump ft. lb. force/lb. mass
h	height, ft.
L	length, ft.
M	general consistency variable, or molecular weight lb. mass/lb. mol.
m	an integer or a constant
N	general consistency variable
n	an integer or a constant
P	pressure, lb. force/ft. ² abs.
P_D	pump discharge pressure, lb. force/in. ² gage
P_S	pump suction pressure, lb. force/in. ² gage

p	wetted perimeter of flow cross section, ft.
p_G	pipe-wall perimeter wetted by gas, ft.
p_L	pipe-wall perimeter wetted by liquid, ft.
Q	total volumetric flow rate, ft. ³ /sec.
Q_f	volumetric flow rate due to fluidity, ft. ³ /sec.
R	gas constant, 10.74 lb. force/in. ² ft. ³ /lb. mol. °R, or tube radius, ft.
r	radius, ft.
R_E	radius of external cylinder, ft.
R_i	radius of internal cylinder, ft.
R_G	volume fraction of pipe filled by gas phase, dimensionless
R_L	volume fraction of pipe filled by liquid phase, dimensionless
Re	Reynolds number, $DU\rho/\mu$, dimensionless
Re_G	Reynolds number of gas phase based on hydraulic diameter, D_G , of equation (I-4), dimensionless
Re'_G	Reynolds number of gas phase based on hydraulic diameter, D_G , of equation (69), dimensionless
Re_L	Reynolds number of liquid phase based on hydraulic diameter, D_L , of equation (I-3), dimensionless
Re_{GP}	superficial Reynolds number of gas phase based on inside pipe diameter, dimensionless
Re_{LP}	superficial Reynolds number of liquid phase based on inside pipe diameter, dimensionless
Re_{WL}	Reynolds number of liquid phase based on hydraulic diameter, D_H , of equation (59), dimensionless
\dot{r}_s	rate of shear at radius r , 1/sec.
$(\dot{r}_s)_W$	rate of shear at tube or cylinder wall, 1/sec.
S	shearing stress at radius r , lb. force/ft. ²
S_E	shearing stress at external cylinder wall, lb. force/ft. ²

S_i	shearing stress at internal cylinder wall, lb. force/ft. ²
S_{IG}	shearing stress in gas phase at interface, lb. force/ft. ²
S_{IL}	shearing stress in liquid phase at interface, lb. force/ft. ²
S_{WG}	shearing stress in gas phase at pipe wall, lb. force/ft. ²
S_{WL}	shearing stress in liquid phase at pipe wall, lb. force/ft. ²
T	absolute temperature, ° K.
T_o	torque, defined by equation (38), ft. lb. force
t_w/t	ratio of surface tension of water to that of other liquid, dimensionless
U	mean velocity, ft./sec.
u	velocity at radius r , ft./sec.
U_G	mean gas velocity based on actual gas flow area, ft./sec.
U_L	mean liquid velocity based on actual liquid flow area, ft./sec.
U_{GP}	superficial mean gas velocity based on inside pipe area, ft./sec.
U_{LP}	superficial mean liquid velocity based on inside pipe area, ft./sec.
U_D	mean liquid or suspension velocity at pump discharge, ft./sec.
U_S	mean liquid or suspension velocity at pump suction, ft./sec.
V	volumetric gas flow rate as metered at 14.7 psia and 21.1° C. ft. ³ /min.
v	specific volume, cm. ³ /gm. mass
W	consistency variable for rotation instrument, defined by equation (44), lb. force/ft. ²
W_G	gas flow rate, lb. mass/sec.
W_L	liquid or suspension flow rate, lb. mass/sec.
W_S	net shaft work, ft. lb. force/lb. mass
X	square root of the ratio of the pressure drop for the flow of liquid alone to the pressure drop for the flow of gas alone, dimensionless

x	consistency variable for tube instrument, defined by equation (12), lb. force/ft. ²
y	consistency variable for tube instrument, defined by equation (11), 1/sec.
z	consistency variable for rotation instrument, defined by equation (43), radians/sec.
α	parameter used by Lockhart and Martinelli (8), defined by equation (I - 3), dimensionless
β	parameter used by Lockhart and Martinelli (8), defined by equation (I - 4), dimensionless, or coefficient of slip, defined by equation (35), ft. ² sec./lb. mass
Γ	condensate rate per unit periphery, lb. mass/hr. ft.
γ	a constant
δ	yield value, lb. force/ft. ²
δ'	yield value of wall layer or intercept of asymptote to pseudoplastic curve, lb. force/ft. ²
ϵ	thickness of wall layer, ft.
η	coefficient of rigidity, lb. mass/ft. sec.
$\dot{\theta}$	angular velocity of fluid, radians/sec.
μ	coefficient of viscosity, lb. mass/ft. sec.
μ_B	Brookfield viscosity reading, lb. mass/ft. sec.
μ_L	viscosity of liquid, lb. mass/ft. sec.
μ_0	viscosity at zero shear, defined on page 7, lb. mass/ft. sec.
μ_W	viscosity of wall layer, lb. mass/ft. sec.
μ_{∞}	viscosity at infinite shear, defined on page 8, lb. mass/ft. sec.
μ'_{∞}	viscosity at infinite shear, defined on page 8, lb. mass/ft. sec.
μ_G	viscosity of gas, lb. mass/ft. sec.
μ_T	turbulent viscosity, lb. mass/ft. sec.

μ_E	viscosity at external cylinder wall, lb. mass/ft. sec.
μ_I	viscosity at internal cylinder wall, lb. mass/ft. sec.
$\mu_{\text{soln.}}$	viscosity of solution, lb. mass/ft. sec.
$\mu_{\text{solv.}}$	viscosity of solvent (dispersing phase), lb. mass/ft. sec.
$\mu_{\text{rel.}}$	relative viscosity, dimensionless
$\mu_{\text{spec.}}$	specific viscosity, dimensionless
μ_I	intrinsic viscosity, gm. mass/cm. ³
ρ	density, lb. mass/ft. ³
ρ_L	density of liquid or suspension, lb. mass/ft. ³
ρ_G	density of gas, lb. mass/ft. ³
ϕ	coefficient of fluidity, ft. sec./lb. mass
ϕ_0	fluidity at zero shear, ft. sec./lb. mass
ϕ_{∞}	fluidity at infinite shear, ft. sec./lb. mass
ϕ_W	fluidity at tube wall, ft. sec./lb. mass
\mathcal{F}	parameter used by lockhart and Martinelli (8), defined by equation (60), the square root of the ratio of the two phase pressure drop per unit length to the pressure drop per unit length of the gas phase (subscript G) or the liquid phase (subscript L) flowing alone in the pipe, dimensionless. To denote the conditions of the liquid and gas phases respectively the following subscripts are used: TT (turbulent-turbulent), TV (turbulent-viscous), VT (viscous-turbulent), and VV (viscous-viscous)
χ	coefficient of structural stability, defined by equation (23), (lb. force/ft. ²) ²
ω_E	angular velocity of external cylinder, radians/sec.
ω_I	angular velocity of internal cylinder, radians/sec.
ΔP_F	frictional pressure drop, lb. force/ft. ²
ΔP_{GP}	superficial frictional pressure drop of gas phase flowing alone in pipe, lb. force/ft. ² abs. or in. Hg

- ΔP_{LP} superficial frictional pressure drop of liquid or suspension flowing alone in pipe, lb. force/ft.² abs. or in. Hg
- ΔP_{TP} pressure drop for two phase flow, lb. force/ft.² or in. Hg
- $\Delta P_{TP \text{ MART}}$ pressure drop for two phase flow calculated by correlation of Lockhart and Martinelli (8), in. Hg

REFERENCES

- (1) Bergelin, Olaf P., "Flow of Gas-Liquid Mixtures," Chem. Eng., May 1949, 104-6.
- (2) Bergelin, Olaf P. and Carl Gazely, Jr., "Co-Current Gas-Liquid Flow I. Flow in Horizontal Tubes," Heat Transfer and Fluid Mechanics Institute, 1949, 5-18.
- (3) Bergelin, Olaf P., P. K. Kegel, F. G. Carpenter, and Carl Gazely, Jr., "Co-Current Gas-Liquid Flow II. Flow in Vertical Tubes," Heat Transfer and Fluid Mechanics Institute, 1949, 19-28.
- (4) Gazely, Carl, Jr., "Co-Current Gas Liquid Flow III. Interfacial Shear and Stability," Heat Transfer and Fluid Mechanics Institute, 1949, 29-40
- (5) Boelter, L. M. K. and R. H. Kepner, "Pressure Drop Accompanying Two-Component Flow Through Pipes," Industrial and Engineering Chemistry, 31 (1939), 426-34.
- (6) Martinelli, R. C., L. M. K. Boelter, T. H. M. Taylor, E. G. Thomsen, and E. H. Morrin, "Isothermal Pressure Drop for Two-Phase Two-Component Flow in a Horizontal Pipe," Trans. A. S. M. E., 66 (1944), 139-51.
- (7) Martinelli, R. C., J. A. Putnam, and R. W. Lockhart, "Two-Phase, Two-Component Flow in the Viscous Region," Trans. A. I. Ch. E., 42 (1947), 681-705.
- (8) Lockhart, R. W. and R. C. Martinelli, "Proposed Correlation of Data for Isothermal Two-Phase, Two-Component Flow in Pipes," Chem. Eng. Progress, 45 (1949), 39-48.
- (9) Gasely, Carl, Jr. and Olaf P. Bergelin, Discussion of "Proposed Correlation of Data for Isothermal Two-Phase, Two-Component Flow in Pipes," by R. W. Lockhart and R. C. Martinelli, Chem. Eng. Progress, 45 (1949), 39-48.
- (10) Alves, George E., "Flow of Non-Newtonian Suspensions," Chem. Eng., May 1949, 107-09.
- (11) Alves, George E., D. F. Boucher, and R. L. Pigford, "Pipe Line Design for Non-Newtonian Solutions and Suspensions," Paper presented at Atlanta, Ga. Meeting, Am. Inst. Chem. Engrs. March 17-19, 1952.

- (12) Babbitt, Harold E. and David H. Caldwell, "Turbulent Flow of Sludges in Pipes," Univ. Ill. Eng. Exper. Sta. Bull., Series No. 323, Vol. 38, No. 13, 1940.
- (13) Wilhelm, Richard H., Donald M. Wroughton and Willis F. Loeffel, "Flow of Suspensions Through Pipes," Ind. Eng. Chem., 31 (1939), 622-29.
- (14) Binder, R. C. and J. E. Busher, "A Study of Flow of Plastics Through Pipes," J. Applied Mech., 13 (June 1946), A-101-05.
- (15) Winding, C. C., G. P. Baumann and W. L. Kranich, "Flow Properties of Pseudoplastic Fluids--Part I. Viscosities of GR-S Latices," Chem. Eng. Progress, 43 (1947), 527-36 and "Flow Properties of Pseudoplastic Fluids--Part II. Flow of GR-S Latices in Commercial Tubing," 613-622.
- (16) Reiner, Markus, "Deformation and Flow," London: Interscience Publishers, Inc. 1949.
- (17) Williamson, R. V., "The Flow of Pseudoplastic Materials," Ind. Eng. Chem., 21 (1929), 1108-11.
- (18) da C. Andrade, E. N., "Viscosity and Plasticity," New York: Chemical Publishing Company, Inc., 1951.
- (19) Green, Henry, "Industrial Rheology and Rheological Structures," New York: John Wiley and Sons, Inc., 1949.
- (20) Scott Blair, G. W., "An Introduction to Industrial Rheology," Philadelphia: P. Blakiston's Son and Co. Inc., 1938.
- (21) Scott Blair, G. W., "A Survey of General and Applied Rheology," New York and Chicago: Pitman Publishing Corp., 1944.
- (22) Lewis, Warren K., Lombard Squires, and Geoffrey Broughton, "Industrial Chemistry of Colloidal and Amorphous Materials," New York: The MacMillan Co., 1942.
- (23) Babbitt, Harold E. and David H. Caldwell, "Laminar Flow of Sludges in Pipes with Special Reference to Sewage Sludge," Univ. Ill. Eng. Exper. Sta. Bull., Series No. 319, Vol. 37, No. 12, 1939.
- (24) McMillen, Elliott L., "Simplified Pressure-Loss Calculations for Plastic Flow," Chem. Eng. Progress, 44, (1948), 537-46.
- (25) Hedström, Bengt O. A., "Flow of Plastics Materials in Pipes," Ind. Eng. Chem., 44 (1952), 651-56.
- (26) Schofield, R. K. and G. W. Scott Blair, "The Influence of the Proximity of a Solid Wall on the Consistency of Viscous and Plastic Materials," J. Chem. Phys., 34 (1930), 248-62.

- (27) Scott Blair, G. W. and E. M. Crowther, "The Flow of Clay Pastes Through Narrow Tubes," J. Phys. Chem., 33 (1929), 321-33.
- (28) Scott Blair, G. W., "A Further Study of the Influence of the Proximity of a Solid Wall on the Consistency of Viscous and Plastic Materials" J. Chem. Phys., 34 (1930), 1505-08.
- (29) Schofield, R. K. and Scott Blair, G. W., "The Influence of the Proximity of a Solid Wall on the Consistency of Viscous and Plastic Materials III," J. Chem. Phys., 35 (1931), 1212-15; "The Influence of the Proximity of a Solid Wall on the Consistency of Viscous and Plastic Materials" IV, 39 (1935), 973-81.
- (30) Mooney, Melvin, "Explicit Formulas for Slip and Fluidity," J. Rheology, 2 (1931), 210-22.
- (31) Gazely, Carl, Jr., and Olaf P. Bergelin, "A Preliminary Investigation of Two-Phase Flow," Univ. of Del. Report TPF-1, May 1947.
- (32) Jenkins, Rodman, "Two-Phase Two-Component Flow of Water and Air," M. Ch. E. Thesis, Univ. of Del., 1947.
- (33) Gazely, Carl, Jr., "Interfacial Shear and Stability in Two-Phase Flow," Ph. D. Thesis, Univ. of Del., 1948.
- (34) Carpenter, F. G., "Condensation Rates at High Vapor Velocities," Ph. D. Thesis, Univ. of Del., 1948.
- (35) Bauer, Edward E., "Hydrometer Computations in Soil Studies Simplified," Eng. News Record, 118 (1937), 662-64.
- (36) Gregory, W. B., "Pumping Clay Slurry Through a Four-Inch Pipe", Mech. Eng., 49 (1927), 609-16.
- (37) O'Brien, Morrrough P. and Richard G. Folsom, "The Transportation of Sand in Pipe Lines," Univ. of Calif. Pub. in Eng., Vol. 3, No. 7, 1937, 369-73.
- (38) Stepanoff, A. J., "Centrifugal and Axial Flow Pumps," New York: John Wiley and Sons, Inc., 1948.
- (39) Perry, John H., "Chemical Engineers' Handbook," 3rd Edition, New York: McGraw-Hill Book Co. Inc., 1950, 374.
- (40) Keenan, Joseph H. and Frederick G. Keyes, "Thermodynamic Properties of Steam," New York: John Wiley and Sons, Inc. 1947.
- (41) Lange, Norbert A., "Handbook of Chemistry," 6th Edition, Sandusky, Ohio: Handbook Publishers, Inc., 1946, 1576.
- (42) Brown, G. G. (editor), "Unit Operations," New York: John Wiley and Sons, Inc., 1950, 140.

LIST OF TABLES

No.	Page
I Data and Results for the Flow of Water in a 1.60 inch, a 1.06 inch and a 0.82 inch Pipe	73
II Data and Results for the Flow of Various Water-Clay Suspen- sions in a 1.60 inch, a 1.06 inch and a 0.82 inch Pipe	
A. Specific Gravity 1.078, 12.1 Weight (5.27 Volume) Percent Solids	74
B. Specific Gravity 1.164, 23.6 Weight (11.1 Volume) Percent Solids	75
C. Specific Gravity 1.313, 39.9 Weight (21.2 Volume) Percent Solids	76
D. Specific Gravity 1.396, 47.5 Weight (26.8 Volume) Percent Solids	77
III Data and Results of Flow Properties of Various Water-Clay Suspensions in a Brookfield Viscometer	
A. Specific Gravity 1.078, 12.1 Weight (5.27 Volume) Percent Solids	78
B. Specific Gravity 1.164, 23.6 Weight (11.1 Volume) Percent Solids	79
C. Specific Gravity 1.313, 39.9 Weight (21.2 Volume) Percent Solids	80
D. Specific Gravity 1.396, 47.5 Weight (26.8 Volume) Percent Solids	81

LIST OF TABLES (continued)

No.	Page
IV	Data and Results of Flow Properties of Various Water-Clay Suspensions in a Capillary Tube Viscometer
A.	Specific Gravity 1.078, 12.1 Weight (5.27 Volume) Percent Solids. 82
B.	Specific Gravity 1.164, 23.6 Weight (11.1 Volume) Percent Solids. 83
C.	Specific Gravity 1.313, 39.9 Weight (21.2 Volume) Percent Solids. 84
D.	Specific Gravity 1.396, 47.5 Weight (26.8 Volume) Percent Solids. 85
V	Data and Results for the Co-Current Flow of Air and Water
A.	Flow in a 1.60 inch Pipe. 86
B.	Flow in a 1.06 inch Pipe. 87
C.	Flow in a 0.82 inch Pipe. 88
VI	Data and Results for the Co-Current Flow of Air and Various Water-Clay Suspensions
A.	Specific Gravity 1.078, 12.1 Weight (5.27 Volume) Percent Solids
1.	Flow in a 1.60 inch Pipe. 89
2.	Flow in a 1.06 inch Pipe. 90
3.	Flow in a 0.82 inch Pipe. 91

LIST OF TABLES (continued)

No.	Page
B. Specific Gravity 1.164, 23.6 Weight (11.1 Volume)	
Percent Solids	
1. Flow in a 1.60 inch Pipe.	92
2. Flow in a 1.06 inch Pipe.	93
3. Flow in a 0.82 inch Pipe.	94
C. Specific Gravity 1.313, 39.9 Weight (21.2 Volume)	
Percent Solids	
1. Flow in a 1.60 inch Pipe.	95
2. Flow in a 1.06 inch Pipe.	96
3. Flow in a 0.82 inch Pipe.	97
D. Specific Gravity 1.396, 47.5 Weight (26.8 Volume)	
Percent Solids	
1. Flow in a 1.60 inch Pipe.	98
2. Flow in a 1.06 inch Pipe.	99
3. Flow in a 0.82 inch Pipe.	100
VII Pump Characteristics: Data and Results for an Ingersoll-Rand	
1 CORVNL Open-Impeller Centrifugal Pump Handling Water and	
Water-Clay Suspensions	
A. Water	101
B. Specific Gravity 1.078, 12.1 Weight (5.27 Volume)	
Percent Solids.	102
C. Specific Gravity 1.164, 23.6 Weight (11.1 Volume)	
Percent Solids.	103

LIST OF TABLES (continued)

No.	Page
D. Specific Gravity 1.313, 39.9 Weight (21.2 Volume)	
Percent Solids.	104
E. Specific Gravity 1.396, 47.5 Weight (26.8 Volume)	
Percent Solids.	105

TABLE I

Data and Results for Flow of Water in a 1.60 Inch, a 1.06 Inch and a 0.82 Inch Pipe

Run No.	Pipe I.D.	Pipe Lgth.	W_L	ΔP_{OBS}	Temp.	$\mu_L \times 10^4$	Re_{OBS}	f_{CALC}	ΔP_{CALC}	f_{OBS}	Re_{CALC}	Du^P	$\mu_T \times 10^4$	$D\Delta P/4L$
	In.	Ft.	#/SEC	In.Hg	$^{\circ}C$	$\#M/ft.Sec \times 10^{-4}$	$\times 10^{-4}$		In.Hg		$\times 10^{-4}$	$\#M/ft.Sec$	$\#M/ft.Sec$	$\#F/ft^2$
1	1.60	15.0	9.15	3.15	16.4	7.40	11.8	0.0176	3.00	0.0185	8.90	87.4	9.81	0.493
2	1.60	15.0	11.98	4.74	17.2	7.24	15.8	0.0165	4.82	0.01622	16.5	114.3	6.93	0.743
3	1.60	15.0	7.18	1.85	18.0	7.10	9.66	0.0181	1.90	0.01762	11.0	68.5	6.23	0.290
4	1.60	15.0	4.65	0.83	19.0	7.00	6.35	0.0197	0.868	0.01885	8.10	44.4	5.49	0.130
14	1.60	15.0	11.95	4.62	16.0	7.47	15.3	0.0166	4.83	0.01590	18.4	114.1	6.20	0.723
15	1.60	15.0	4.56	0.78	16.5	7.18	6.06	0.0200	0.846	0.01841	9.15	43.5	4.76	0.122
5	1.06	16.5	9.66	24.2	20.6	6.66	20.9	0.0156	25.7	0.01486	25.7	139.3	5.42	2.28
6	1.06	16.5	8.01	17.82	21.7	6.47	17.9	0.0160	18.10	0.01573	19.3	115.5	5.98	1.68
7	1.06	16.5	5.91	10.37	22.0	6.44	13.3	0.0170	10.48	0.01681	13.8	85.3	6.18	0.976
8	1.06	16.5	3.10	3.21	22.5	6.36	7.05	0.0194	3.28	0.01896	7.85	44.7	5.69	0.302
9	1.06	16.5	1.375	0.70	23.9	6.16	3.22	0.0231	0.769	0.0210	4.89	19.82	4.06	0.066
16	1.06	16.5	1.501	0.90	18.0	7.10	3.06	0.0233	0.925	0.0227	3.48	21.7	6.24	0.085
10	0.82	17.25	1.366	2.71	24.7	6.05	4.11	0.0218	2.70	0.0219	4.08	25.4	6.23	0.189
11	0.82	17.25	2.78	10.02	25.1	5.99	8.64	0.0186	9.57	0.0195	6.85	51.8	7.56	0.700
12	0.82	17.25	3.63	16.10	25.6	5.92	11.4	0.0178	15.60	0.01838	9.20	67.6	7.35	1.122
13	0.82	17.25	4.30	21.9	26.0	5.87	13.6	0.0170	20.9	0.01781	10.5	80.1	7.63	1.527
17	0.82	17.25	1.332	2.70	17.0	7.28	3.41	0.0229	2.70	0.0229	3.35	24.8	7.41	0.188
18	0.82	17.25	2.65	9.42	18.0	7.10	6.95	0.0194	9.06	0.0202	5.80	49.4	8.52	0.656

TABLE II A

Data and Results for Flow of a Water-Clay Suspension of Specific Gravity 1.078 Containing
12.1 Weight Per Cent (5.27 Volume Per Cent) Solids in a 1.60 Inch, a 1.06 Inch and a 0.82 Inch Pipe

Run No.	Pipe I.D.	Pipe Lgth.	W_L	ΔP_{OBS}	Temp.	$\mu_{H_2O} \times 10^4$	$8Q/\pi D^3$	$\Delta P/4L$	Du^{ρ}	f_L	$Re_L \times 10^{-4}$	$\mu_T \times 10^4$	μ_T/μ_{H_2O}
	In.	Ft.	#/Sec	In. Hg.	°C	# _m /Ft.-Sec	1/Sec	# _F /Ft. ²	# _m /Ft.-Sec			# _m /Ft.-Sec	
57	1.60	15.0	12.25	4.62	22.8	6.32	195.9	0.724	117.0	0.01629	16.0	7.32	1.16
58	1.60	15.0	15.79	7.42	23.4	6.23	252	1.164	150.8	0.01580	18.5	8.15	1.31
59	1.60	15.0	9.27	2.80	24.2	6.12	148.2	0.439	88.5	0.01722	12.5	7.08	1.16
60	1.60	15.0	7.36	1.75	24.8	6.03	117.8	0.274	70.3	0.01708	12.8	5.49	0.910
61	1.60	15.0	4.83	0.80	25.0	6.01	77.2	0.1255	46.1	0.01817	9.8	4.71	0.783
71	1.60	15.0	4.77	0.79	23.2	6.26	76.3	0.1240	45.6	0.01835	9.1	5.01	0.800
74	1.60	15.0	4.52	0.79	25.0	6.01	72.3	0.1240	43.2	0.0204	5.55	7.78	1.29
78	1.60	15.0	8.15	2.01	26.1	5.86	130.3	0.315	77.8	0.01600	17.6	4.42	0.755
82	1.60	15.0	13.70	5.61	27.2	5.72	219	0.880	130.9	0.01581	18.6	7.04	1.23
62	1.06	16.5	1.582	0.91	25.4	5.95	87.2	0.0857	22.8	0.0222	3.8	6.00	1.01
63	1.06	16.5	3.35	3.57	25.7	5.91	184.7	0.336	48.3	0.01942	7.0	6.90	1.17
64	1.06	16.5	5.68	9.18	25.9	5.88	313	0.865	82.0	0.01737	11.9	6.90	1.17
65	1.06	16.5	7.97	17.01	26.3	5.83	439	1.602	115.1	0.01633	16.0	7.19	1.23
66	1.06	16.5	9.56	22.98	26.5	5.80	527	2.165	138.0	0.01533	22.0	6.27	1.08
86	1.06	16.5	1.727	1.04	28.3	5.58	95.1	0.0981	24.9	0.0213	4.55	5.47	0.981
90	1.06	16.5	4.08	5.07	29.1	5.48	225	0.478	58.9	0.01857	8.7	6.77	1.23
94	1.06	16.5	6.31	10.77	29.9	5.39	348	1.014	91.1	0.01648	15.3	5.95	1.10
67	0.82	17.25	1.416	2.85	26.9	5.75	168.3	0.1986	26.4	0.0230	3.3	8.00	1.39
68	0.82	17.25	2.81	9.64	27.2	5.72	334	0.671	52.4	0.01977	6.4	8.18	1.43
69	0.82	17.25	3.75	15.95	27.3	5.70	446	1.112	69.9	0.01837	9.15	7.64	1.34
70	0.82	17.25	4.62	22.98	27.4	5.69	550	1.602	86.2	0.01740	11.7	7.37	1.30
98	0.82	17.25	1.525	3.16	30.6	5.31	181.5	0.220	28.4	0.0220	4.0	7.10	1.34
102	0.82	17.25	2.61	8.20	31.1	5.26	311	0.571	48.6	0.01946	7.0	6.95	1.32
106	0.82	17.25	3.53	14.03	31.4	5.22	420	0.978	65.8	0.01822	9.7	6.79	1.30

TABLE II B

Data and Results for Flow of a Water-Clay Suspension of Specific Gravity 1.164 Containing
23.6 Weight Per Cent (11.1 Volume Per Cent) Solids in a 1.60 Inch, a 1.06 Inch and a 0.82 Inch Pipe

Run No.	Pipe I.D.	Pipe Lgth.	W_L	ΔP_{OBS}	Temp.	$\mu_{H_2O} \times 10^4$	$8Q/\pi D^3$	$\Delta P/4L$	Du^0	f_L	$Re_L \times 10^{-4}$	$\mu_T \times 10^4$	μ_T/μ_{H_2O}
	In.	Ft.	#/Sec	In. Hg.	°C	# _m /Ft. Sec	1/Sec	# _F /Ft ²	# _m /Ft-Sec			# _m /Ft-Sec	
110	1.60	15.0	5.50	0.97	26.5	5.81	81.4	0.1522	52.5	0.01837	9.2	5.70	0.981
114	1.60	15.0	8.12	1.99	28.5	5.56	120.2	0.312	77.5	0.01725	12.2	6.35	1.14
118	1.60	15.0	14.10	5.72	29.1	5.48	209	0.897	134.8	0.01650	15.1	8.92	1.63
123	1.06	16.5	3.23	3.20	30.2	5.36	164.9	0.302	46.6	0.0202	5.8	8.03	1.50
127	1.06	16.5	4.94	7.04	30.6	5.31	252	0.663	71.3	0.0190	7.75	9.20	1.73
131	1.06	16.5	7.38	14.22	30.6	5.31	376	1.340	106.5	0.01722	12.4	8.59	1.62
135	0.82	17.25	1.268	2.15	31.1	5.26	139.7	0.150	23.6	0.0234	3.07	7.69	1.46
139	0.82	17.25	2.19	5.95	31.0	5.27	241	0.415	40.8	0.0217	4.25	9.60	1.82
143	0.82	17.25	3.31	12.46	31.3	5.23	365	0.869	61.7	0.01987	6.3	9.80	1.87

TABLE II C

Data and Results for Flow of a Water-Clay Suspension of Specific Gravity 1.313 Containing
39.9 Weight Per Cent (21.2 Volume Per Cent) Solids in a 1.60 Inch, a 1.06 Inch and a 0.82 Inch Pipe

Run No.	Pipe I.D. In.	Pipe Lgth. Ft.	W_L #/Sec	ΔP_{OBS} In.Hg.	Temp. °C	$\mu_{H_2O} \times 10^4$ #/Ft.Sec	$8Q/\pi D^3$ 1/Sec	$D\Delta P/4L$ #/Ft ²	Du^{ρ} #/Ft-Sec	f_L	$Re_L \times 10^{-4}$	$\mu_T \times 10^4$ #/Ft-Sec	μ_T/μ_{H_2O}
147	1.60	15.0	0.978	1.10	28.3		12.83	0.1725	9.34	0.0742			
151	1.60	15.0	0.848	1.00	28.6		11.12	0.1568	8.10	0.0897			
152	1.60	15.0	10.48	3.05	28.8	5.52	137.5	0.478	100.0	0.01792	10.3	9.71	1.76
156	1.60	15.0	10.63	3.03	29.6	5.42	139.7	0.475	101.6	0.01730	12.0	8.47	1.56
157	1.60	15.0	13.85	5.21	29.7	5.41	181.8	0.817	132.2	0.01753	11.4	11.60	2.14
161	1.60	15.0	13.83	5.20	30.4	5.33	181.4	0.815	132.0	0.01753	11.4	11.58	2.17
162	1.06	16.5	0.580	2.10	31.3		26.2	0.198	8.37	0.0465			
166	1.06	16.5	0.367	1.90	31.5		16.6	0.179	5.30	0.1047			
167	1.06	16.5	4.47	5.41	31.7	5.19	202	0.510	64.5	0.0202	5.8	11.11	2.14
171	1.06	16.5	4.33	5.20	32.3	5.13	196	0.490	62.5	0.0206	5.3	11.80	2.30
172	1.06	16.5	6.22	10.28	32.4	5.12	282	0.969	89.9	0.01968	6.7	13.41	2.62
176	1.06	16.5	5.89	9.20	32.9	5.06	266	0.867	85.0	0.01976	6.5	13.09	2.58
177	0.82	17.25	0.252	2.77	33.0		24.6	0.193	4.70	0.0860			
181	0.82	17.25	0.1431	2.58	34.0		13.98	0.180	2.67	0.248			
182	0.82	17.25	2.42	6.65	34.0	4.95	236	0.463	45.1	0.0224	3.7	12.20	2.46
186	0.82	17.25	2.01	4.52	34.0	4.95	196.1	0.315	37.5	0.0221	3.9	9.62	1.94
187	0.82	17.25	3.18	10.80	34.0	4.95	310	0.753	59.3	0.0211	4.8	12.35	2.50
191	0.82	17.25	3.09	10.38	34.0	4.95	302	0.724	57.6	0.0214	4.5	12.80	2.58

TABLE II D

Data and Results for Flow of a Water-Clay Suspension of Specific Gravity 1.396 Containing
47.5 Weight Per Cent (26.8 Volume Per Cent) Solids in a 1.60 Inch, a 1.06 Inch and a 0.82 Inch Pipe

Run No.	Pipe I.D. In.	Pipe Lgth. Ft.	W_L #/Sec	ΔP_{OBS} In. Hg.	Temp. °C	$\rho_{H_2O} \times 10^4$ #/Ft-Sec.	$8Q/\pi D^3$ 1/Sec	$\Delta P/4L$ #/Ft ²	Du_0 #/Ft-Sec	f_L	$Re_L \times 10^{-4}$	$\mu_T \times 10^4$ #/Ft-Sec	μ_T, μ_{H_2O}
192	1.60	15.0	0.927	2.95	25.0		11.43	0.462	8.85	0.235			
196	1.60	15.0	0.482	2.60	27.5		5.94	0.408	4.60	0.769			
197	1.60	15.0	13.17	5.00	27.5	5.68	162.2	0.784	125.8	0.0198	6.35	19.80	3.48
201	1.60	15.0	13.20	5.02	30.0	5.38	162.8	0.787	126.0	0.0198	6.35	19.83	3.68
202	1.60	15.0	15.71	6.51	30.0	5.38	193.9	1.022	150.0	0.01812	9.8	15.30	2.84
206	1.60	15.0	15.60	6.51	30.0	5.38	191.1	1.022	149.0	0.01851	8.9	16.73	3.11
207	1.06	16.5	0.732	5.32	31.0		31.1	0.501	10.58	0.785			
211	1.06	16.5	0.595	5.07	31.5		25.3	0.478	8.59	1.133			
212	1.06	16.5	5.13	7.65	31.5	5.21	218	0.720	74.1	0.0229	3.35	22.1	4.24
216	1.06	16.5	4.98	7.31	31.5	5.21	212	0.689	71.9	0.0233	3.1	23.2	4.45
217	1.06	16.5	6.21	10.26	31.5	5.21	264	0.966	89.7	0.0210	4.9	18.30	3.51
221	1.06	16.5	6.09	9.90	31.5	5.21	259	0.933	87.9	0.0211	4.8	18.30	3.51
222	0.82	17.25	0.390	6.65	31.5		35.8	0.463	7.27	0.916			
226	0.82	17.25	0.154	5.90	32.0		14.13	0.411	2.87	5.15			
227	0.82	17.25	2.98	10.38	32.0	5.16	273	0.724	55.5	0.0246	2.45	22.6	4.38
231	0.82	17.25	2.84	10.02	32.0	5.16	261	0.699	53.0	0.0260	1.95	27.2	5.27
232	0.82	17.25	3.99	16.63	32.0	5.16	366	1.160	74.4	0.0220	4.0	18.60	3.60
235	0.82	17.25	3.96	16.17	32.0	5.16	363	1.127	73.9	0.0216	4.3	17.20	3.33

TABLE III A

Data and Results of Flow Properties in a Brookfield Viscometer of a Water-Clay Suspension of Specific Gravity 1.078 Containing 12.1 Weight Per Cent (5.27 Volume Per Cent) Solids.

$$\left(\frac{\text{Inner Cylinder Radius}}{\text{External Cylinder Radius}} \right)^2 = \left(\frac{R_i}{R_E} \right)^2 = \left(\frac{0.742/2}{3.25/2} \right)^2 = 0.0521$$

Angular Velocity of Inner Cylinder (ω) radians/second	Brookfield Viscosity (μ_B) Centipoises	Shearing Stress at Inner Cylinder Wall (W) $\#_F/Pt^2$	Temperature $^{\circ}C$
$\pi/5$	69.5	0.00192	26.0
$2\pi/5$	40.8	0.00226	
π	21.0	0.00290	
2π	12.6	0.00348	25.9

TABLE III B

Data and Results of Flow Properties in a Brookfield Viscometer of a Water-Clay Suspension of Specific Gravity 1.164 Containing 23.6 Weight Per Cent (11.1 Volume Per Cent) Solids.

$$\left(\frac{\text{Inner Cylinder Radius}}{\text{External Cylinder Radius}} \right)^2 = \left(\frac{R_i}{R_e} \right)^2 = \left(\frac{0.742/2}{3.25/2} \right)^2 = 0.0521$$

Angular Velocity of Inner Cylinder (ω_i) radians /second	Brookfield Viscosity (μ_B) Centipoises	Shearing Stress at Inner Cylinder Wall (W) $\frac{F}{Ft^2}$	Temperature $^{\circ}C$
$\pi/5$	520	0.01433	26.9
$2\pi/5$	287	0.01588	
π	133.1	0.0184	
2π	73.1	0.2024	26.6

TABLE III C

Data and Results of Flow Properties in a Brookfield Viscometer of a Water-Clay Suspension of Specific Gravity 1.313 Containing 39.9 Weight Per Cent (21.2 Volume Per Cent) Solids.

$$\left(\frac{\text{Inner Cylinder Radius}}{\text{External Cylinder Radius}} \right)^2 = \left(\frac{R_i}{R_e} \right)^2 = \left(\frac{0.1254/2}{3.25/2} \right)^2 = 0.00149$$

Angular Velocity of Inner Cylinder (ω_i) radians / second	Brookfield Viscosity (μ_B) Centipoises	Shearing Stress at Inner Cylinder Wall (τ) $\#_f / Ft^2$	Temperature $^{\circ}C$
$\pi/5$	500	0.0131	2.67
$2\pi/5$	400	0.0210	
π	1100	0.144	
2π	580	0.152	27.0

TABLE III D

Data and Results of Flow Properties in a Brookfield Viscometer of a Water-Clay Suspension of Specific Gravity 1.396 Containing 47.5 Weight Per Cent (26.8 Volume Per Cent) Solids

$$\left(\frac{\text{Inner Cylinder Radius}}{\text{External Cylinder Radius}} \right)^2 = \left(\frac{R_i}{R_E} \right)^2 = \left(\frac{0.1254/2}{3.25/2} \right)^2 = 0.00149$$

Angular Velocity of Inner Cylinder (ω) radians/second	Brookfield Viscosity (μ_B) Centipoises	Shearing Stress at Inner Cylinder Wall (τ) $\frac{F}{A}$ /ft ²	Temperature °C
$\pi/5$	1500	0.0393	27.0
$2\pi/5$	900	0.0472	
π	1120	0.147	
2π	1195	0.314	27.5

TABLE IV A

Data and Results of Flow Properties in a Capillary Tube Viscometer of a Water-Clay Suspension
of Specific Gravity 1.078 Containing 12.1 Weight Per Cent (5.27 Volume Per Cent) Solids

Tube Diameter = 0.1339 cm.

Tube Length = 64.37 cm.

Temperature = 30.0° C

Measured Pressure Drop gm_F/cm^2	Volume Collected cm^3	Time Seconds	Average Velocity cm/sec	Kinetic Energy and Contraction Loss gm_F/cm^2	Frictional Pressure Drop gm_F/cm^2	$\frac{\Delta P_F}{4L}$ $\frac{\text{#}_F/\text{Ft}^2}{\text{#}_F/\text{Ft}^2}$	$\frac{8Q}{\pi D^3}$ l/sec
73.5	53.58	76.6	49.69	3.04	70.46	0.0751	742
39.1	53.58	145.0	26.24	0.848	38.3	0.0408	392
123.4	53.58	43.8	86.92	9.31	114.1	0.1215	1299
168.6	53.58	32.2	118.1	17.18	151.4	0.1612	1764

TABLE IV B

Data and Results of Flow Properties in a Capillary Tube Viscometer of a Water-Clay Suspension
of Specific Gravity 1.164 Containing 23.6 Weight Per Cent (11.1 Volume Per Cent) Solids

Tube Diameter = 0.1339 cm.

Tube Length = 64.37 cm.

Temperature = 30.0° C

Measured Pressure Drop $\frac{gm_F}{cm^2}$	Volume Collected cm^3	Time Seconds	Average Velocity cm/sec	Kinetic Energy and Contraction Loss $\frac{gm_F}{cm^2}$	Frictional Pressure Drop $\frac{gm_F}{cm^2}$	$\frac{\Delta P_F}{4L}$ $\frac{\#_F}{Ft^2}$	$\frac{8Q}{\pi D^3}$ 1/sec
79.5	53.58	171.8	22.16	0.65	78.8	0.0839	331
158.6	53.58	61.0	62.37	5.17	153.4	0.163	932
231.6	53.58	37.6	101.2	13.62	218.0	0.232	1512
306	53.58	27.8	136.8	24.89	281.1	0.299	2043

TABLE IV C

Data and Results of Flow Properties in a Capillary Tube Viscometer of a Water-Clay Suspension
of Specific Gravity 1.313 Containing 39.9 Weight Per Cent (21.2 Volume Per Cent) Solids

Tube Diameter = 0.1339 cm.

Tube Length = 64.37 cm.

Temperature = 30.0 °C.

Measured Pressure Drop $\frac{\text{gm}_F}{\text{cm}^2}$	Volume Collected cm^3	Time Seconds	Average Velocity cm/sec	Kinetic Energy & Contraction Loss $\frac{\text{gm}_F}{\text{cm}^2}$	Frictional Pressure Drop $\frac{\text{gm}_F}{\text{cm}^2}$	$\frac{DAF_F}{4L}$ $\frac{\#_F}{\text{ft}^2}$	$\frac{8Q}{\pi D^3}$ 1/Sec	Slippage 1/Sec	$\frac{8Q\phi}{\pi D^3}$ 1/Sec
89.7	53.58	2762	1.378	0.0029	89.7	0.0955	20.6		
172.5	53.58	415.6	9.151	0.126	172.4	0.184	136.7	40	96.7
276.3	53.58	137.4	27.68	1.15	275.1	0.293	414	67	347
385.4	53.58	69.4	54.81	4.51	380.9	0.406	819	86	733
500	53.58	44.0	86.59	11.25	488.8	0.521	1294	111	1183

TABLE IV D

Data and Results of Flow Properties in a Capillary Tube Viscometer of a Water-Clay Suspension
of Specific Gravity 1.396 Containing 47.5 Weight Per Cent (26.8 Volume Per Cent) Solids

Tube Diameter = 0.1339 cm.
Tube Length = 64.37 cm.
Temperature = 30.0 °C.

Measured Pressure Drop $\frac{\text{gm}_F}{\text{cm}^2}$	Volume Collected cm^3	Time Seconds	Average Velocity cm/sec	Kinetic Energy & Contraction Loss $\frac{\text{gm}_F}{\text{cm}^2}$	Frictional Pressure Drop $\frac{\text{gm}_F}{\text{cm}^2}$	$\frac{D\Delta P_F}{4L}$ $\frac{\#_F}{\text{ft}^2}$	$8Q/\pi D^3$ 1/Sec	Slippage 1/Sec	$\frac{8Q_0}{\eta \eta^3}$ 1/Sec
234.6	53.58	2338	1.627	0.0041	234.6	0.250	24.3		
337.4	27.33	1160	1.671	0.0045	337.4	0.359	25.0		
560	27.33	130.6	14.86	0.352	559.6	0.596	222	51	171
773	27.33	55.6	34.93	1.95	771	0.821	522	70	452
244	27.33	1059	1.832	0.0054	244	0.260	27.4		
374	27.33	343	5.658	0.051	374	0.398	84.5	34	50.5
919	27.33	32.8	59.04	5.56	913.4	0.974	885	82	803
<p>Tube Diameter = 0.1074 cm. Tube Length = 64.16 cm. Temperature = 30.4 °C.</p>									
856	27.33	151.0	19.99	0.637	855.4	0.733	372	62	310
663	27.33	306.0	9.86	0.155	662.8	0.568	183.6	48	135.6

TABLE V A

Data and Results for Co-Current Flow of Air and Water in a 1.60 Inch Pipe 15.0 Feet Long

Run No.		24	25	26	27	28	29	30	31	32	33	34
W_L	#/Sec	11.55	11.26	10.91	12.00	8.53	8.51	8.30	8.11	4.53	4.49	4.46
W_G	#/Sec	0	0.00516	0.01169	0.01567	0	0.00382	0.00865	0.01641	0	0.001755	0.01636
ΔP_{OBS}	In. Hg.	4.68	5.94	6.91	8.50	2.65	3.64	4.24	4.91	0.80	1.04	1.78
T_{AVG}	$^{\circ}C$	12.8	14.3	14.9	15.3	16.3	17.0	17.3	18.0	18.4	19.0	19.7
P_{AVG}	PSIA	22.3	25.5	28.1	33.0	18.7	20.9	23.0	25.3	15.7	16.3	19.2
$Re_{LP} \times 10^{-4}$		13.7	13.8	13.6	15.1	11.0	11.2	11.0	10.9	6.15	6.22	6.25
$f_{LP\text{ CALC}}$		0.0171	0.0170	0.0171	0.0167	0.0178	0.0178	0.0178	0.0178	0.0199	0.0199	0.0198
$f_{LP\text{ OBS}}$		0.0172				0.01772				0.0191		
ΔP_{LP}	In. Hg.	4.65	4.39	4.15	4.90	2.64	2.63	2.50	2.39	0.833	0.817	0.802
$Re_{GP} \times 10^{-3}$			4.14	9.33	12.6		3.03	6.86	13.0		1.39	12.8
f_{GP}			0.0396	0.0312	0.0289		0.0439	0.0340	0.0287		0.0560	0.0288
ΔP_{GP}	In. Hg.		0.001004	0.00369	0.00524		0.000750	0.00271	0.00751		0.000261	0.00993
X^2			4370	1125	935		3510	922	318		3130	808
$E^2_{LTT\text{ OBS}}$			1.353	1.667	1.735		1.383	1.697	2.05		1.272	2.22
$E^2_{LTT\text{ MART}}$			1.39	1.78	1.84		1.44	1.85	2.30		1.47	1.89
$R_G\text{ MART}$			0.168	0.265	0.277		0.184	0.279	0.360		0.193	0.288
$\Delta P_{TP\text{ MART}}$	In. Hg.		6.10	7.39	9.01		3.79	4.62	5.50		1.20	1.52
DEVIATION	%	+0.645	-2.62	-6.50	-5.66	+0.41	-3.96	-8.23	-10.7	-3.96	-13.3	+17.1

TABLE V B

Data and Results for Co-Current Flow of Air and Water in a 1.06 Inch Pipe 16.5 Feet Long

Run No.		35	36	37	38	39	40	41	42	43	44	45
W_L	#/Sec	2.24	2.21	2.14	2.11	6.14	5.81	5.45	5.16	7.36	6.26	6.00
W_G	#/Sec	0	0.00319	0.00968	0.01671	0	0.006575	0.00980	0.01659	0	0.00839	0.01355
ΔP_{OBS}	In. Hg.	1.70	3.53	5.68	6.65	11.02	15.02	16.82	18.82	14.43	18.43	20.40
T_{AVG}	$^{\circ}C$	20.0	20.7	20.9	21.0	21.3	21.7	22.3	22.6	22.9	23.0	23.2
P_{AVG}	PSIA	16.0	17.8	20.2	22.3	24.6	31.3	33.5	36.8	29.2	36.5	39.0
$Re_{LP} \times 10^{-4}$		4.79	4.80	4.67	4.63	13.5	13.0	12.3	11.7	16.9	14.4	13.8
f_{LP}^{CALC}		0.0212	0.0212	0.0213	0.0213	0.0170	0.0171	0.0174	0.0176	0.0163	0.0168	0.0169
f_{LP}^{OBS}		0.0192				0.01658				0.01512		
ΔP_{LP}	In. Hg.	1.875	1.825	1.720	1.672	11.30	10.18	9.12	8.27	15.57	11.61	10.72
$Re_{GP} \times 10^{-3}$			3.79	11.5	19.9		7.77	11.6	19.6		9.86	15.9
f_{GP}			0.0409	0.0295	0.0259		0.0329	0.0295	0.0260		0.0308	0.0273
ΔP_{GP}	In. Hg.		0.00503	0.0294	0.0699		0.00981	0.01842	0.0420		0.01288	0.0279
X^2			363	58.5	24.0		1037	495	197		902	384
$\bar{h}^2_{LTT OBS}$			1.933	3.30	3.97		1.478	1.844	2.28		1.588	1.902
$\bar{h}^2_{LTT MART}$			2.23	3.62	4.89		1.81	2.09	2.56		1.85	2.21
R_G MART			0.350	0.508	0.570		0.271	0.324	0.403		0.280	0.345
$\Delta P_{TP MART}$	In. Hg.		4.07	6.22	8.18		18.40	19.10	21.2		21.50	23.70
DEVIATION	%	-9.34	-13.3	-8.67	-18.7	-2.48	-18.4	-11.9	-11.2	-7.33	-14.3	-13.9

TABLE V C

Data and Results for Co-Current Flow of Air and Water in a 0.82 Inch Pipe 17.25 Feet Long

Run No.		46	47	48	49	50	51	52	53	54	55	56
W_L	#/Sec	1.191	1.170	1.137	1.086	2.60	2.395	2.21	2.12	3.535	3.05	2.90
W_G	#/Sec	0	0.00321	0.00654	0.01269	0	0.00558	0.01138	0.01468	0	0.00688	0.00983
ΔP_{OBS}	In. Hg.	2.30	5.70	7.22	10.57	9.03	17.21	19.40	20.80	15.00	23.58	24.78
T_{AVG}	$^{\circ}C$	12.5	13.6	14.0	14.8	16.1	17.2	18.0	18.8	19.0	19.5	20.0
P_{AVG}	PSIA	16.1	18.5	20.2	22.5	20.2	27.7	31.7	33.5	25.0	34.1	35.8
$Re_{LP} \times 10^{-4}$		2.70	2.74	2.69	2.62	6.50	6.16	5.79	5.67	9.50	8.30	7.98
$f_{LP} \text{ CALC}$		0.0240	0.0240	0.0240	0.0241	0.0198	0.0200	0.0203	0.0204	0.0182	0.0187	0.0189
$f_{LP} \text{ OBS}$		0.0244				0.0201				0.01808		
ΔP_{LP}	In. Hg.	2.26	2.18	2.06	1.89	8.89	7.63	6.60	6.10	15.1	11.6	10.6
$Re_{GP} \times 10^{-3}$			5.02	10.2	19.7		8.64	17.6	22.6		10.6	15.0
f_{GP}			0.0372	0.0302	0.0260		0.0318	0.0266	0.0250		0.0300	0.0277
ΔP_{GP}	In. Hg.		0.0164	0.0506	0.1479		0.0286	0.0871	0.1298		0.0336	0.0604
X^2			133	40.7	12.8		267	75.8	47.1		344	175
$E^2_{LTT} \text{ OBS}$			2.61	3.51	5.59		2.26	2.94	3.41		2.04	2.34
$E^2_{LTT} \text{ MART}$			2.83	4.09	6.13		2.39	3.33	3.88		2.26	2.64
$R_G \text{ MART}$			0.441	0.533	0.616		0.377	0.489	0.522		0.355	0.415
$\Delta P_{TP} \text{ MART}$	In. Hg.		6.17	8.43	11.60		18.23	22.0	23.7		26.1	27.9
DEVIATION	%	+1.77	-7.62	-14.4	-8.88	+1.46	-5.60	-11.8	-12.2	-0.73	-9.65	-11.2

TABLE VI A1

Data and Results for Co-Current Flow of Air and a Water-Clay Suspension of Specific Gravity 1.078
Containing 12.1 Weight Per Cent (5.27 Volume Per Cent) Solids in a 1.60 Inch Pipe 15.0 Feet Long

Run No.		71	72	74	75	76	77	78	79	80	82	83	84	85
W_L	#/Sec	4.77	4.51	4.52	4.47	4.43	4.34	8.15	8.03	7.91	13.70	13.11	12.71	12.36
W_G	#/Sec	0	0.001741	0	0.001606	0.00421	0.01975	0	0.00412	0.01155	0	0.00836	0.01603	0.0231
ΔP_{OBS}	In. Hg.	0.79	1.01	0.79	0.97	1.41	2.20	2.01	3.08	3.75	5.61	7.41	8.45	9.00
T_{AVG}	$^{\circ}C$	23.2	24.0	25.0	25.1	25.6	26.0	26.1	26.7	27.0	27.2	27.7	28.0	28.0
P_{AVG}	PSIA	15.7	16.5	15.7	16.2	16.5	19.5	17.9	20.3	22.3	24.4	29.6	32.8	34.9
$8Q/\pi D^3$	1/Sec	76.3	72.1	72.3	71.5	70.8	69.4	130.3	128.4	126.7	219	210	203	197.5
$\Delta P_{LP}/4L$	#/ft ²	0.1240	0.114	0.1240	0.112	0.110	0.108	0.315	0.330	0.320	0.880	0.820	0.768	0.729
ΔP_{LP}	In. Hg.		0.727		0.715	0.702	0.689		2.10	2.04		5.13	4.90	4.65
$Re_{GP} \times 10^{-3}$			1.36		1.25	3.29	15.4		3.22	9.01		6.52	12.5	18.0
f_{GP}			0.0567		0.0580	0.0425	0.0276		0.0430	0.0315		0.0345	0.0289	0.0264
ΔP_{GP}	In. Hg.		0.000262		0.000233	0.001153	0.01395		0.000911	0.00477		0.00207	0.00576	0.01030
X^2			2780		3070	609	49.4		2300	427		2480	850	452
$\bar{h}^2_{LTT OBS}$			1.39		1.356	2.01	3.19		1.467	1.84		1.445	1.725	1.935
$\bar{h}^2_{LTT MART}$			1.50		1.47	2.01	3.81		1.56	2.16		1.53	1.88	2.13
R_G MART			0.201		0.193	0.308	0.519		0.215	0.337		0.209	0.285	0.331
$\Delta P_{TP MART}$	In. Hg.		1.09		1.05	1.41	2.62		3.28	4.40		7.85	9.21	9.91
DEVIATION	%		-7.34		-7.62	0	-16.0		-6.10	-14.8		-5.60	-8.25	-9.19

TABLE VI A2

Data and Results for Co-Current Flow of Air and a Water-Clay Suspension of Specific Gravity 1.078
Containing 12.1 Weight Per Cent (5.27 Volume Per Cent) Solids in a 1.06 Inch Pipe 16.5 Feet Long

Run No.		86	87	88	89	90	91	92	93	94	95	96	97
W_L	#/Sec	2.727	1.687	1.625	1.602	4.08	4.00	3.86	3.68	6.31	5.85	5.50	5.19
W_G	#/Sec	0	0.00157	0.0188	0.0232	0	0.00332	0.0105	0.0223	0	0.00577	0.01215	0.01853
ΔP_{OBS}	In.Hg.	1.04	1.91	5.90	7.24	5.07	8.41	11.91	14.43	10.77	15.02	18.43	19.90
T_{AVG}	$^{\circ}C$	28.3	28.9	29.0	29.1	29.1	29.5	29.6	29.7	29.9	30.0	30.2	30.2
P_{AVG}	PSIA	15.4	16.5	20.9	21.8	18.7	22.4	27.0	32.2	23.9	31.0	35.4	37.8
$8Q/\pi D^3$	1/Sec	95.1	93.0	89.6	88.4	225	220	213	203	348	322	303	286
$\Delta P_{IP}/4L$	#/Ft ²	0.0981	0.97	0.90	0.88	0.478	0.455	0.43	0.395	1.014	0.91	0.82	.735
ΔP_{IP}	In.Hg.		0.971	0.955	0.934		4.83	4.56	4.19		9.66	8.70	7.80
$Re_{GP} \times 10^{-3}$			1.84	22.1	27.2		3.90	12.3	26.2		6.77	14.3	21.8
f_{GP}			0.0507	0.0251	0.0240		0.0402	0.0290	0.0242		0.0340	0.0279	0.0253
ΔP_{GP}	In.Hg.		0.001877	0.0938	0.1311		0.00438	0.0262	0.0829		0.00810	0.0258	0.0510
K^2			580	10.18	7.12		1102	174	50.5		1193	337	153
$B^2_{LTT OBS}$			1.968	6.18	7.75		1.741	2.61	3.45		1.554	2.12	2.55
$B^2_{LTT MART}$			2.03	6.70	7.65		1.78	2.64	3.79		1.76	2.27	2.73
$R_G MART$			0.311	0.634	0.658		0.266	0.417	0.518		0.260	0.357	0.429
$\Delta P_{TP MART}$	In.Hg.		1.97	6.40	7.14		8.60	12.03	15.90		17.0	19.75	21.3
DEVIATION	%		-3.05	-7.81	-1.40		-2.21	-1.0	-9.25		-11.6	-6.68	-6.57

TABLE VI A3

Data and Results for Co-Current Flow of Air and a Water-Clay Suspension of Specific Gravity 1.078
Containing 12.1 Weight Per Cent (5.27 Volume Per Cent) Solids in a 0.82 Inch Pipe 17.25 Feet Long

Run No.		98	99	100	101	102	103	104	105	106	107	108	109
W_L	#/Sec	1.525	1.459	1.345	1.197	2.61	2.55	2.36	2.09	3.53	3.41	2.96	2.74
W_G	#/Sec	0	0.00175	0.01118	0.02338	0	0.00197	0.00869	0.01919	0	0.00236	0.01012	0.01527
ΔP_{OBS}	In. Hg.	3.16	5.80	13.04	17.82	8.20	12.35	18.42	22.38	14.03	18.33	25.33	26.74
T_{AVG}	$^{\circ}C$	30.6	31.0	31.0	31.0	31.1	31.2	31.3	31.3	31.4	31.8	31.8	31.8
P_{AVG}	PSIA	16.7	18.7	24.7	29.0	19.7	23.5	30.1	35.2	23.9	28.6	36.4	38.8
$8Q/\pi D^3$	1/Sec	181.5	173.5	160	142.4	311	304	281	249	420	406	352	326
$\Delta P_{LP}/4L$	$\#_F/Ft^2$	0.220	0.212	0.187	0.155	0.571	0.555	0.481	0.390	0.978	0.940	0.724	0.630
ΔP_{LP}	In. Hg.		3.04	2.68	2.22		7.96	6.90	5.60		13.49	10.39	9.04
$Re_{GP} \times 10^{-3}$			2.64	16.9	36.0		2.98	13.1	29.0		3.57	15.3	23.1
f_{GP}			0.046	0.0270	0.0226		0.0440	0.0288	0.0237		0.0416	0.0277	0.0248
ΔP_{GP}	In. Hg.		0.00632	0.1146	0.356		0.00610	0.0605	0.209		0.00681	0.0656	0.1253
X^2			481	23.4	6.23		1305	114	26.8		1980	158.2	72.0
$\bar{h}^2_{LTT OBS}$			1.91	4.87	8.03		1.551	2.67	4.00		1.36	2.44	2.96
$\bar{h}^2_{LTT MART}$			2.10	4.92	8.03		1.73	2.94	4.69		1.59	2.70	3.39
$R_G MART$			0.326	0.572	0.662		0.255	0.457	0.562		0.225	0.425	0.492
$\Delta P_{TP MART}$	IN. Hg.		6.38	13.20	17.82		13.78	20.3	26.3		21.4	28.0	30.6
DEVIATION	%		-9.10	-1.21	0		-10.4	-9.26	-14.9		-14.3	-9.54	-12.6

TABLE VI B1

Data and Results for Co-Current Flow of Air and a Water-Clay Suspension of Specific Gravity 1.164
Containing 23.6 Weight Per Cent (11.1 Volume Per Cent) Solids in a 1.60 Inch Pipe 15.0 Feet Long

Run No.		110	111	112	113	114	115	116	117	118	119	120	121	122
W_L	#/Sec	5.50	5.72	5.44	5.24	8.12	8.05	7.99	7.71	14.10	13.76	13.11	13.22	5.04
W_G	#/Sec	0	0.00153	0.00434	0.0263	0	0.00202	0.00462	0.0257	0	0.00315	0.0115	0.0231	0.00455
ΔP_{OBS}	In. Hg.	0.97	1.24	1.80	3.37	1.99	2.57	3.30	4.74	5.72	6.53	8.04	8.60	1.80
T_{AVG}	$^{\circ}C$	26.5	26.6	28.0	28.0	28.5	29.0	29.0	28.8	29.1	29.4	29.9	29.8	30.2
P_{AVG}	PSIA	16.1	16.8	17.4	21.3	17.9	19.0	20.3	25.8	23.9	27.2	31.2	34.8	17.4
$8Q/\pi D^3$	1/Sec	81.4	80.3	80.5	77.5	120.2	119.2	118.3	114.2	209	204	194	195.8	74.5
$\Delta P_{LP}/4L$	$\#_2/\text{Ft}^2$	0.1522	0.1520	0.152	0.1443	0.312	0.310	0.307	0.287	0.397	0.860	0.775	0.787	0.132
ΔP_{LP}	In. Hg.		0.970	0.970	0.921		1.98	1.96	1.83		5.48	4.94	5.02	0.842
$Re_{GP} \times 10^{-3}$			1.19	3.38	20.5		1.57	3.59	20.0		2.45	8.95	13.0	3.54
f_{GP}			0.0595	0.0422	0.0257		0.0535	0.0413	0.0258		0.0470	0.0317	0.0265	0.0417
ΔP_{GP}	In. Hg.		0.000209	0.001162	0.0213		0.000293	0.001109	0.01686		0.000438	0.00344	0.01040	0.001270
X^2_{GP}			4640	834	43.2		6750	1768	108.5		12,500	1437	483	663
$E^2_{LTT OBS}$			1.279	1.856	3.66		1.30	1.684	2.59		1.192	1.628	1.712	2.14
$E^2_{LTT MART}$			1.38	1.88	3.99		1.30	1.63	2.97		1.18	1.69	2.10	1.97
$R_G \text{ MART}$			0.164	0.286	0.529		0.134	0.233	0.462		0.080	0.248	0.326	0.302
$\Delta P_{TP \text{ MART}}$	In. Hg.		1.34	1.82	3.67		2.57	3.20	5.44		6.47	8.35	10.54	1.66
DEVIATION	%		-7.47	-1.10	-8.13		0	+3.13	-12.9		+0.62	-3.71	-18.4	+8.44

TABLE VI B2

Data and Results for Co-Current Flow of Air and a Water-Clay Suspension of Specific Gravity 1.164
Containing 23.6 Weight Per Cent (11.1 Volume Per Cent) Solids in a 1.06 Inch Pipe 16.5 Feet Long

Run No.		123	124	125	126	127	128	129	130	131	132	133	134
W_L	#/Sec	3.23	3.19	3.05	2.97	4.94	4.89	4.67	4.51	7.38	6.96	6.61	6.14
W_G	#/Sec	0	0.00221	0.01396	0.0240	0	0.00256	0.01213	0.0200	0	0.00416	0.00852	0.01589
ΔP_{OBS}	In. Hg.	3.20	5.31	9.60	12.90	7.04	9.81	15.87	18.02	14.22	17.01	19.83	22.14
T_{AVG}	$^{\circ}C$	30.2	30.0	30.5	30.3	30.6	30.6	30.6	30.4	30.6	30.8	30.9	30.9
P_{AVG}	PSIA	17.3	19.1	25.4	29.8	20.2	23.6	31.0	35.1	26.8	32.6	36.6	40.2
$8Q/\pi D^3$	1/Sec	164.9	162.8	155.6	151.4	252	249	238	230	376	355	337	313
$\Delta P_{LP/4L}$	#/Ft ²	0.302	0.301	0.278	0.265	0.663	0.64	0.59	0.553	1.340	1.216	1.11	0.97
ΔP_{LP}	In. Hg.		3.19	2.95	2.81		6.79	6.26	5.87		12.90	11.78	10.30
$Re_{GP} \times 10^{-3}$			2.59	16.4	28.1		3.00	14.2	23.4		4.87	9.98	18.6
f_{GP}			0.0460	0.0273	0.0238		0.0440	0.0269	0.0248		0.0375	0.0307	0.0264
ΔP_{GP}	In. Hg.		0.00261	0.0465	0.1020		0.00271	0.0284	0.0628		0.00443	0.01354	0.0369
X^2			1222	63.5	27.5		2510	220	92.0		2910	870	279
$E^2_{LTT OBS}$			1.665	3.26	4.59		1.445	2.53	3.07		1.32	1.685	2.15
$E^2_{LTT MART}$	In. Hg.		1.75	3.52	4.66		1.53	2.50	3.13		1.49	1.87	2.36
$R_G MART$			0.259	0.501	0.560		0.208	0.394	0.474		0.198	0.283	0.373
$\Delta P_{TP MART}$	In. Hg.		5.58	10.39	13.10		10.40	15.65	18.40		19.20	22.0	24.3
DEVIATION	%		-4.84	-7.61	-1.53		-5.67	+1.41	-2.06		-11.4	-9.87	-8.89

TABLE VI B3

Data and Results for Co-Current Flow of Air and a Water-Clay Suspension of Specific Gravity 1.164 Containing 23.6 Weight Per Cent (11.1 Volume Per Cent) Solids in a 0.82 Inch Pipe 17.25 Feet Long

Run No.		135	136	137	138	139	140	141	142	143	144	145	146
W_L	#/Sec	1.268	1.177	1.098	1.029	2.19	2.12	1.985	1.811	3.31	3.17	2.86	2.64
W_G	#/Sec	0	0.001684	0.01208	0.0244	0	0.00244	0.00943	0.0209	0	0.00286	0.01003	0.01618
ΔP_{OBS}	In. Hg.	2.15	4.33	11.52	16.45	5.95	10.56	16.02	22.38	12.46	18.44	23.38	25.94
T_{AVG}	$^{\circ}C$	31.1	31.0	31.2	31.0	31.0	31.2	31.2	31.3	31.3	31.3	31.4	31.4
P_{AVG}	PSIA	16.1	17.6	22.8	27.6	18.3	22.1	27.5	33.1	22.6	28.1	34.4	38.1
$8Q/\pi D^3$	1/Sec	139.7	129.7	121	113.3	241	234	219	200	365	349	315	291
$D\Delta P_{LP}/4L$	$\#_F/Ft^2$	0.150	0.13	0.12	0.10	0.415	0.397	0.352	0.30	0.869	0.80	0.668	0.58
ΔP_{LP}	In. Hg.		1.865	1.72	1.435		5.70	5.05	4.30		11.49	9.59	8.32
$Re_{GP} \times 10^{-3}$			2.55	18.3	36.9		3.69	14.3	31.6		4.32	15.2	24.4
f_{GP}			0.0462	0.0263	0.0224		0.0410	0.0280	0.0233		0.0390	0.0277	0.0246
ΔP_{GP}	In. Hg.		0.00625	0.1412	0.405		0.00926	0.0760	0.259		0.00954	0.0682	0.142
X^2_{GP}			298	12.2	3.54		615	66.5	16.6		1204	140.5	58.6
$B^2_{LLT OBS}$			2.32	6.70	11.47		1.851	3.17	5.20		1.650	2.44	3.12
$B^2_{LTT MART}$	In. Hg.		2.33	6.25	10.2		2.00	3.46	5.58		1.75	2.78	3.61
$R_G MART$			0.368	0.620	0.700		0.307	0.498	0.598		0.260	0.437	0.507
$\Delta P_{TP MART}$	In. Hg.		4.35	10.76	14.63		11.40	17.48	24.0		20.1	26.7	30.0
DEVIATION	%		-0.46	+7.06	+12.4		-7.55	-8.35	-6.75		-8.26	-12.8	-13.5

TABLE VI C1

Data and Results for Co-Current Flow of Air and a Water-Clay Suspension of Specific Gravity 1.313
Containing 39.9 Weight Per Cent (21.2 Volume Per Cent) Solids in a 1.60 Inch Pipe 15.0 Feet Long

Run No.		147	148	149	150	152	153	154	155	157	158	159	160
W_L	#/Sec	0.978	1.464	0.888	0.832	10.48	10.31	10.24	10.89	13.85	13.70	13.46	12.84
W_G	#/Sec	0	0.001954	0.00483	0.0220	0	0.00236	0.00611	0.0246	0	0.00249	0.00671	0.0225
ΔP_{OBS}	In. Hg.	1.10	0.47	0.40	1.82	3.05	3.97	4.94	7.65	5.21	6.00	7.40	9.60
T_{AVG}	$^{\circ}C$	28.3			28.5		29.0				29.9		30.4
P_{AVG}	PSIA	15.8	15.2	15.1	15.9	19.5	20.1	23.1	29.0	22.8	21.1	28.2	34.6
$8Q/\pi D^3$	1/Sec	12.83	19.2	11.65	10.92	137.5	135.3	134.4	142.9	181.8	179.8	176.5	168.3
$\Delta P_{LP}/4L$	#/Ft ²	0.1725	0.182	0.168	0.165	0.478	0.460	0.456	0.508	0.817	0.783	0.760	0.690
ΔP_{LP}	In.Hg.		1.16	1.07	1.05		2.93	2.91	3.24		4.99	4.85	4.40
$Re_{GP} \times 10^{-3}$			1.52	3.76	17.1		1.84	4.75	19.1		1.93	5.22	17.5
f_{GP}			0.0421	0.0409	0.0269		0.0507	0.0378	0.0261		0.0501	0.0367	0.0267
ΔP_{GP}	In. Hg.		0.000269	0.00161	0.208		0.000358	0.001561	0.0139		0.000378	0.001501	0.01002
X^2							8190	1863	233		13,200	3230	439
$\bar{b}^2_{LTT OBS}$							1.355	1.698	2.36		1.202	1.526	2.18
$\bar{b}^2_{LTT MART}$							1.27	1.62	2.47		1.18	1.46	2.15
$R_G MART$							0.118	0.229	0.389		0.075	0.189	0.336
$\Delta P_{TP MART}$	In.Hg.						3.72	4.71	8.00		5.89	7.08	9.46
DEVIATION	%						+6.72	+4.88	-4.37		+1.87	+4.52	+1.48

TABLE VI C2

Data and Results for Co-Current Flow of Air and a Water-Clay Suspension of Specific Gravity 1.313
Containing 39.9 Weight Per Cent (21.2 Volume Per Cent) Solids in a 1.06 Inch Pipe 16.5 Feet Long

Run No.		162	163	164	165	167	168	169	170	172	173	174	175
W_L	#/Sec	0.580	0.515	0.407	0.390	4.47	4.35	4.26	4.03	6.22	6.07	5.75	5.42
W_G	#/Sec	0	0.00186	0.00541	0.0216	0	0.00243	0.00685	0.0211	0	0.00278	0.00790	0.01782
ΔP_{OBS}	In. Hg.	2.10	1.00	1.22	2.77	5.41	8.84	12.10	17.42	10.28	13.76	18.20	22.38
T_{AVG}	$^{\circ}C$	31.3		31.5			31.8		32.1	32.4		32.7	
P_{AVG}	PSIA	16.0	15.7	15.8	17.2	18.8	22.0	25.5	34.0	23.0	26.9	32.5	38.2
$8Q/A D^3$	1/Sec	26.2	23.3	18.4	17.62	202	196.6	192.6	182.2	282	274	260	245
$\Delta P_{LP}/4L$	#/Ft ²	0.193	0.191	0.181	0.179	0.510	0.491	0.470	0.428	0.969	0.917	0.825	0.735
ΔP_{LP}	In. Hg.		2.03	1.92	1.90		5.21	4.99	4.54		9.74	8.76	7.80
$Re_{GP} \times 10^{-3}$			2.18	6.33	25.3		2.84	8.01	24.7		3.25	9.24	20.8
f_{GP}			0.049	0.0349	0.0244		0.0447	0.0325	0.0245		0.043	0.0313	0.0257
ΔP_{GP}	In. Hg.		0.00241	0.01444	0.1478		0.00268	0.01338	0.0718		0.00276	0.01343	0.0478
X^2							1945	373	63.3		3530	652	163.1
$E^2_{LTT OBS}$							1.695	2.43	3.84		1.403	2.08	2.87
$E^2_{LTT MART}$							1.60	2.22	3.52		1.44	1.98	2.68
$R_G MART$							0.226	0.348	0.502		0.184	0.304	0.422
$\Delta P_{TP MART}$	In. Hg.						8.34	11.09	16.08		14.03	17.35	20.9
DEVIATION	%						+6.00	+11.0	+12.0		-2.56	+4.90	+7.08

TABLE VI C3

Data and Results for Co-Current Flow of Air and a Water-Clay Suspension of Specific Gravity 1.313
Containing 39.9 Weight Per Cent (21.2 Volume Per Cent) Solids in a 0.82 Inch Pipe 17.25 Feet Long

Run No.		177	178	179	180	182	183	184	185	187	188	189	190
W_L	#/Sec	0.252	0.191	0.1423	0.080	2.42	2.35	2.23	1.884	3.18	3.05	2.91	2.68
W_G	#/Sec	0	0.00147	0.00528	0.0164	0	0.00253	0.00800	0.0188	0	0.00281	0.00896	0.01344
ΔP_{OBS}	In. Hg.	2.77	0.81	1.60	2.77	6.65	12.28	19.00	22.38	10.80	18.02	23.38	27.35
T_{AVG}	$^{\circ}C$	33.0		33.1			34.0		34.0	34.0		34.0	
P_{AVG}	PSIA	16.2	15.2	15.5	16.5	18.6	23.0	29.3	35.2	21.3	27.3	32.3	38.4
$8Q/\pi D^3$	1/Sec	24.6	18.64	13.9	7.81	236	229	218	184	310	298	284	262
$\Delta P_{LP}/4L$	#/Ft ²	0.1930	0.181	0.173	0.158	0.463	0.426	0.39	0.283	0.753	0.702	0.640	0.548
ΔP_{LP}	In.Hg.		2.60	2.48	2.27		6.11	5.60	4.06		10.08	9.19	7.86
$Re_{GP} \times 10^{-3}$			2.22	7.98	24.8		3.82	12.1	28.4		4.24	13.5	20.3
f_{GP}			0.0484	0.0324	0.0245		0.0405	0.0292	0.0237		0.0390	0.0285	0.0258
ΔP_{GP}	In.Hg.		0.00581	0.0492	0.338		0.00955	0.0540	0.202		0.00957	0.0600	0.103
X^2							640	103.8	20.1		1053	153	76.3
$E^2_{LTT OBS}$							2.01	3.39	5.51		1.79	2.55	3.48
$E^2_{LTT MART}$							1.99	3.02	5.19		1.80	2.73	3.32
$R_G MART$							0.305	0.467	0.584		0.269	0.429	0.489
$\Delta P_{TP MART}$	In.Hg.						12.17	17.00	21.1		18.13	25.1	26.1
DEVIATION	%						+0.91	+11.8	+6.06		-0.61	-6.85	+4.79

TABLE VI D1

Data and Results for Co-Current Flow of Air and Water-Clay Suspension of Specific Gravity 1.396
Containing 47.5 Weight Per Cent (26.8 Volume Per Cent) Solids in a 1.60 Inch Pipe 15.0 Feet Long

Run No.		192	193	194	195	197	198	199	200	202	203	204	205
W_L	#/Sec	0.927	0.839	0.655	0.522	13.17	12.97	12.80	12.52	15.71	15.50	15.02	14.64
W_G	#/Sec	0	0.00207	0.00710	0.01748	0	0.00274	0.00618	0.01501	0	0.00261	0.00747	0.01476
ΔP_{OBS}	In. Hg.	2.95	1.00	0.40	0.23	5.00	6.36	7.31	8.85	6.51	7.43	9.10	10.37
T_{AVG}	$^{\circ}C$	25.0	25.0	25.0	25.0	27.5	27.5	27.5	27.5	30.0	30.0	30.0	30.0
P_{AVG}	PSIA	16.7	15.7	14.6	14.56	22.1	24.7	26.6	30.4	25.0	27.3	31.1	34.2
$8Q/\pi D^3$	1/Sec	11.43	10.34	8.08	6.44	162.2	159.9	157.8	154.3	193.9	191.0	185	180.5
$\Delta P_{LP}/4L$	#/Ft ²	0.462	0.450	0.430	0.413	0.784	0.761	0.750	0.719	1.022	1.02	0.970	0.930
ΔP_{LP}	In. Hg.		2.87	2.74	2.64		4.86	4.78	4.59		6.50	6.19	5.93
$Re_{GP} \times 10^{-3}$			1.62	5.54	13.6		2.14	4.82	11.7		2.03	5.80	11.5
f_{GP}			0.0396	0.0360	0.0284		0.049	0.0375	0.0298		0.0495	0.0357	0.0299
ΔP_{GP}	In. Hg.		0.000272	0.00313	0.0150		0.000378	0.001368	0.00560		0.000317	0.001641	0.00487
X^2							12,860	3500	819		20,500	3770	1217
\bar{v}^2 LTT OBS							1.31	1.53	1.93		1.142	1.47	1.748
\bar{v}^2 LTT MART							1.18	1.44	1.89		1.12	1.43	1.75
R_G MART							0.076	0.185	0.287		0.0375	0.180	0.259
ΔP_{TP} MART	In. Hg.						5.73	6.88	8.68		7.28	8.85	10.38
DEVIATION	%						+11.0	+6.25	+1.96		+2.06	+2.83	-0.96

TABLE VI D2

Data and Results for Co-Current Flow of Air and a Water-Clay Suspension of Specific Gravity 1.396
Containing 47.5 Weight Per Cent (26.8 Volume Per Cent) Solids in a 1.06 Inch Pipe 16.5 Feet Long

Run No.		207	208	209	210	212	213	214	215	217	218	219	220
W_L	#/Sec	0.732	0.654	0.626	0.589	5.13	4.98	4.80	4.64	6.21	6.07	5.85	5.53
W_G	#/Sec	0	0.00216	0.00556	0.01840	0	0.00259	0.00764	0.01527	0	0.00284	0.00856	0.01737
ΔP_{OBS}	In. Hg.	5.32	2.20	2.20	3.76	7.65	11.75	15.04	18.83	10.26	14.34	19.40	22.38
T_{AVG}	$^{\circ}C$	31.0				31.5				31.5			
P_{AVG}	PSIA	17.8	16.0	16.0	17.4	20.9	23.9	28.1	33.0	22.6	27.1	33.0	38.2
$8Q/\pi D^3$	l/Sec	31.1	27.8	26.6	25.0	218	212	204	197	264	258	249	235
$\Delta P_{LP}/4L$	#/ft ²	0.501	0.488	0.483	0.477	0.720	0.680	0.647	0.612	0.966	0.932	0.88	0.80
ΔP_{LP}	In. Hg.		5.18	5.13	5.07		7.22	6.87	6.50		9.89	9.34	8.49
$Re_{GP} \times 10^{-3}$			2.53	6.51	21.5		3.03	8.94	17.9		3.28	10.0	20.3
f_{GP}			0.0465	0.0346	0.0255		0.044	0.0317	0.0264		0.0427	0.0306	0.0258
ΔP_{GP}	In. Hg.		0.00302	0.0149	0.1105		0.00276	0.01469	0.0416		0.00276	0.01517	0.0455
K^2							2620	468	156.3		3580	615	186.5
$E^2_{LTT OBS}$							1.629	2.19	2.90		1.451	2.08	2.64
$E^2_{LTT MART}$							1.52	2.12	2.71		1.44	2.00	2.60
$R_G MART$							0.205	0.328	0.427		0.183	0.308	0.410
$\Delta P_{TP MART}$	In. Hg.						10.98	14.57	17.61		14.24	18.68	22.1
DEVIATION	%						+7.01	+3.23	+6.93		+0.70	+3.86	+1.27

TABLE VI D3

Data and Results for Co-Current Flow of Air and a Water-Clay Suspension of Specific Gravity 1.396
Containing 47.5 Weight Per Cent (26.8 Volume Per Cent) Solids in a 0.82 Inch Pipe 17.25 Feet Long

Run No.		222	223	224	225	227	228	229	230	232	233	234
W_L	#/Sec	0.390	0.312	0.307	0.273	2.98	2.84	2.62	2.31	3.99	3.84	3.67
W_G	#/Sec	0	0.001923	0.00559	0.01819	0	0.00276	0.00788	0.01654	0	0.00250	0.00440
ΔP_{OBS}	In. Hg.	6.65	2.05	2.77	6.68	10.38	17.66	22.38	26.75	16.63	23.38	26.92
T_{AVG}	$^{\circ}C$	31.5				32.0				32.0		
P_{AVG}	PSIA	18.2	16.0	16.2	18.6	20.8	26.3	32.1	37.2	24.9	30.8	34.4
$8Q/nD^3$	1/Sec	35.8	28.6	28.2	25.0	273	261	240	212	366	352	337
$\Delta P_{LP/4L}$	#/Ft ²	0.463	0.448	0.447	0.440	0.724	0.678	0.602	0.513	1.160	1.08	1.007
ΔP_{LP}	In. Hg.		6.43	6.42	6.31		9.73	8.64	7.36		15.50	14.43
$Re_{GP} \times 10^{-3}$			2.91	8.45	27.5		4.17	11.9	25.0		3.78	6.65
f_{GP}			0.0443	0.0319	0.0240		0.0395	0.0292	0.0245		0.0406	0.0342
ΔP_{GP}	In. Hg.		0.00861	0.0517	0.359		0.00964	0.0476	0.1519		0.00694	0.0162
X^2							1010	181.5	48.5		2230	891
\bar{E}_2^2							1.815	2.59	3.64		1.51	1.863
\bar{E}_2^2 LTT OBS							1.82	2.61	3.84		1.56	1.86
\bar{E}_2^2 LTT MART							0.273	0.411	0.520		0.217	0.281
R_G MART							17.70	22.5	28.3		24.2	26.8
ΔP_{TP} MART	In. Hg.											
DEVIATION	%						-0.23	-0.53	-5.48		-3.39	+0.45

TABLE VII A

Pump Characteristics

Data and Results for an Ingersoll-Rand 1 CORVNL Open Impeller Centrifugal Pump Handling Water

Run No.	W_L #/Sec	Temperature °C	V' Gals/Min	Discharge Pressure (P_D) PSIG	Suction Pressure (P_S) PSIG	$\frac{2.31 (P_D - P_S)}{\text{Sp. Gr}}$ Ft. # _F /# _M	$\frac{U_D^2 - U_S^2}{2g_c}$ Ft. # _F /# _M	Head*' Ft. # _F /# _M	Motor Power Input HP	Overall Efficiency %
1	9.15	16.4	65.9	56.3	1.1	127.6	8.70	139.7	7.24	32.1
2	11.98	17.2	86.2	48.1	0.8	109.3	14.91	127.6	7.62	36.4
3	7.18	18.1	51.7	63.1	1.4	142.7	5.35	151.5	6.43	30.8
4	4.65	18.9	33.5	68.6	1.7	154.5	2.25	160.2	6.17	21.9
5	9.66	20.6	69.5	57.3	1.2	129.8	9.71	142.9	7.27	34.5
6	8.01	21.7	57.7	62.0	1.3	140.3	6.67	150.4	6.97	31.4
7	5.91	22.0	42.6	66.8	1.6	150.9	3.64	159.0	6.44	26.4
8	3.10	22.4	22.3	69.9	1.9	157.1	1.00	161.5	5.74	15.8
9	1.375	23.9	9.90	70.4	1.9	158.2	0.197	161.8	5.40	7.49
10	1.366	24.7	9.84	70.4	1.9	158.2	0.194	161.8	5.39	7.45
11	2.78	25.1	20.0	69.9	1.9	157.1	0.773	161.3	5.72	14.2
12	3.63	25.6	26.1	69.7	1.8	156.9	1.37	161.7	5.93	18.0
13	4.30	26.0	31.0	68.9	1.8	155.2	1.92	160.5	5.98	21.0
24	11.55	12.8	83.2	48.4	0.9	109.9	13.90	127.2	7.65	34.9
28	8.53	16.3	61.4	58.9	1.2	133.4	7.57	144.4	6.77	33.1

$$* \frac{U_D^2 - U_S^2}{2g_c} = 0.104 \frac{W_L^2}{\text{SpGr}}$$

$$*' \text{ HEAD} = \frac{2.31 (P_D - P_S)}{\text{Sp. Gr.}} + \frac{U_D^2 - U_S^2}{2g_c} + 3.42$$

TABLE VII B

Pump Characteristics

Data and Results for an Ingersoll-Rand 1 CORVNL Open Impeller Centrifugal Pump Handling a Water-Clay
Suspension of Specific Gravity 1.078 Containing 12.1 Weight Per Cent (5.27 Volume Per Cent) Solids

Run No.	W_L #/Sec	Temperature °C	V Gals/Min	Discharge	Suction	$2.31 (P_D - P_S)$	$\frac{U_D^2 - U_S^2}{2g_c}$ *	Head* ¹ Ft. #/ft	Motor Power	Overall
				Pressure (P _D) PSIG	Pressure (P _S) PSIG	Sp. Gr. Ft. #/ft	Input HP		Efficiency %	
57	12.25	22.8	31.8	55.2	1.0	116.1	13.41	132.7	8.20	36.0
58	15.79	23.4	105.3	19.0	0.5	39.6	22.3	65.1	8.96	20.9
59	9.27	24.2	61.9	64.7	1.3	135.8	7.68	146.7	7.30	33.9
60	7.36	24.8	49.1	69.4	1.5	145.2	4.85	153.3	6.84	30.0
61	4.83	25.0	32.2	74.2	1.8	155.0	2.09	160.3	6.20	22.7
62	1.582	25.4	10.57	75.7	2.0	158.0	0.22	161.4	5.39	8.62
63	3.35	25.7	22.4	75.3	2.0	157.0	1.00	161.2	5.79	17.3
64	5.68	25.9	37.9	73.1	1.7	152.9	2.78	158.9	6.42	25.6
65	7.97	26.3	53.2	68.0	1.5	142.5	5.68	151.4	7.01	31.3
66	9.56	26.5	63.9	63.8	1.3	134.0	8.17	145.4	7.34	34.5
67	1.416	26.9	9.45	75.6	2.0	157.8	0.18	161.2	5.36	7.74
68	2.81	27.2	18.8	75.2	2.0	156.9	0.73	160.8	5.61	14.6
69	3.75	27.3	25.0	74.6	2.0	155.7	1.26	160.2	5.87	18.6
70	4.62	27.4	30.8	74.1	1.9	154.7	1.91	159.8	6.06	22.2

$$* \frac{U_D^2 - U_S^2}{2g_c} = 0.104 \left(\frac{W_L}{SpGr} \right)^2$$

$$*^1 \text{ HEAD} = \frac{2.31 (P_D - P_S)}{Sp.Gr.} + \frac{U_D^2 - U_S^2}{2g_c} + 3.17$$

TABLE VII C

Pump Characteristics

Data and Results for an Ingersoll-Rand 1 CORVNL Open Impeller Centrifugal Pump Handling a Water-Clay

Suspension of Specific Gravity 1.164 Containing 23.6 Weight Per Cent (11.1 Volume Per Cent) Solids

Run No.	W_L #/Sec	Temperature °C	V ¹ Gals/Min	Discharge	Suction	$2.31 (P_D - P_S)$	$\frac{U_D^2 - U_S^2}{2g_c}$	Head ^{*1} Ft. #/##	Motor Power Input HP	Overall Efficiency %
				Pressure (P _D) PSIG	Pressure (P _S) PSIG	Sp. Gr. Ft. #/##	Ft. #/##			
110	5.50	26.5	34.0	79.4	2.0	153.3	2.31	158.6	6.18	25.6
114	8.12	28.5	50.2	74.3	1.6	144.2	5.05	152.2	6.82	32.9
116	7.99	29.0	49.4	74.7	1.7	144.8	4.90	152.6	6.76	32.8
118	14.10	30.1	87.2	54.2	0.9	105.8	15.23	124.0	8.21	38.7
123	3.23	30.2	20.0	80.6	2.2	155.3	0.80	159.0	5.61	16.6
127	4.94	30.6	30.5	79.9	2.0	154.3	1.87	159.1	6.06	23.6
131	7.38	30.6	45.6	75.2	1.7	145.8	4.17	152.9	6.65	30.8
135	1.268	31.1	7.84	81.3	2.2	157.0	0.12	160.1	5.15	7.15
139	2.19	31.0	13.5	81.1	2.2	156.4	0.37	159.7	5.36	11.9
143	3.31	31.3	20.5	80.4	2.2	155.2	0.84	159.0	5.61	17.1

$$* \frac{U_D^2 - U_S^2}{2g_c} = 0.104 \left(\frac{W_L}{\text{Sp.Gr.}} \right)^2$$

$$*1 \text{ HEAD} = 2.31 \frac{(P_D - P_S)}{\text{Sp.Gr.}} + \frac{U_D^2 - U_S^2}{2g_c} + 2.94$$

TABLE VII D

Pump Characteristics

Data and Results for an Ingersoll-Rand 1 CORVNL Open Impeller Centrifugal Pump Handling a Water-Clay Suspension of Specific Gravity 1.313 Containing 39.9 Weight Per Cent (21.2 Volume Per Cent) Solids

Run No.	W_L #/Sec	Temperature ° C	V^1 Gals/Min	Discharge Pressure (P_D) PSIG	Suction Pressure (P_S) PSIG	$\frac{2.31 (P_D - P_S)}{\text{Sp. Gr.}}$ Ft. #F/#M	$\frac{U_D^2 - U_S^2}{2g_c}$ Ft. #F/#M	Head** Ft. #F/#M	Motor Power Input HP	Overall Efficiency %
147	0.978	28.3	5.36	90.4	2.5	154.3	0.06	157.0	5.47	5.10
152	10.48	28.8	57.4	80.9	1.7	139.2	6.60	148.4	7.81	36.2
157	13.85	29.7	75.9	69.4	1.3	119.8	11.53	133.9	8.60	39.2
162	0.580	31.3	3.18	92.0	2.5	157.2	0.02	159.8	5.27	3.20
167	4.47	31.6	24.5	90.9	2.4	155.6	1.20	159.4	6.21	20.9
172	6.22	32.4	34.1	89.3	2.2	153.1	2.33	158.0	6.61	27.1
177	0.252	33.0	1.38	92.0	2.5	157.2	0	159.8	5.15	1.42
182	2.42	34.0	13.3	92.0	2.5	157.2	0.35	160.2	5.67	12.4
187	3.18	34.0	17.4	90.9	2.5	155.2	0.60	158.4	5.81	15.7

$$* \frac{U_D^2 - U_S^2}{2g_c} = 0.104 \left(\frac{W_L}{\text{Sp. Gr.}} \right)^2$$

$$*^1 \text{ HEAD} = \frac{2.31 (P_D - P_S)}{\text{Sp. Gr.}} + \frac{U_D^2 - U_S^2}{2g_c} + 2.61$$

TABLE VII E

Pump Characteristics

Data and Results for an Ingersoll-Rand 1 CORVNL Open Impeller Centrifugal Pump Handling a Water-Clay

Suspension of Specific Gravity 1.396 Containing 47.5 Weight Per Cent (26.8 Volume Per Cent) Solids

Run No.	W_L #/Sec	Temperature °C	V^1 Gals/Min	Discharge Pressure (P_D) PSIG	Suction Pressure (P_S) PSIG	$\frac{2.31 (P_D - P_S)}{\text{Sp. Gr.}}$ Ft. #/ft.	$\frac{U_D^2 - U_S^2}{2g_c}$ Ft. #/ft.	Head ^{*1} Ft. #/ft.	Motor Power Input HP	Overall Efficiency %
192	0.927	25.0	4.77	95.1	2.7	152.4	0.05	154.9	5.89	4.43
197	13.17	27.5	67.7	78.8	1.5	127.6	9.21	139.3	8.88	37.6
200	12.52	27.5	64.5	79.9	1.6	129.2	8.32	140.0	8.65	36.8
202	15.71	30.0	80.9	70.4	1.3	114.1	13.11	129.7	9.35	39.6
205	14.64	30.0	75.4	74.1	1.4	120.0	11.40	133.9	9.08	39.2
207	0.732	31.0	3.77	95.1	2.7	152.4	0.03	154.9	5.68	3.63
212	5.13	31.5	26.4	92.0	2.5	147.8	1.40	151.7	6.66	21.2
217	6.21	31.5	32.0	91.4	2.4	146.9	2.05	151.4	6.93	24.7
222	0.390	31.5	2.01	96.7	2.7	155.1	0.01	157.6	5.52	2.02

$$* \frac{U_D^2 - U_S^2}{2g_c} = 0.104 \left(\frac{W_L}{\text{SpGr}} \right)^2$$

$$*^1 \text{ HEAD} = \frac{2.31 (P_D - P_S)}{\text{Sp. Gr.}} + \frac{U_D^2 - U_S^2}{2g_c} + 2.46$$

LIST OF FIGURES

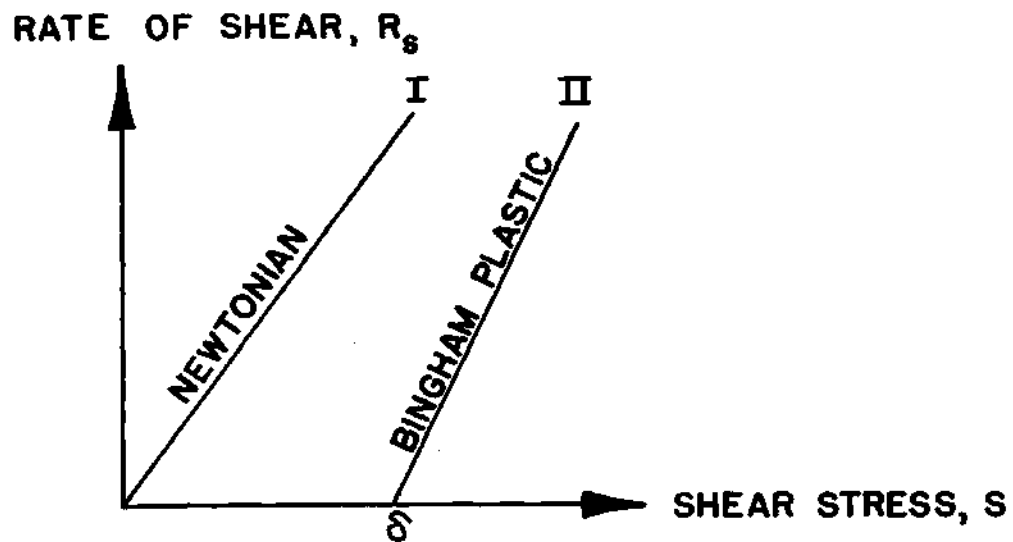
No.	Page
1. a)	Typical Flow Curves of Newtonian and Bingham Plastic Materials 109
b)	Typical Flow Curves of Pseudoplastic and Generalized Newtonian Materials 109
2. a)	Typical Flow Curves of Dilatant and Generalized Bingham Plastic Materials 110
b)	Typical Flow Curves of a Thixotropic Material in a Rotation Viscometer 110
3. a)	Typical Flow Curves of a Bingham Plastic Material in a Cylindrical Tube. 111
b)	Typical Flow Curves of a Thixotropic Material in Cylindrical Tubes 111
4. a)	Typical Flow Curve of a Bingham Plastic in a Cylindrical Tube with Buckingham Slippage Occurring 112
b)	Typical Flow Curves of Materials in Cylindrical Tubes Exhibiting "Sigma Phenomenon" 112
5. a)	Typical Flow Curve of a Bingham Plastic in a Rotation Viscometer. 113
b)	Typical Flow Curves of a Non-Newtonian Material in Cylindrical Tubes in the Laminar and Turbulent Regions. . . 113
6.	Schematic Diagram of Experimental Apparatus 114
7.	General View of Experimental Equipment (Photograph) 115

LIST OF FIGURES (continued)

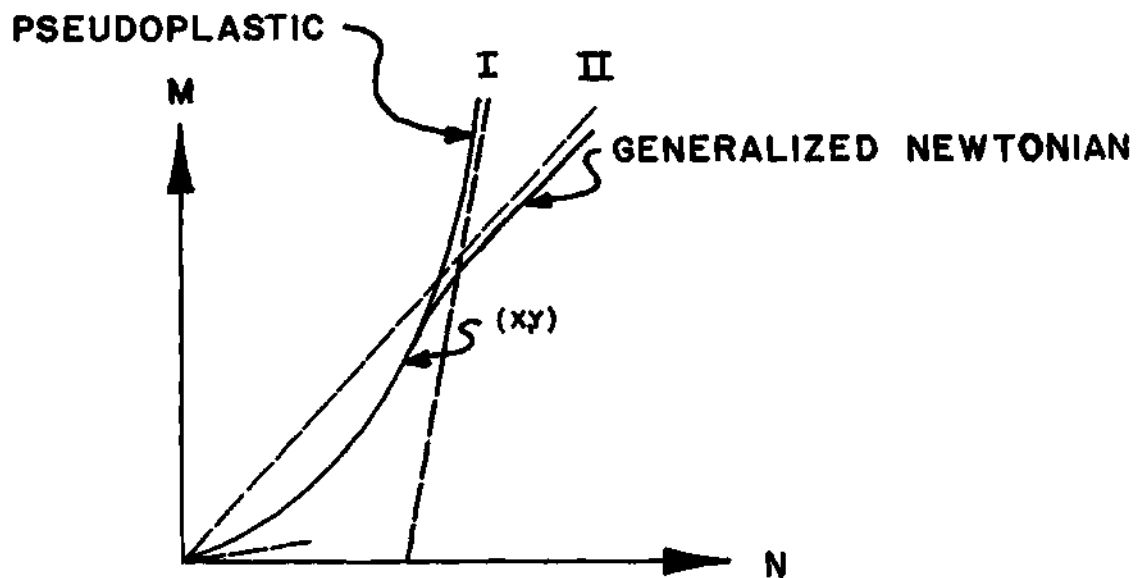
No.	Page
8. Upstream End of Experimental Equipment (Photograph)	116
9. Downstream End of Experimental Equipment (Photograph)	117
10. Schematic Diagram of Entrance Section	118
11. Schematic Diagram of Mud Trap	119
12. Instrument Panel (Photograph)	120
13. Schematic Diagram of Capillary Tube Viscometer.	121
14. Particle-Size Distribution Curves of Clays by Hydrometer Method.	122
15. a) Electron Microscope Photograph of Kaolin Clay	123
b) Electron Microscope Photograph of Kaolin Clay	124
16. Friction Factor vs. Reynolds Number for Flow of Water Alone . .	125
17. Pressure Drop vs. Volumetric Flow Rate (Water-Clay Suspensions in a 1.60 inch Pipe 15.0 feet Long)	126
18. Flow Curves of Water-Clay Suspensions in a Rotation Viscometer (Brookfield).	127
19. Flow Curves of Water-Clay Suspensions in a Rotation Viscometer (Brookfield)	128
20. Flow Curves of a 12.1 Weight Percent Suspension in Various Size Tubes.	129
21. Flow Curves of a 23.6 Weight Percent Suspension in Various Size Tubes.	130
22. Flow Curves of a 39.9 Weight Percent Suspension in Various Size Tubes.	131

LIST OF FIGURES (continued)

No.	Page
23. Flow Curves of a 47.5 Weight Percent Suspension in Various Size Tubes.	132
24. Friction Factor vs. $(DU\rho)$ Suspension.	133
25. Turbulent Viscosity vs. Shearing Stress at Pipe Wall.	134
26. Turbulent Viscosity vs. Shearing Stress at Pipe Wall.	135
27. Total Pressure Drop vs. Air Rate(Co-Current Turbulent- Turbulent Flow of Air and Water-Clay Suspensions in a 1.60 inch Pipe 15.0 feet Long)	136
28. Total Pressure Drop vs. Air Rate (Co-Current Turbulent- Turbulent Flow of Air and Water-Clay Suspensions in a 1.06 inch Pipe 16.50 feet Long).	137
29. Total Pressure Drop vs. Air Rate(Co-Current Turbulent- Turbulent Flow of Air and Water-Clay Suspensions in a 0.82 inch Pipe 17.25 feet Long).	138
30. Comparison of Data for Co-Current Turbulent-Turbulent Flow of Air and Water-Clay Suspensions in 1.60, 1.06 and 0.82 inch Pipes with Correlation of Lockhart and Martinelli (8). . .	139
31. Predicted Pump Characteristic Curves.	140
32. Head vs. Capacity Curves for Centrifugal Pump Handling Water-Clay Suspensions.	141
33. Power vs. Capacity Curves for Centrifugal Pump Handling Water-Clay Suspensions.	142

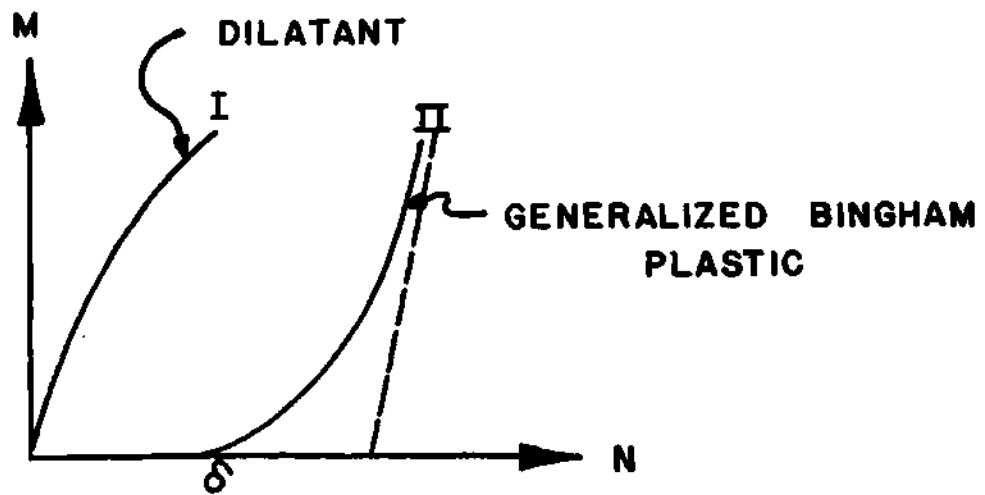


A) TYPICAL FLOW CURVES OF NEWTONIAN
AND BINGHAM PLASTIC MATERIALS

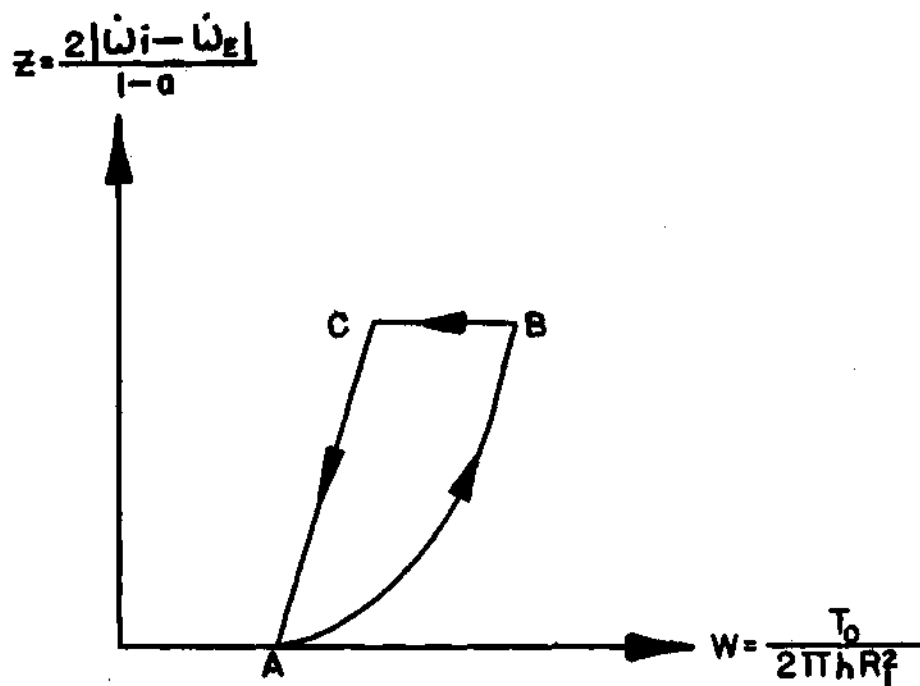


B) TYPICAL FLOW CURVES OF PSEUDOPLASTIC
AND GENERALIZED NEWTONIAN MATERIALS

FIGURE 1

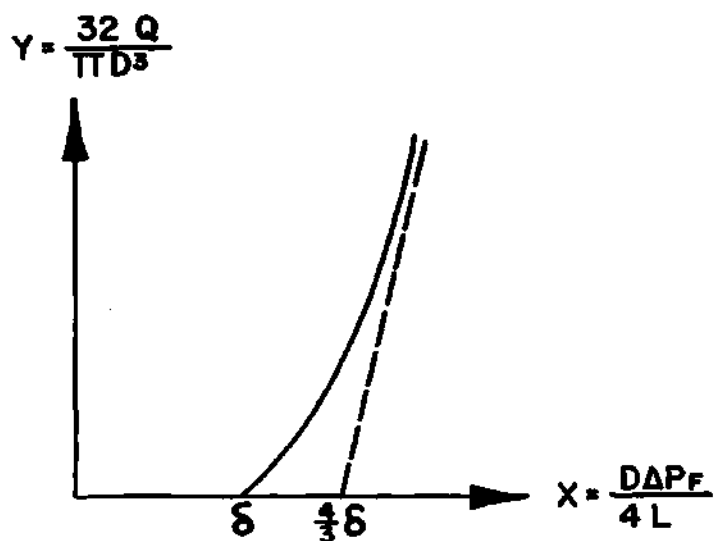


A) TYPICAL FLOW CURVES OF DILATANT AND GENERALIZED BINGHAM PLASTIC MATERIALS

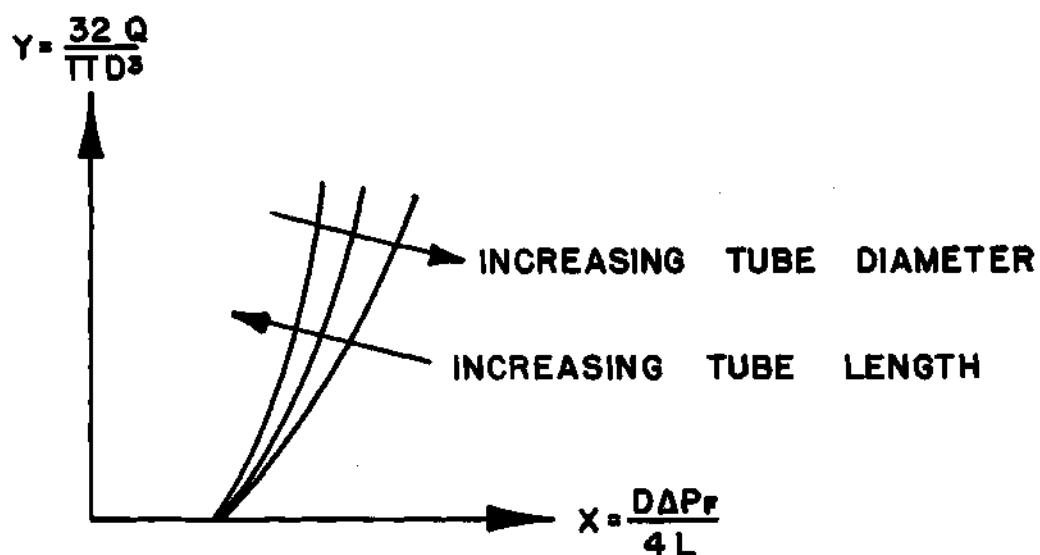


B) TYPICAL FLOW CURVES OF A THIXOTROPIC MATERIAL IN A ROTATION VISCOMETER

FIGURE 2

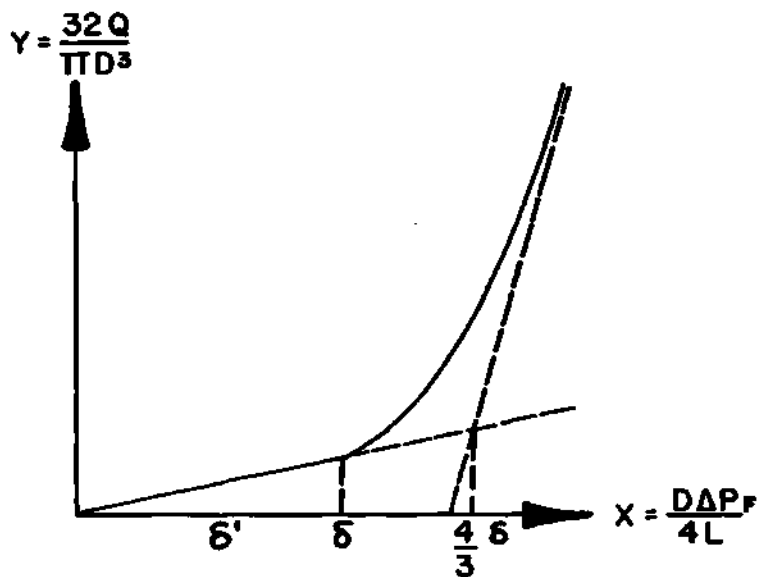


A) TYPICAL FLOW CURVE OF A BINGHAM PLASTIC MATERIAL IN A CYLINDRICAL TUBE

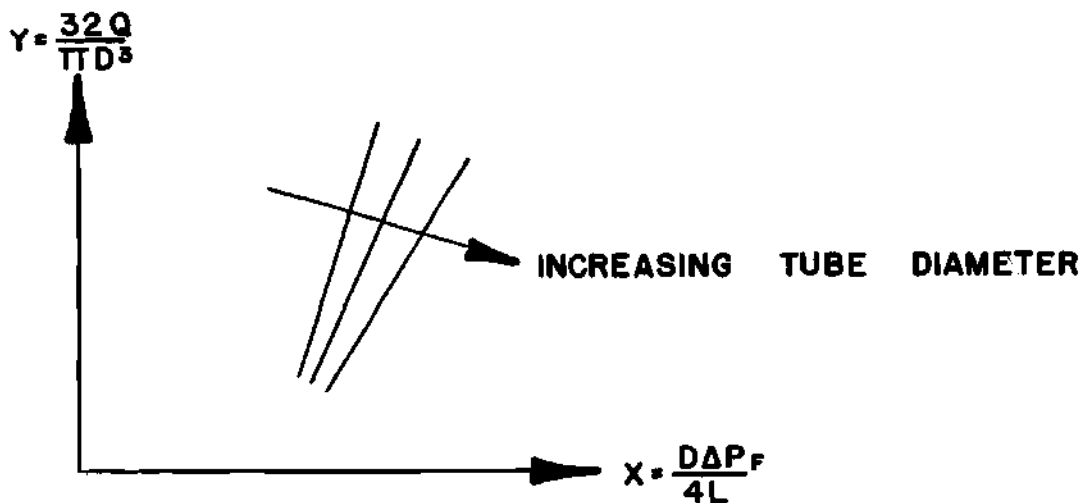


B) TYPICAL FLOW CURVES OF A THIXOTROPIC MATERIAL IN CYLINDRICAL TUBES

FIGURE 3

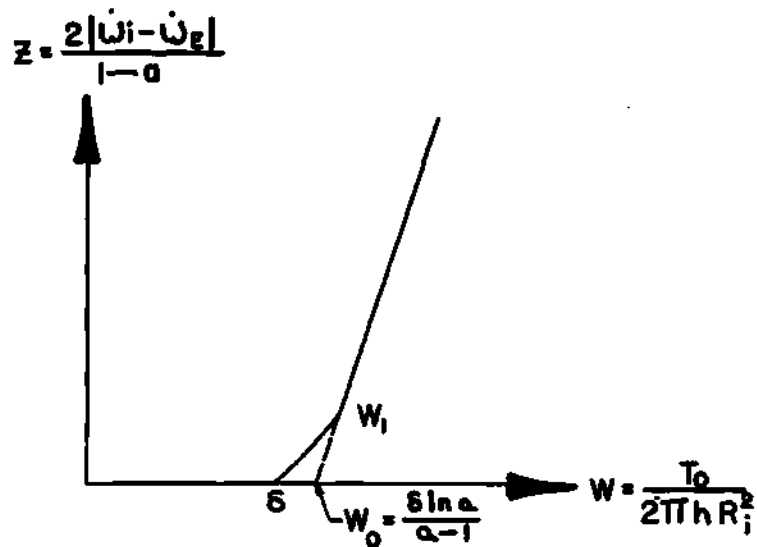


A) TYPICAL FLOW CURVE OF A BINGHAM PLASTIC IN A CYLINDRICAL TUBE WITH BUCKINGHAM SLIPPAGE OCCURRING

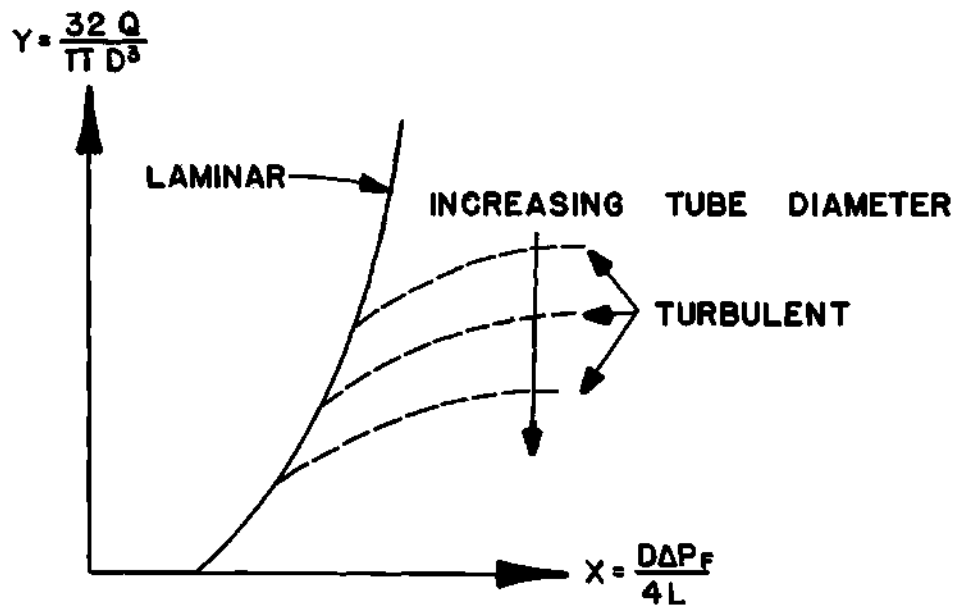


B) TYPICAL FLOW CURVES OF MATERIALS IN CYLINDRICAL TUBES EXHIBITING "SIGMA PHENOMENON"

FIGURE 4

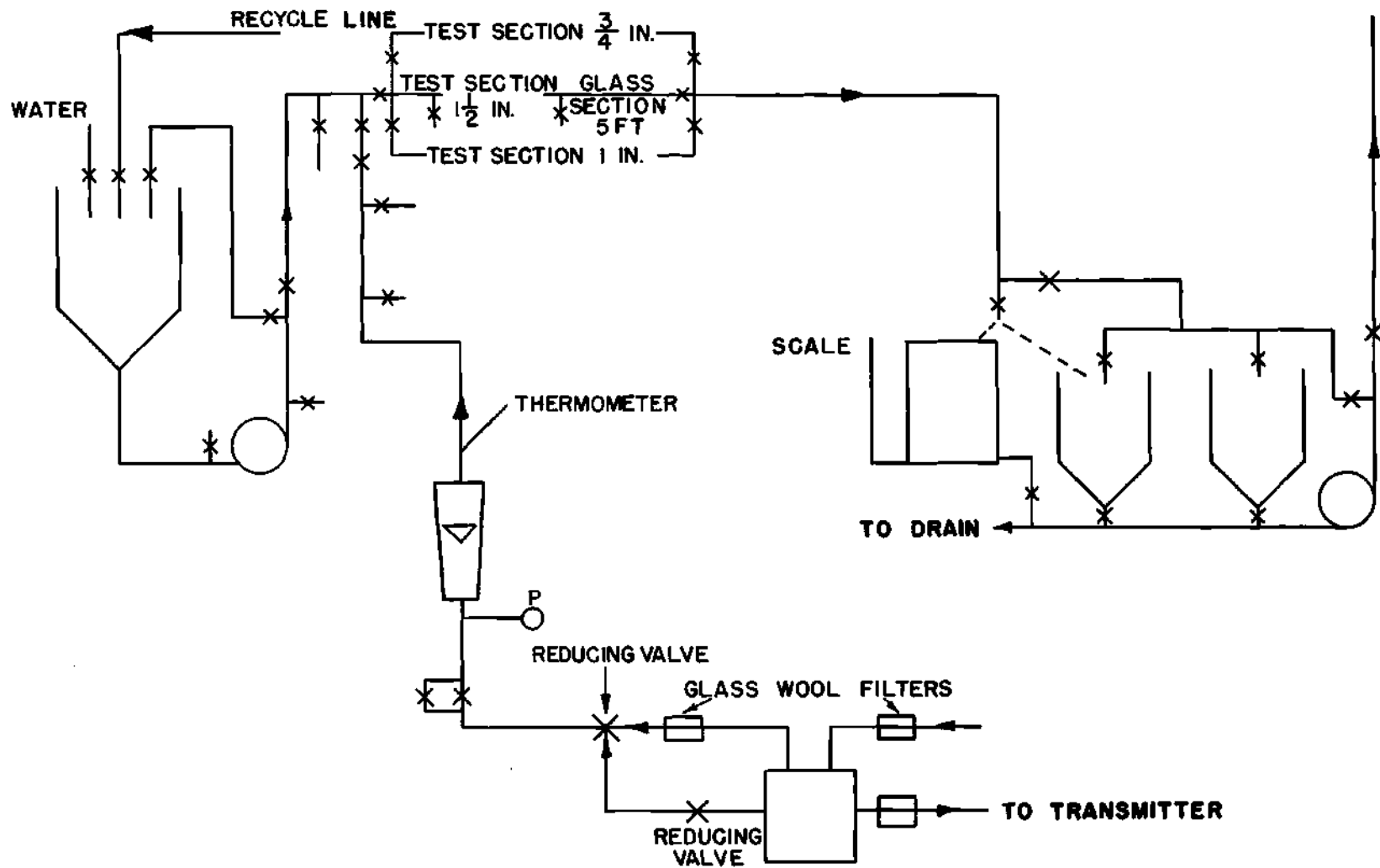


A) TYPICAL FLOW CURVE OF A BINGHAM PLASTIC IN A ROTATION VISCOMETER



B) TYPICAL FLOW CURVES OF A NON-NEWTONIAN MATERIAL IN CYLINDRICAL TUBES IN THE LAMINAR AND TURBULENT REGIONS

FIGURE 5



SCHEMATIC DIAGRAM OF EXPERIMENTAL APPARATUS
 FIGURE 6

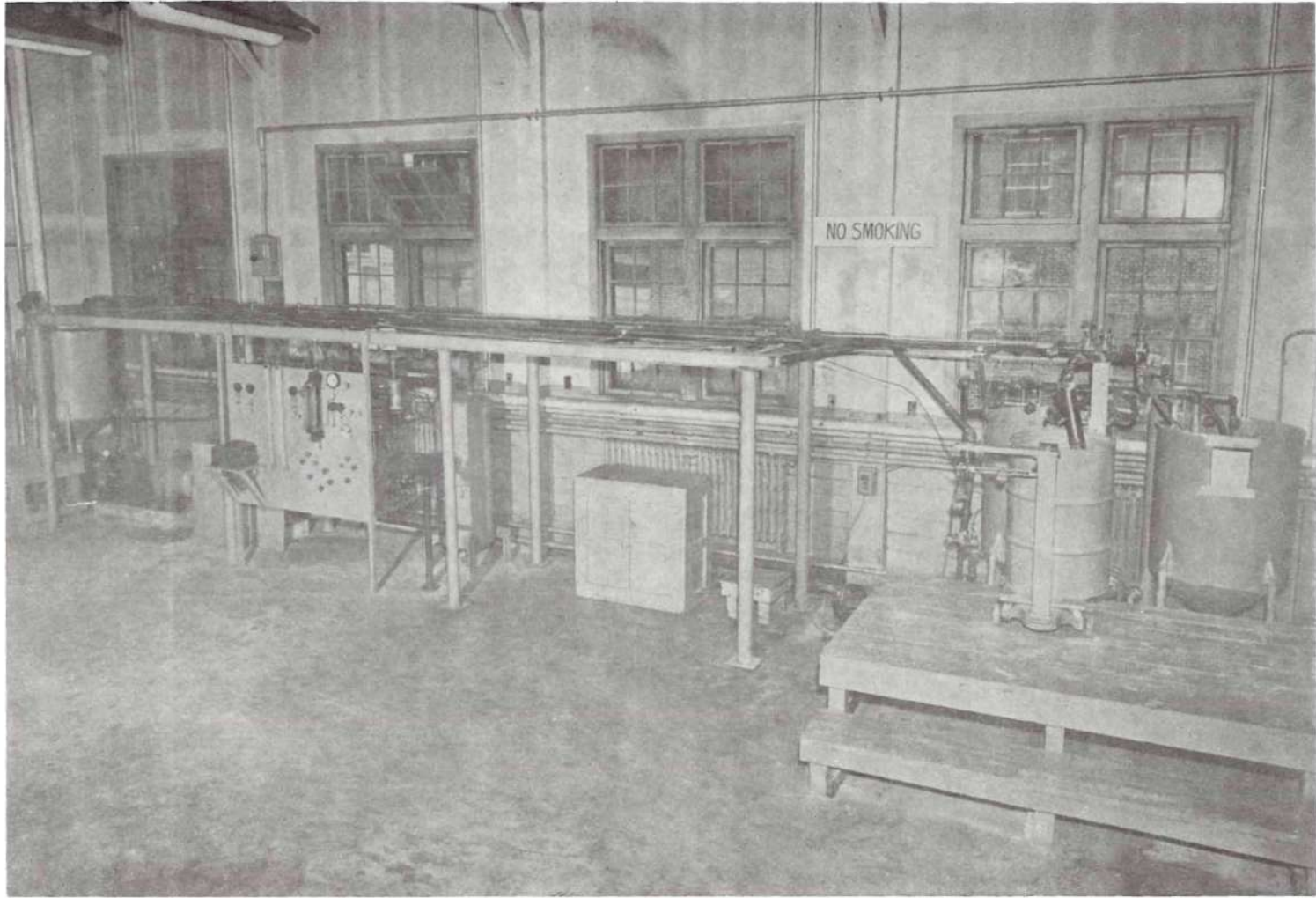


Figure 7. General View of Experimental Equipment.

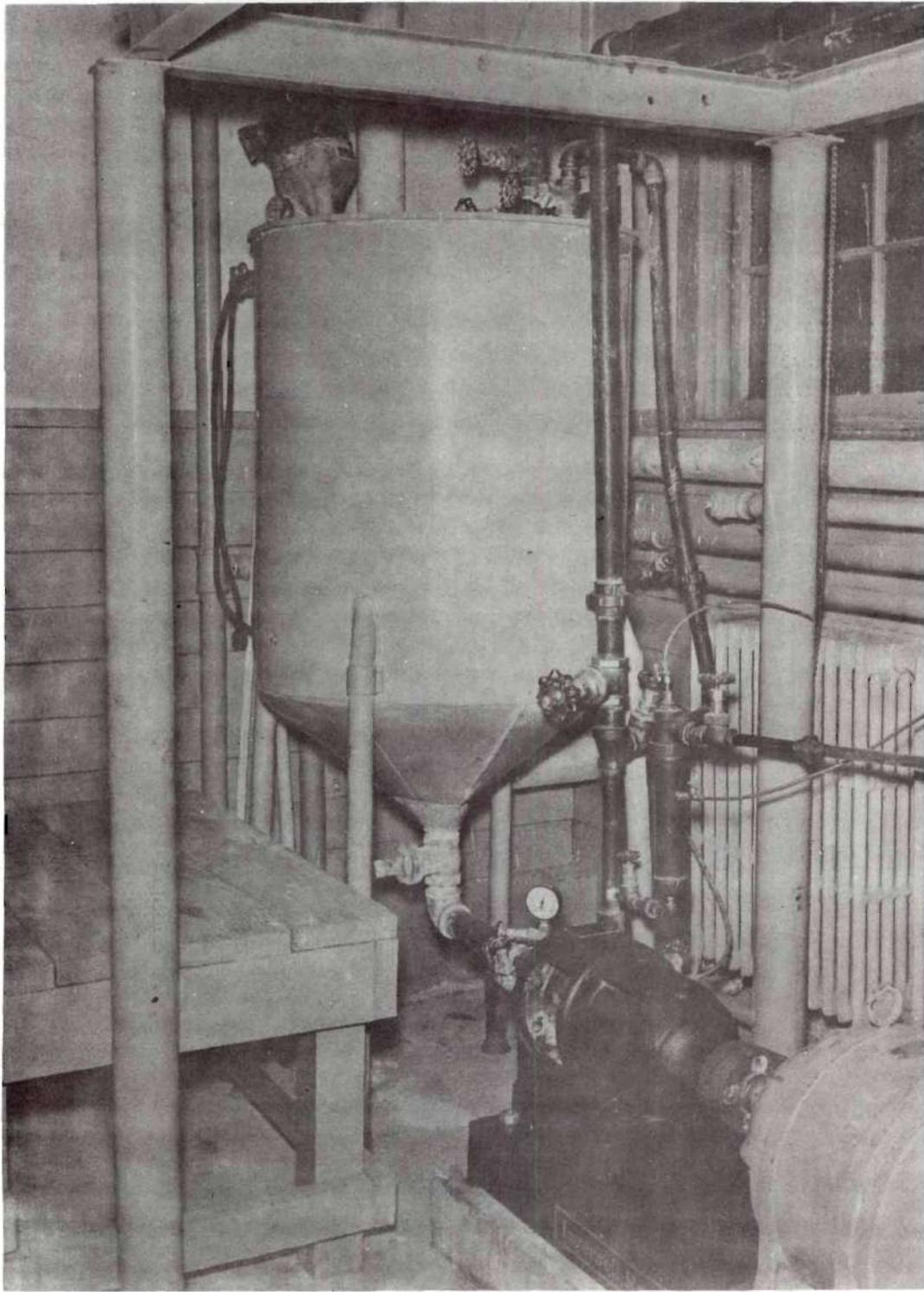


Figure 8. Upstream End of Experimental Equipment.

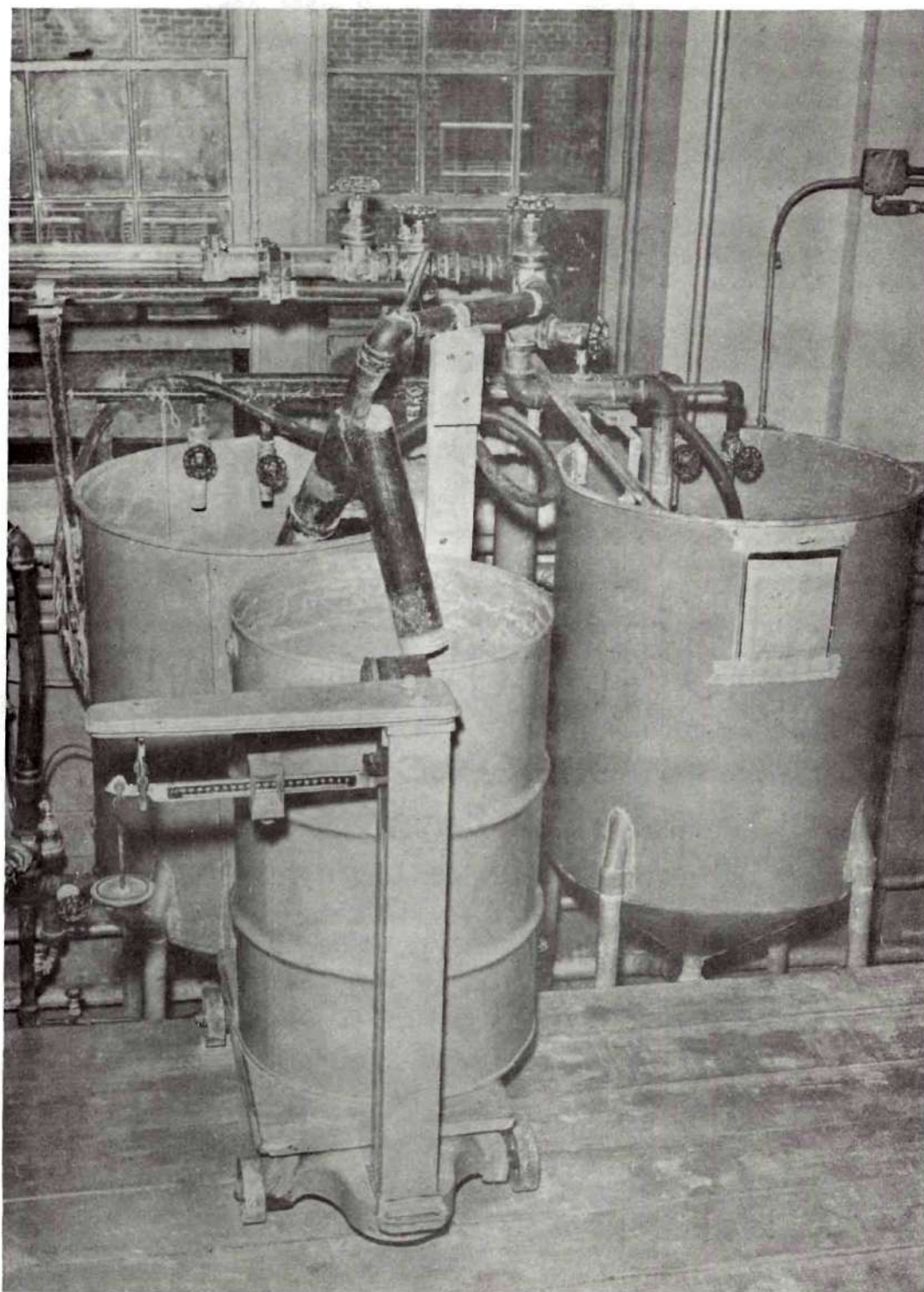
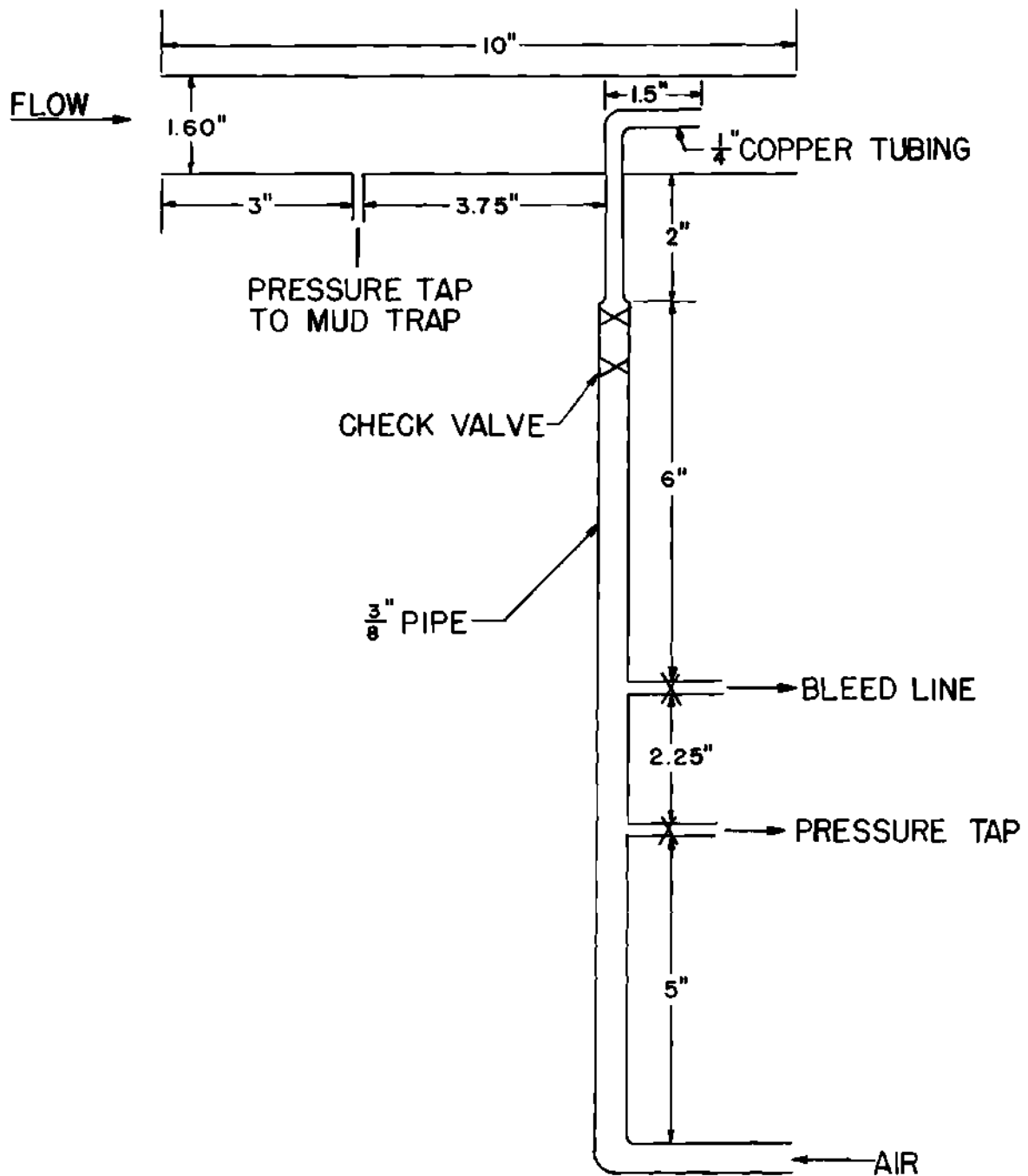
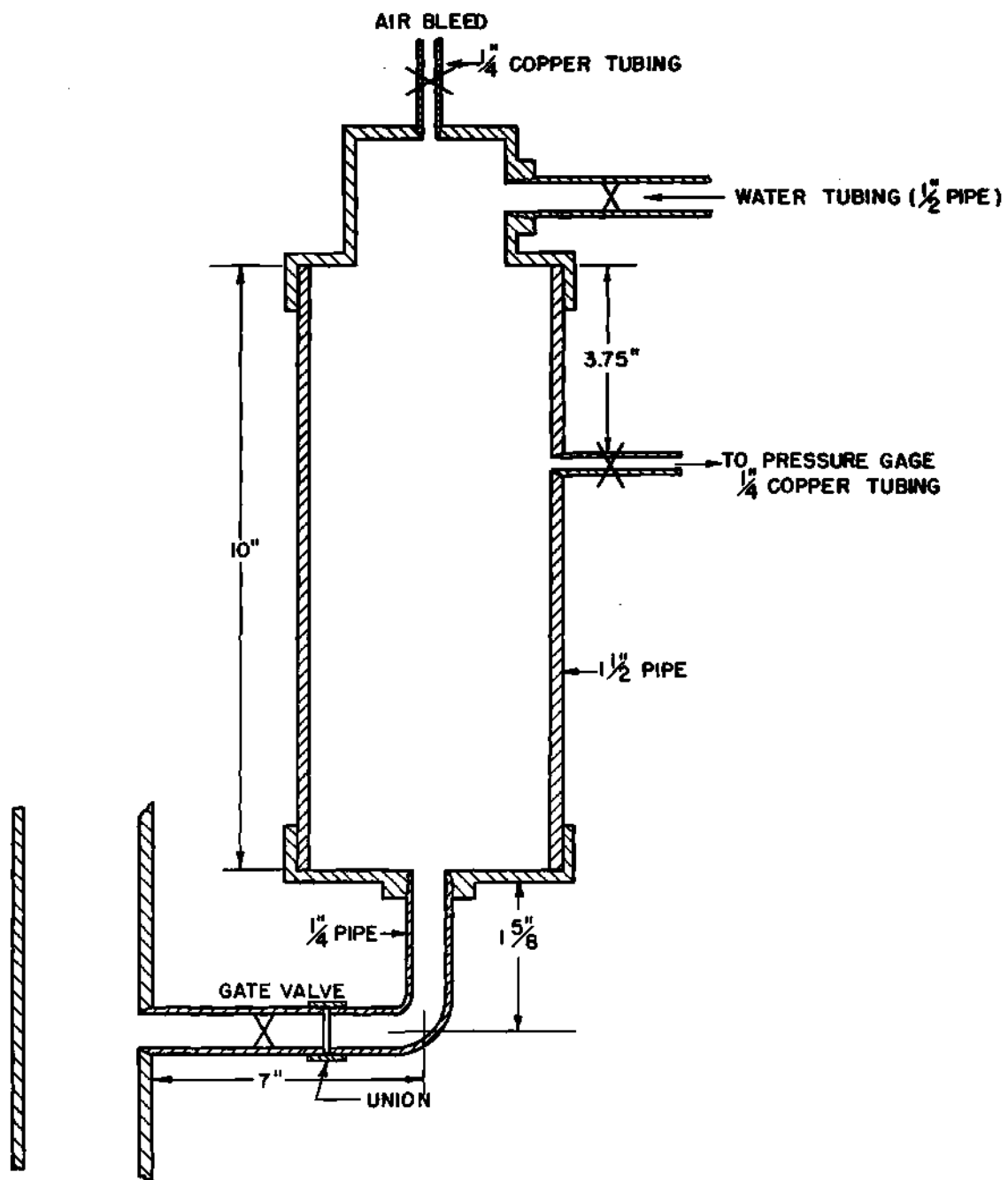


Figure 9. Downstream End of Experimental Equipment.



SCHEMATIC DIAGRAM OF ENTRANCE SECTION

FIGURE 10



MUD TRAP
FIGURE 11

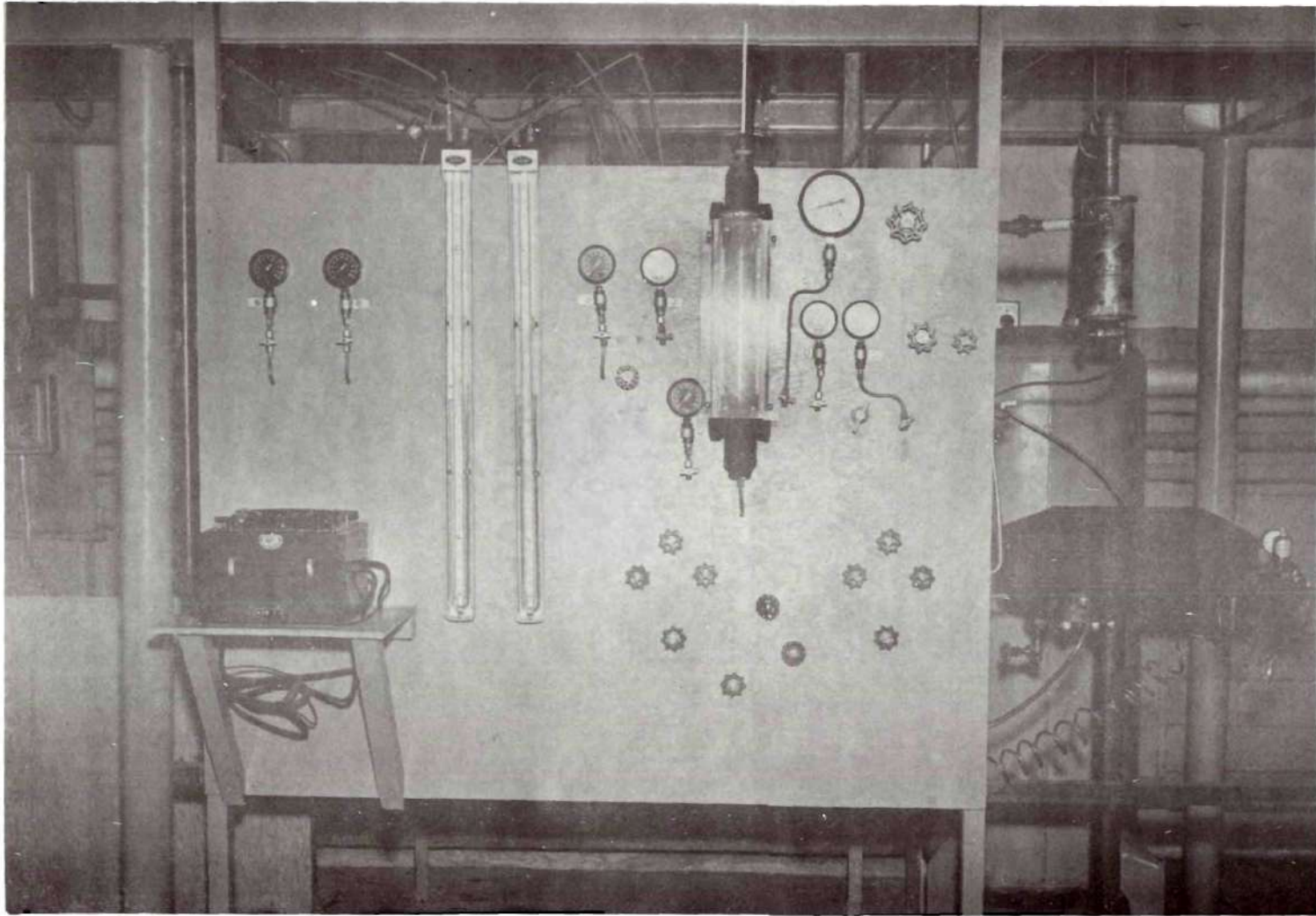
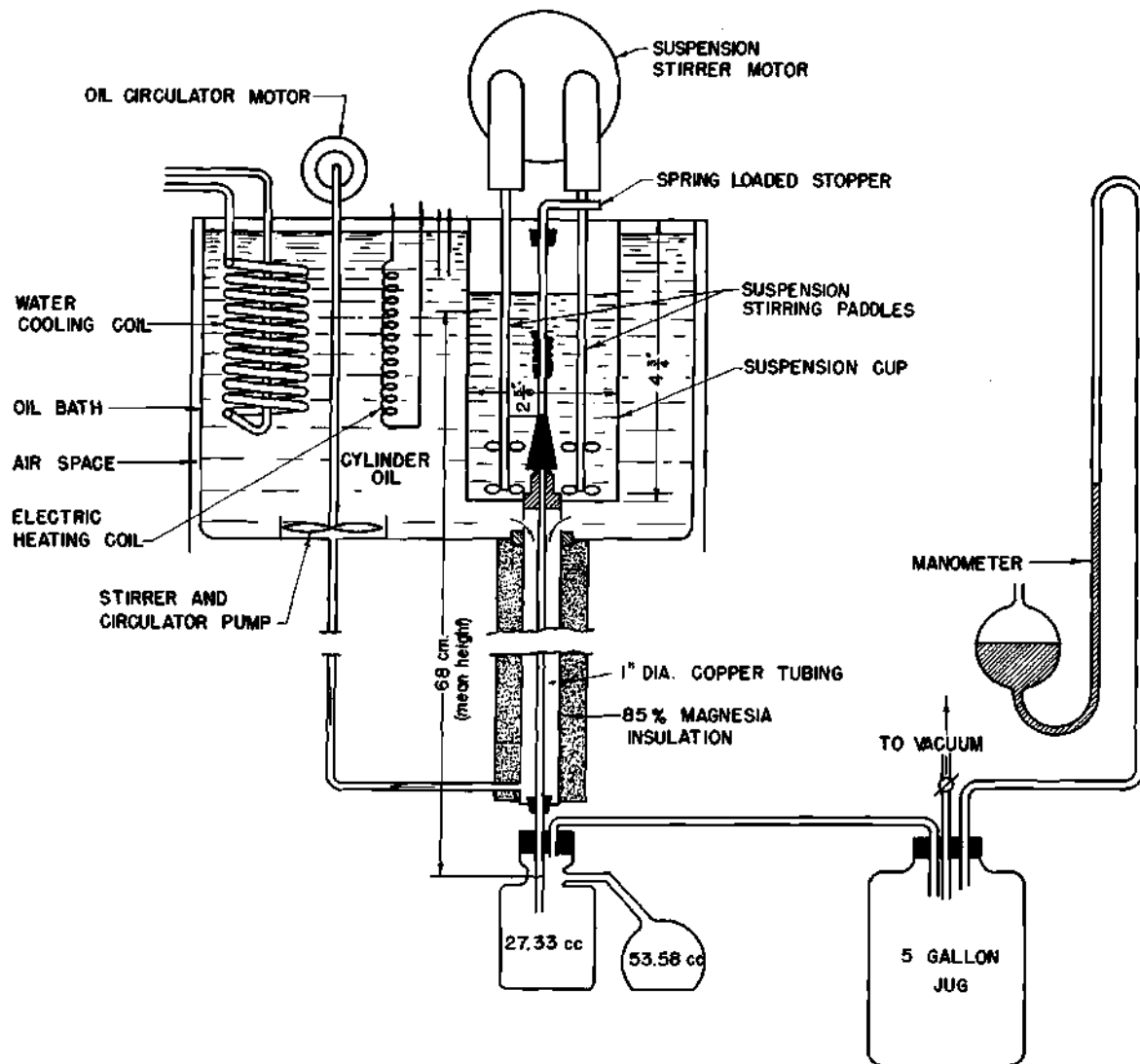
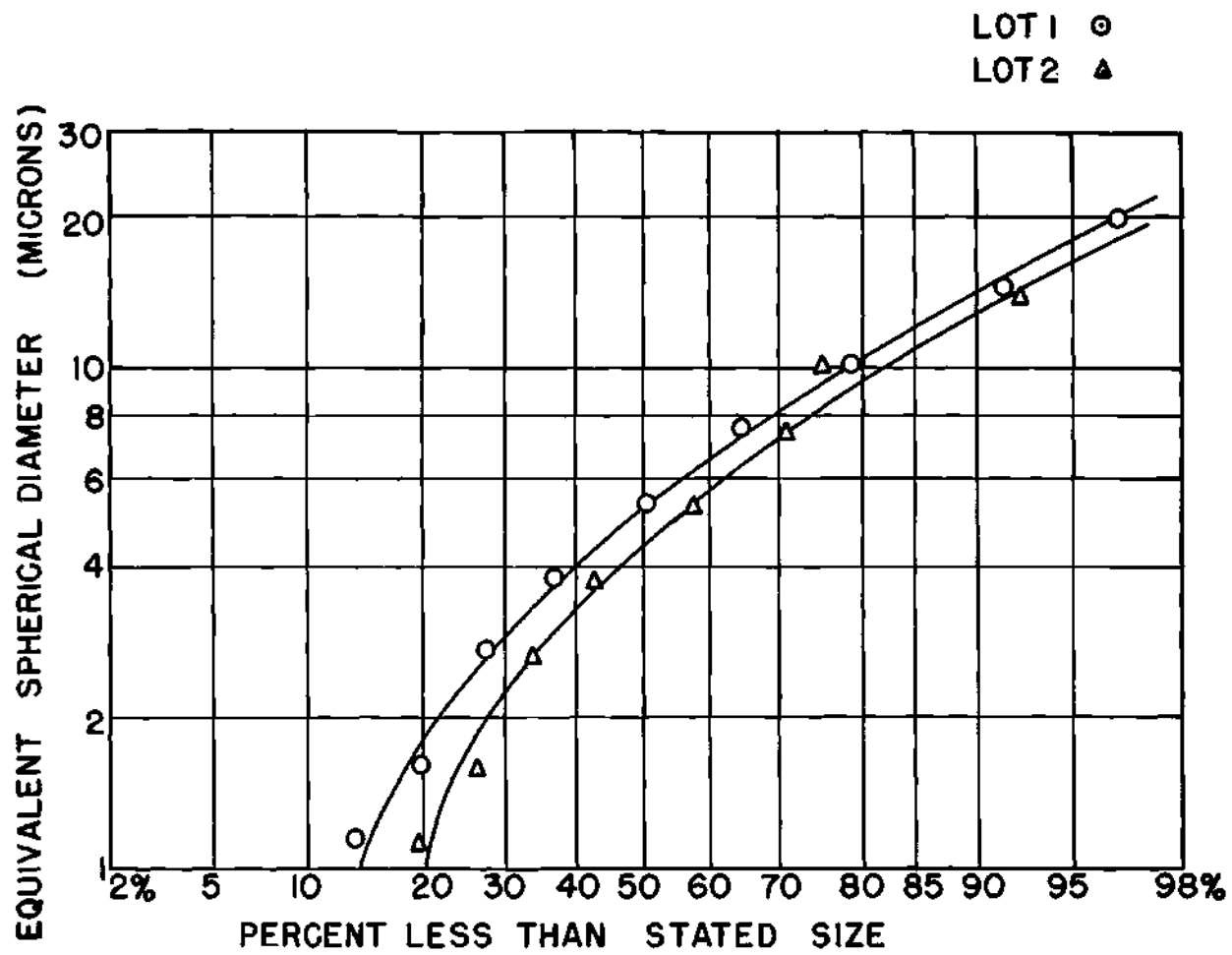


Figure 12. Instrument Panel.



SCHEMATIC DIAGRAM OF CAPILLARY TUBE VISCOMETER

FIGURE 13



PARTICLE SIZE DISTRIBUTION CURVES OF CLAYS BY THE
HYDROMETER METHOD

FIGURE 14

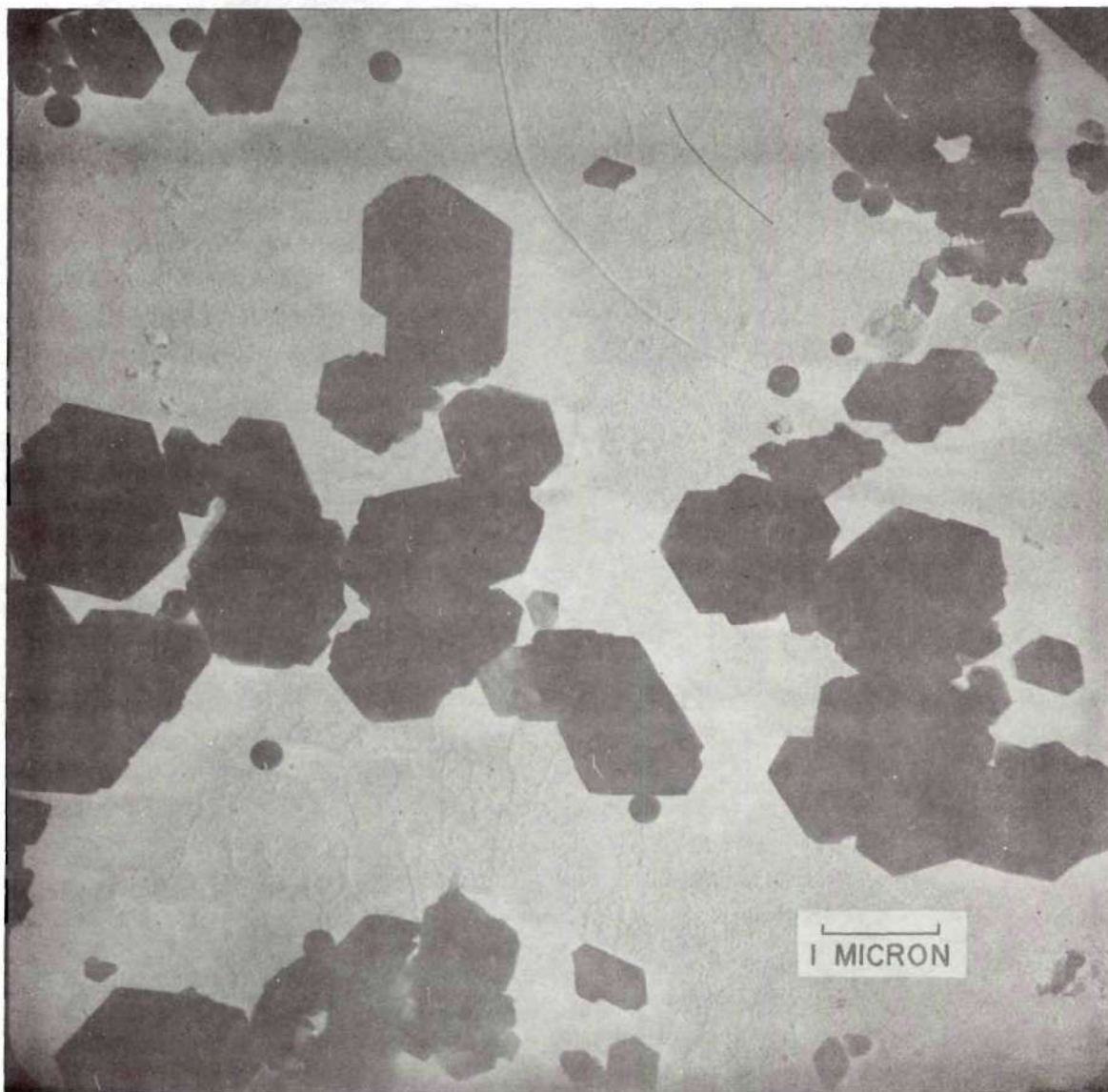


Figure 15. a) Electron Microscope Photograph of Kaolin Clay.

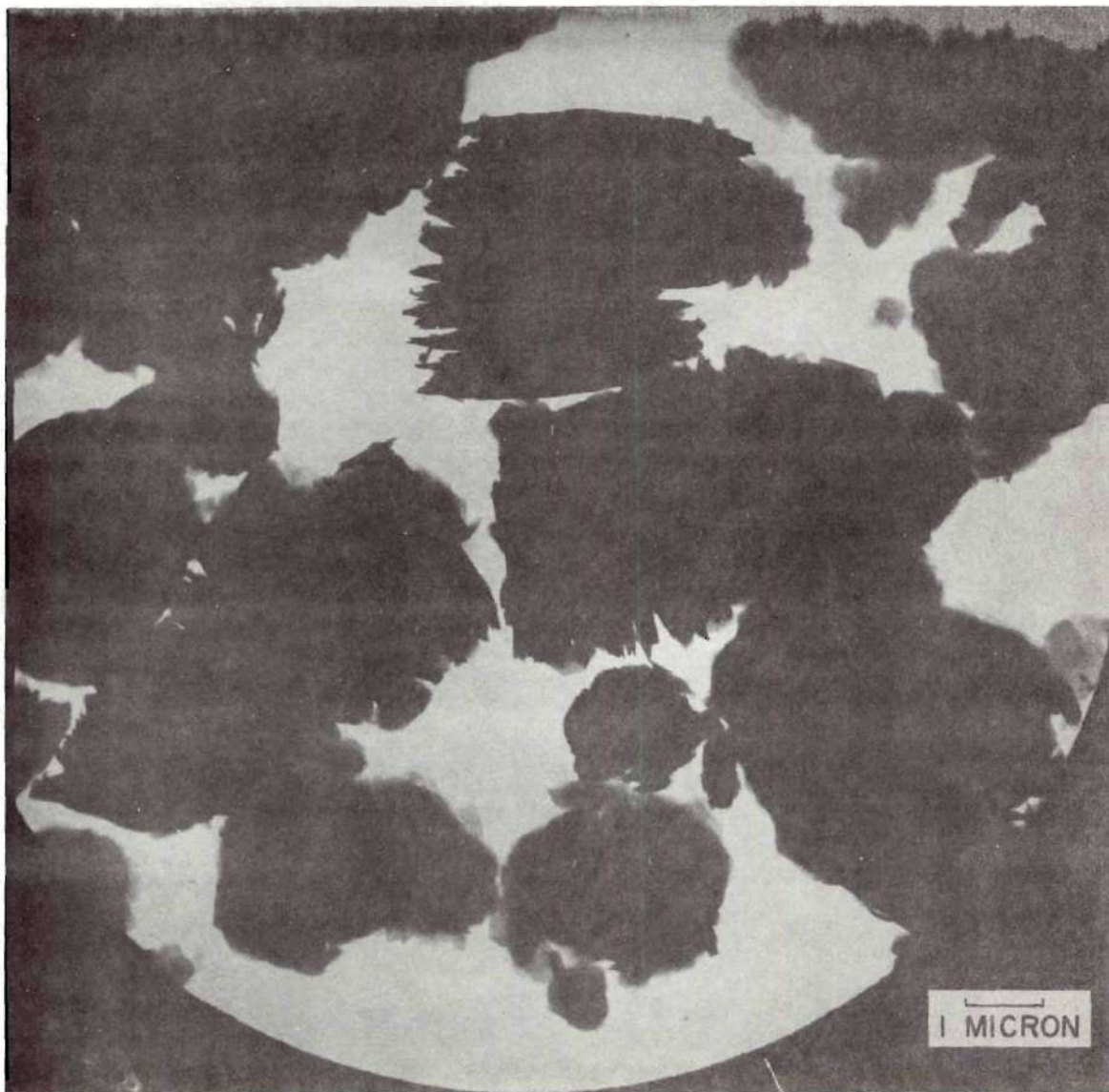
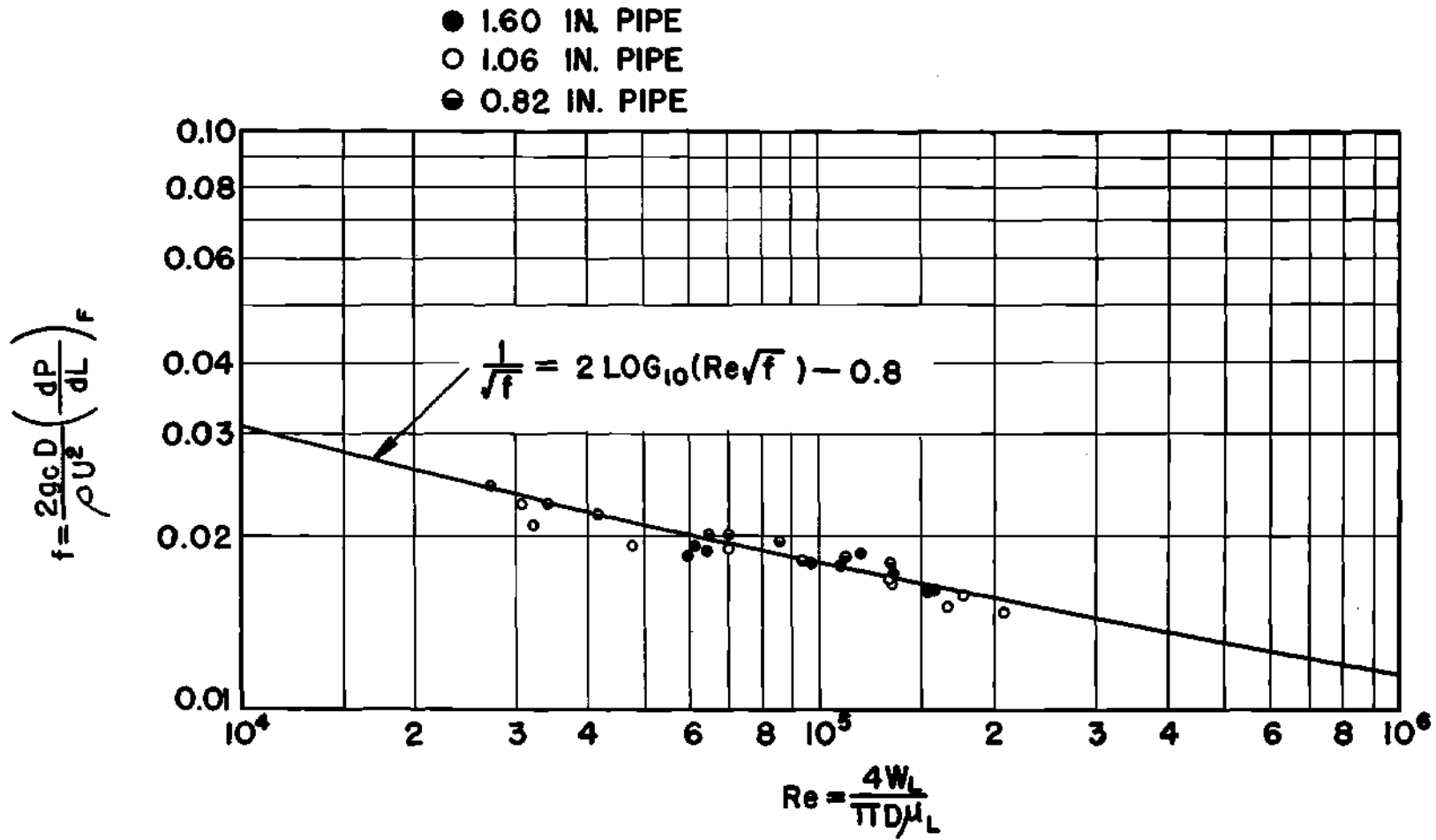


Figure 15. b) Electron Microscope Photograph of Kaolin Clay.



FRICTION FACTOR vs. REYNOLDS NUMBER
 FLOW OF WATER ALONE

FIGURE 16

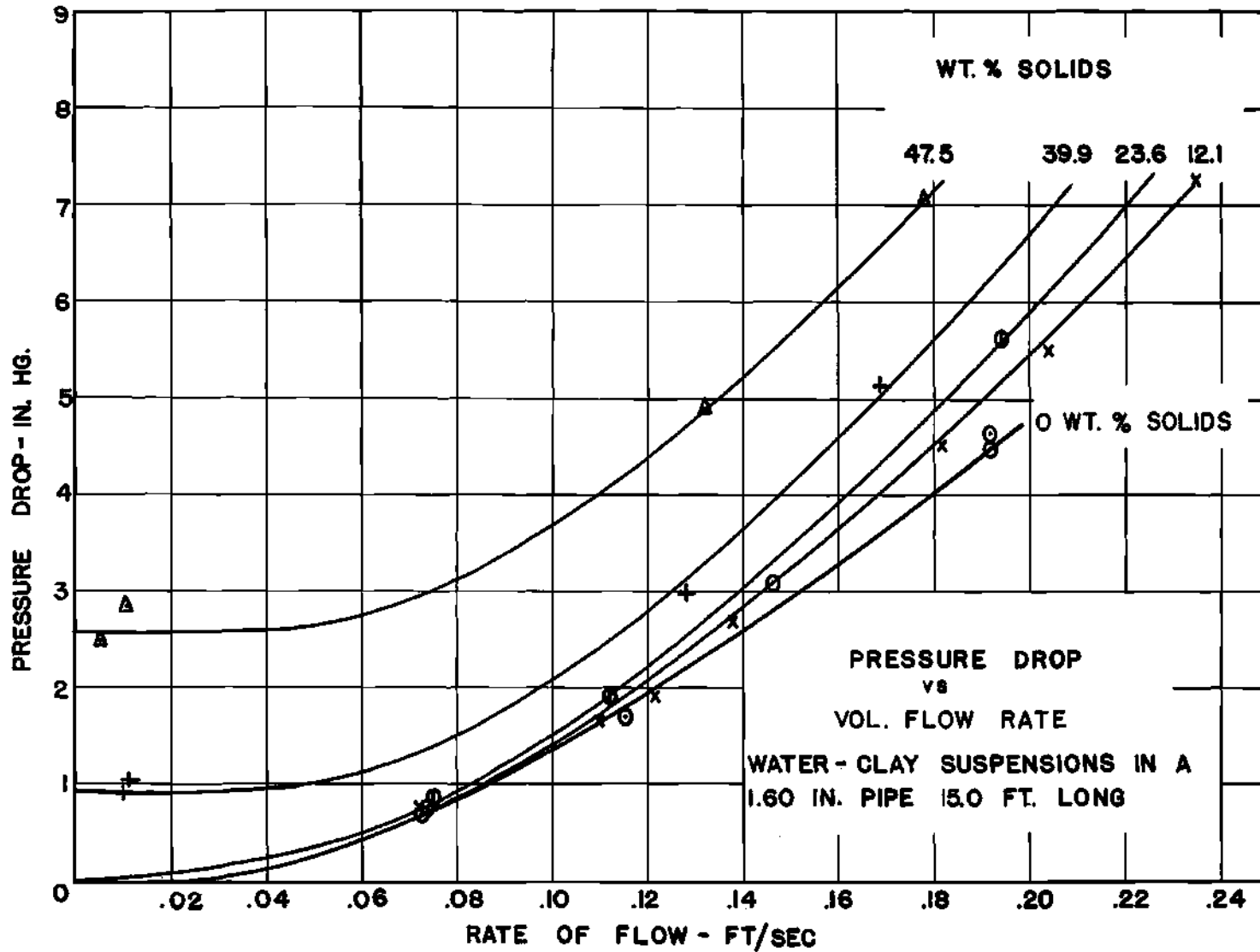


FIGURE 17

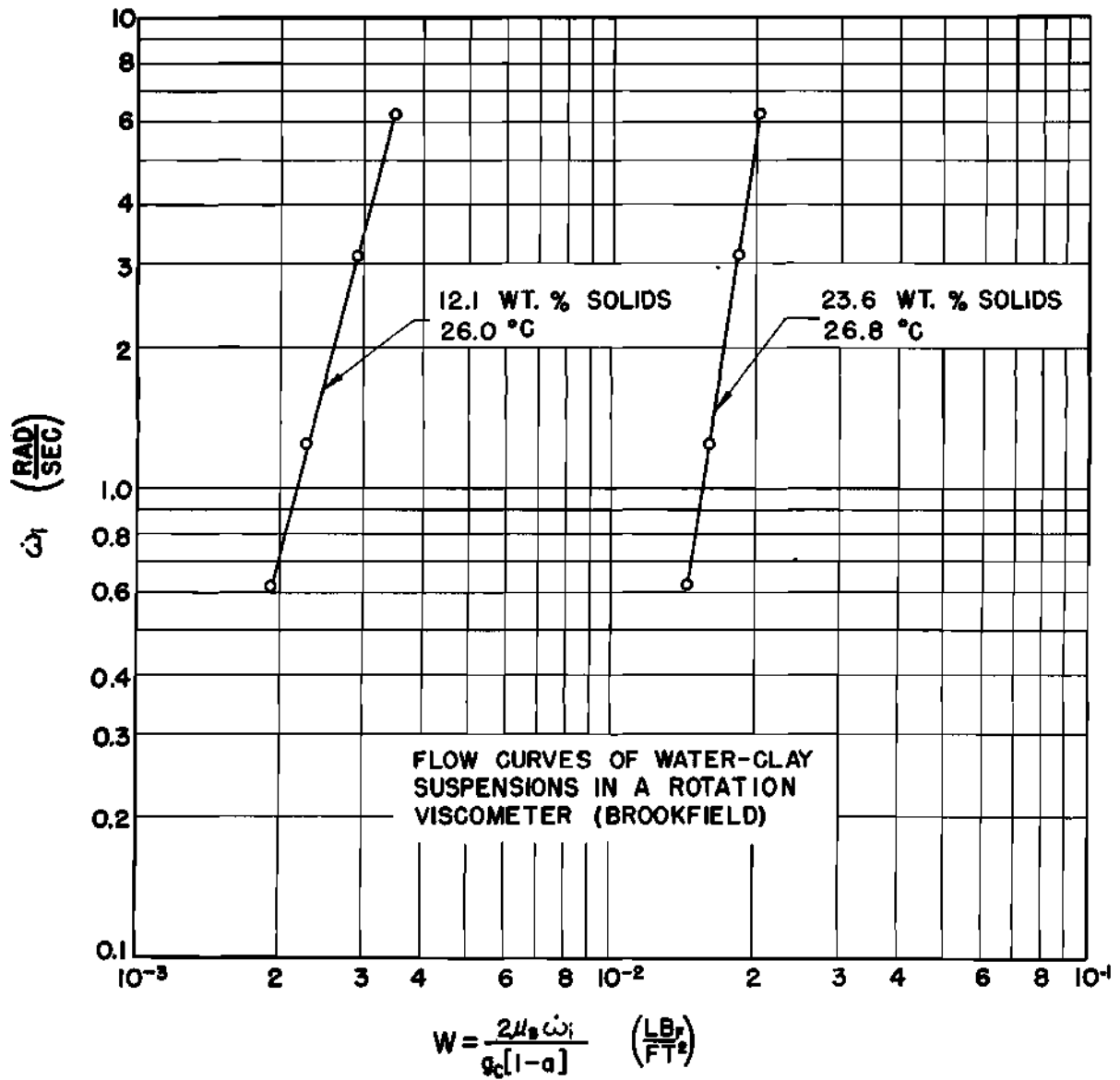
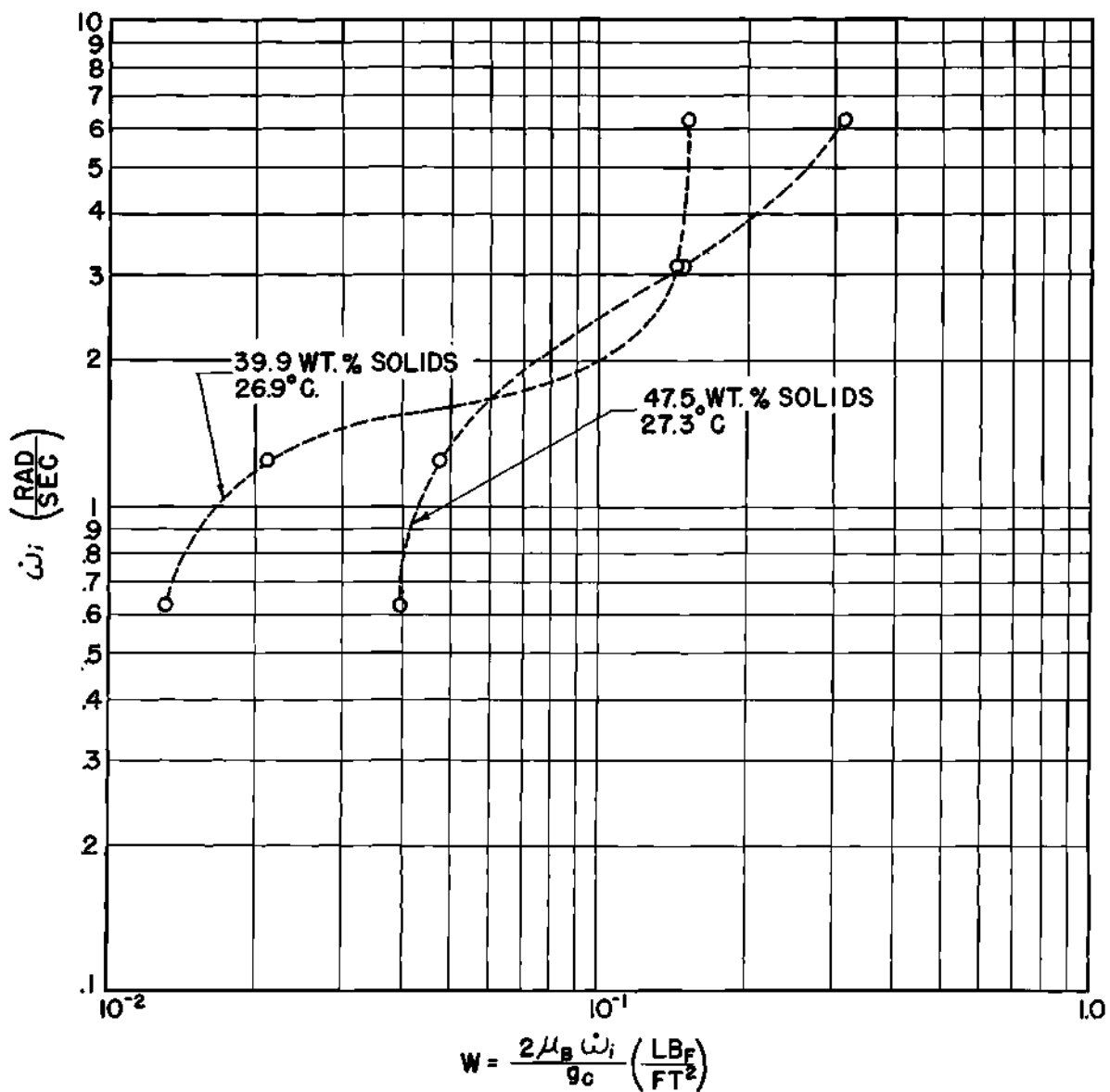


FIGURE 18



FLOW CURVES OF WATER-CLAY SUSPENSIONS IN A ROTATION
VISCOMETER (BROOKFIELD)

FIGURE 19

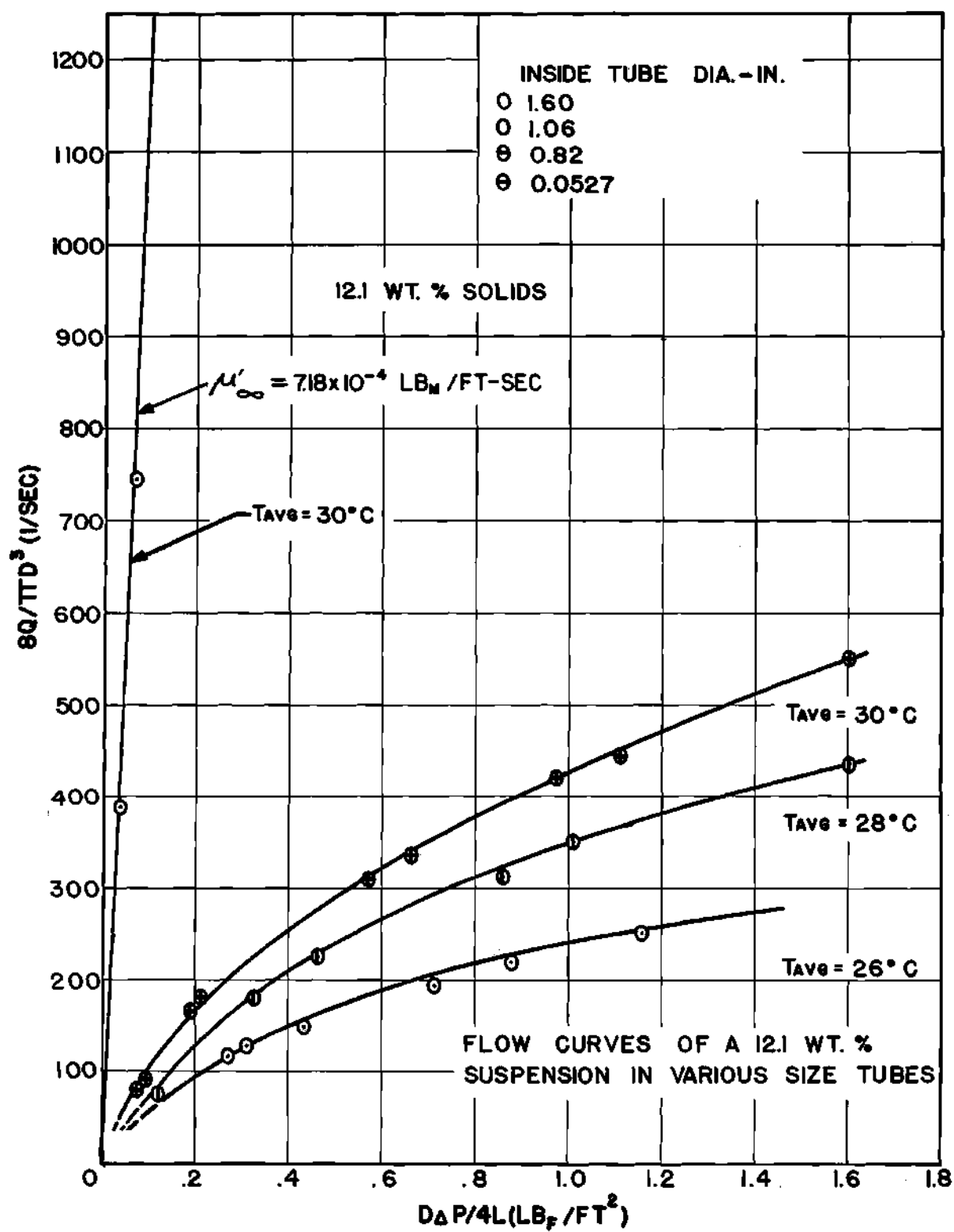


FIGURE 20

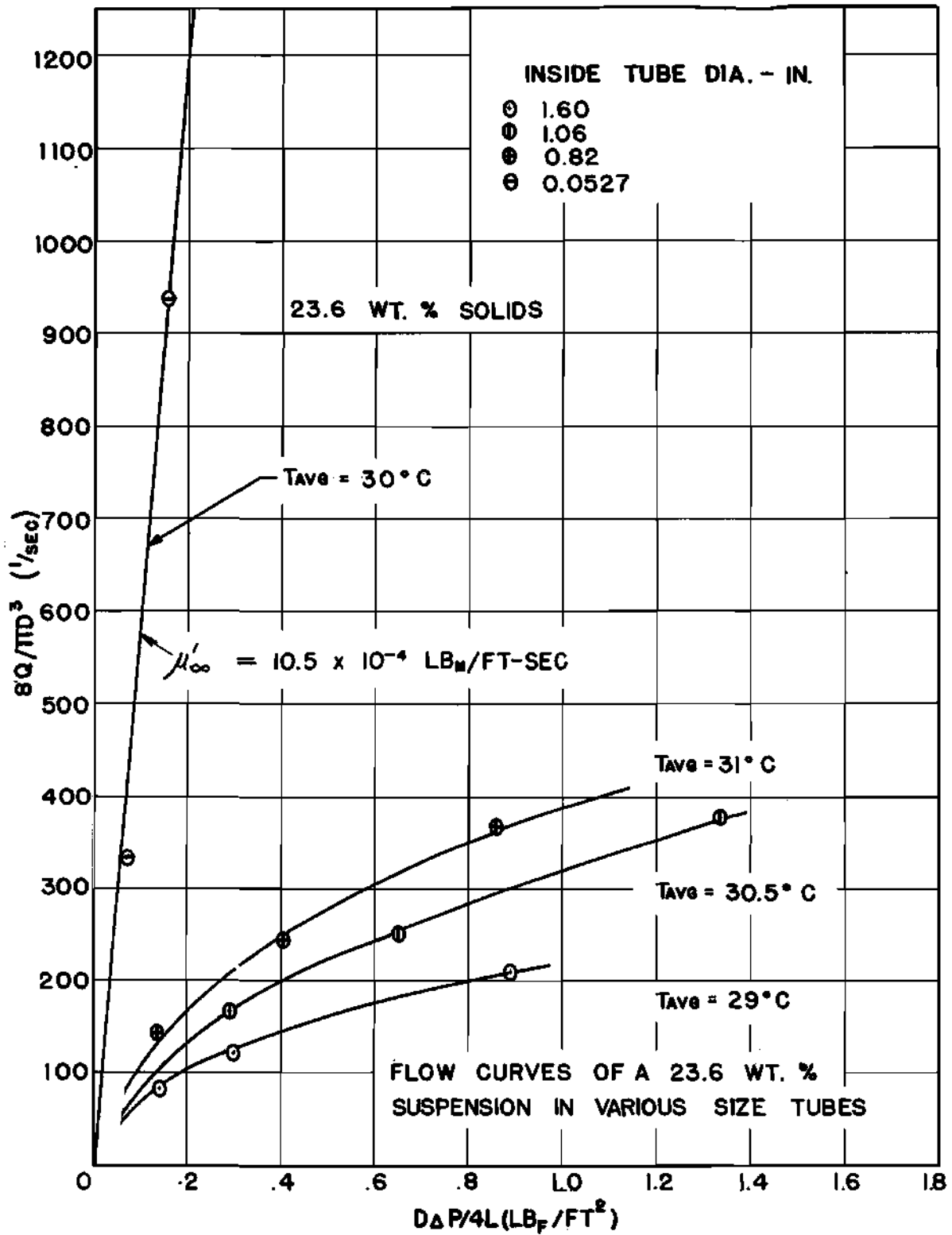


FIGURE 21

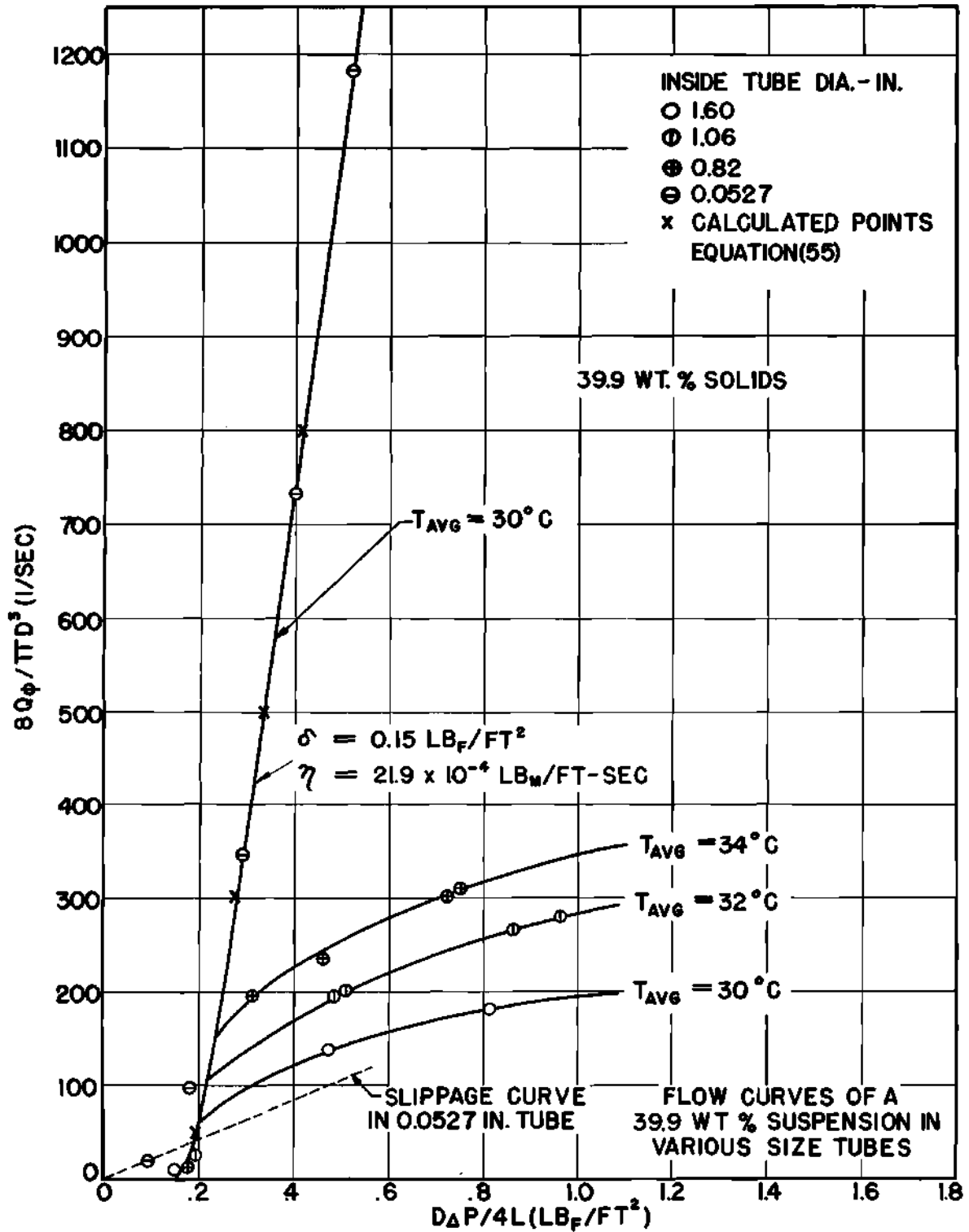


FIGURE 22

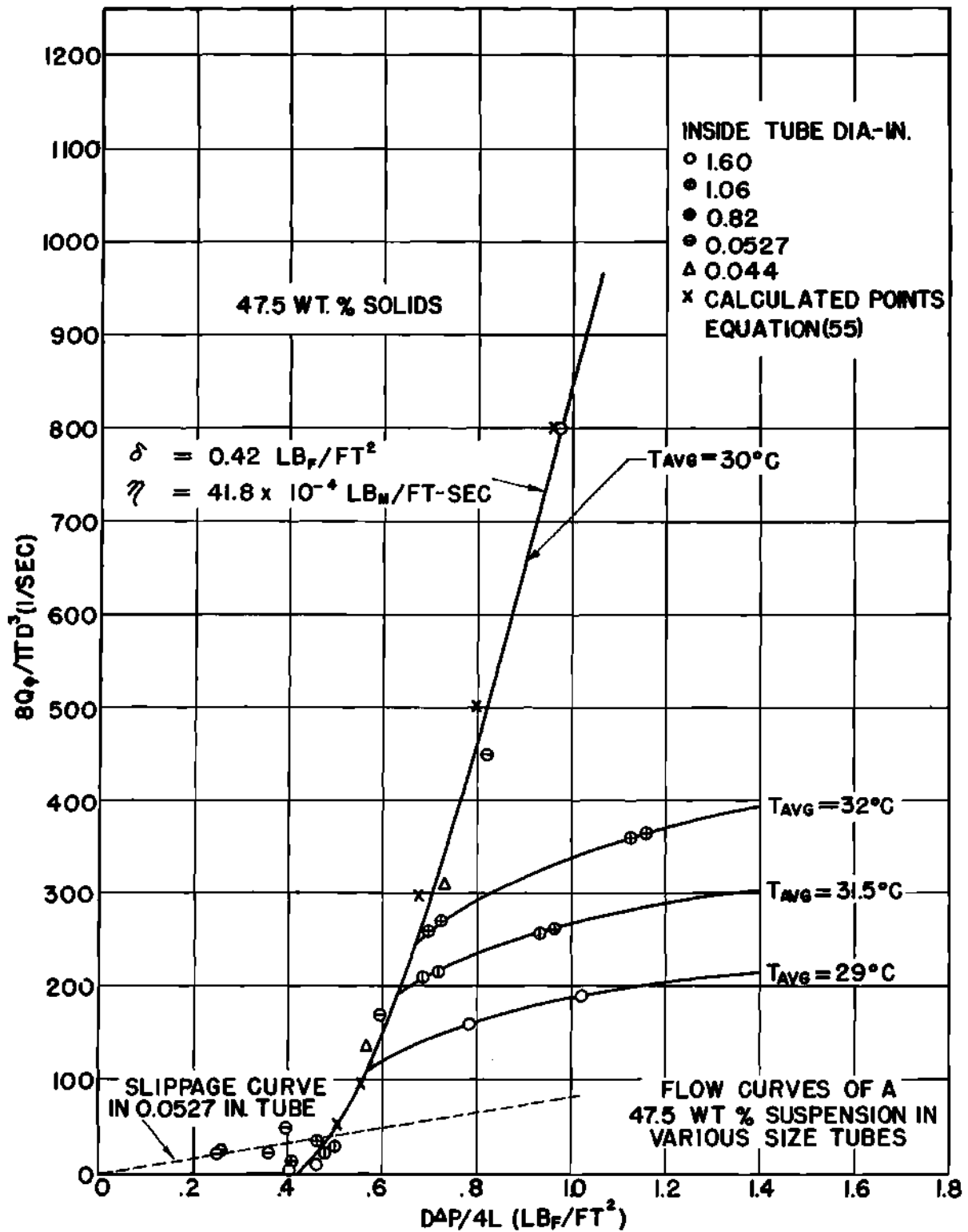
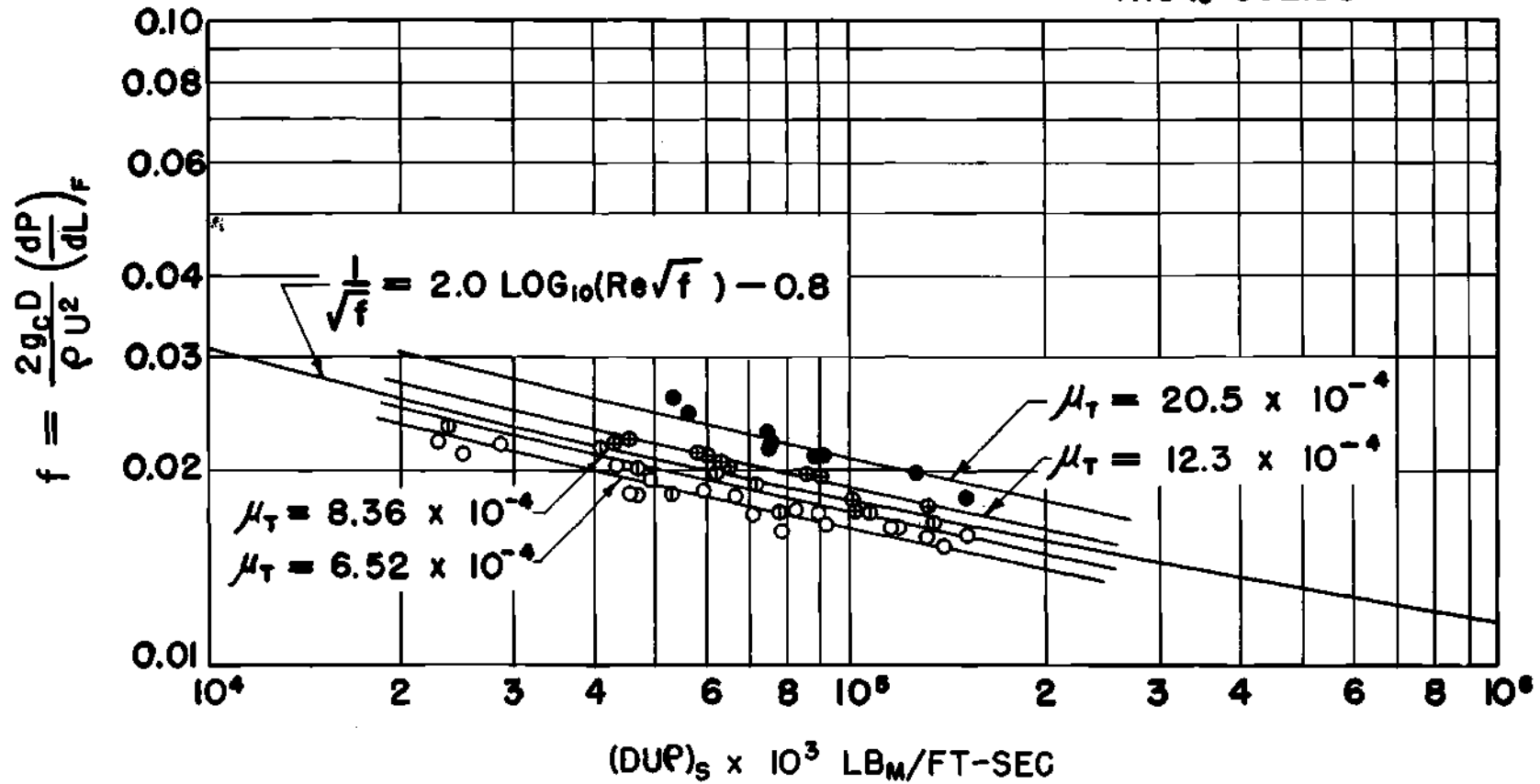


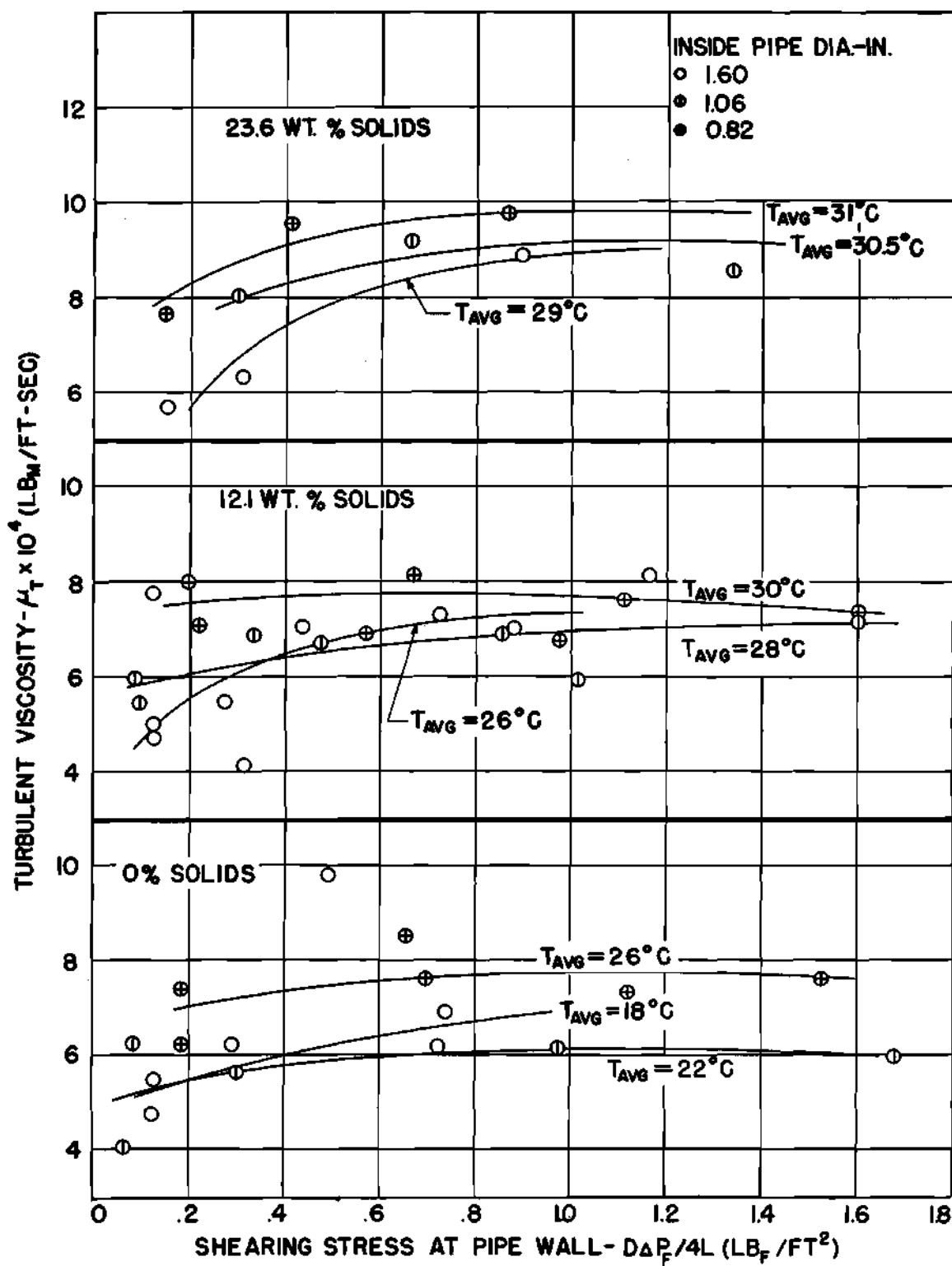
FIGURE 23

- 12.1% SOLIDS
- ◐ 23.6% SOLIDS
- 39.9% SOLIDS
- 47.5% SOLIDS

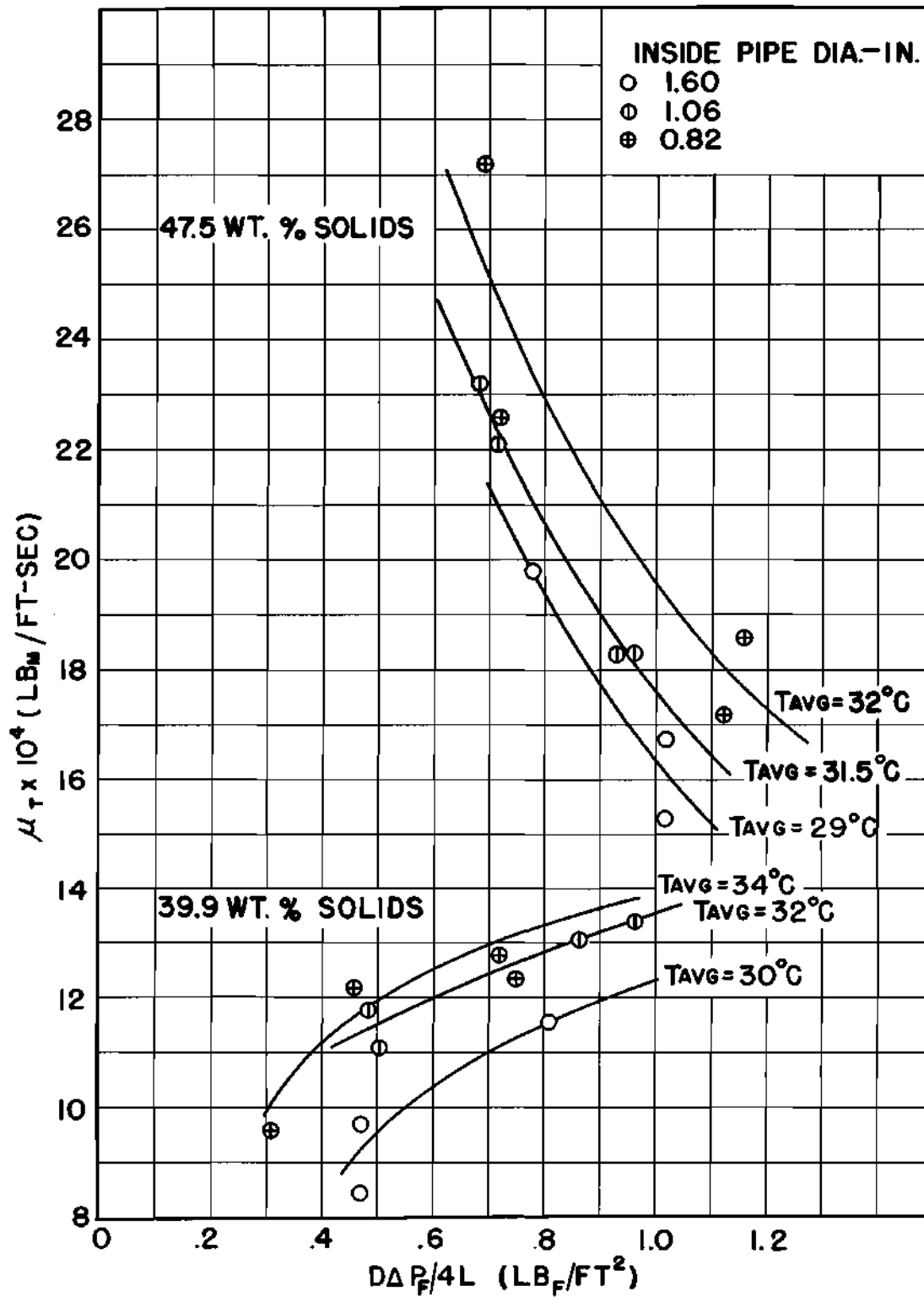


FRICION FACTOR vs. $(DUP)_{\text{SUSPENSION}}$

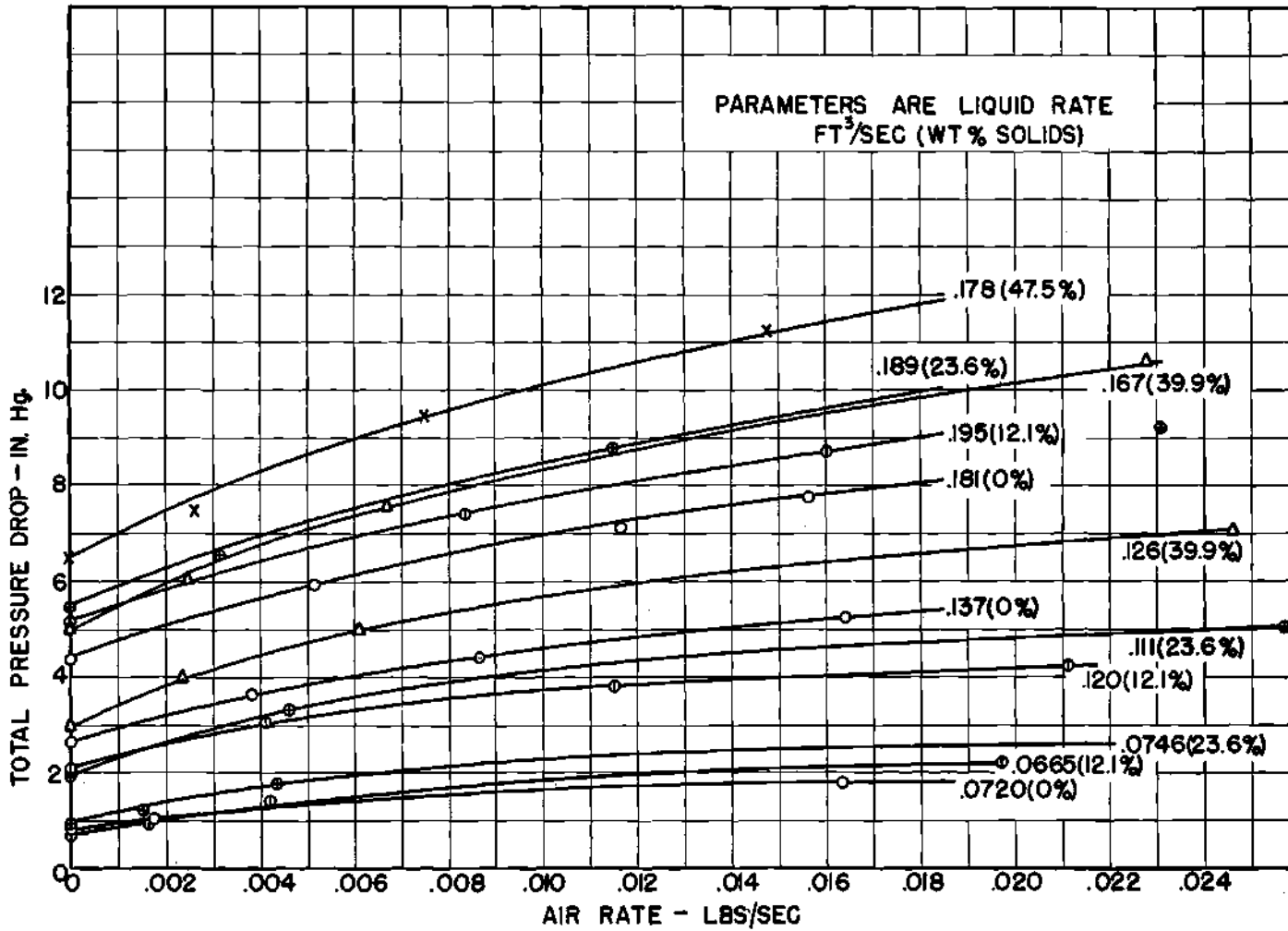
FIGURE 24



TURBULENT VISCOSITY vs. SHEARING STRESS AT PIPE WALL
 FIGURE 25

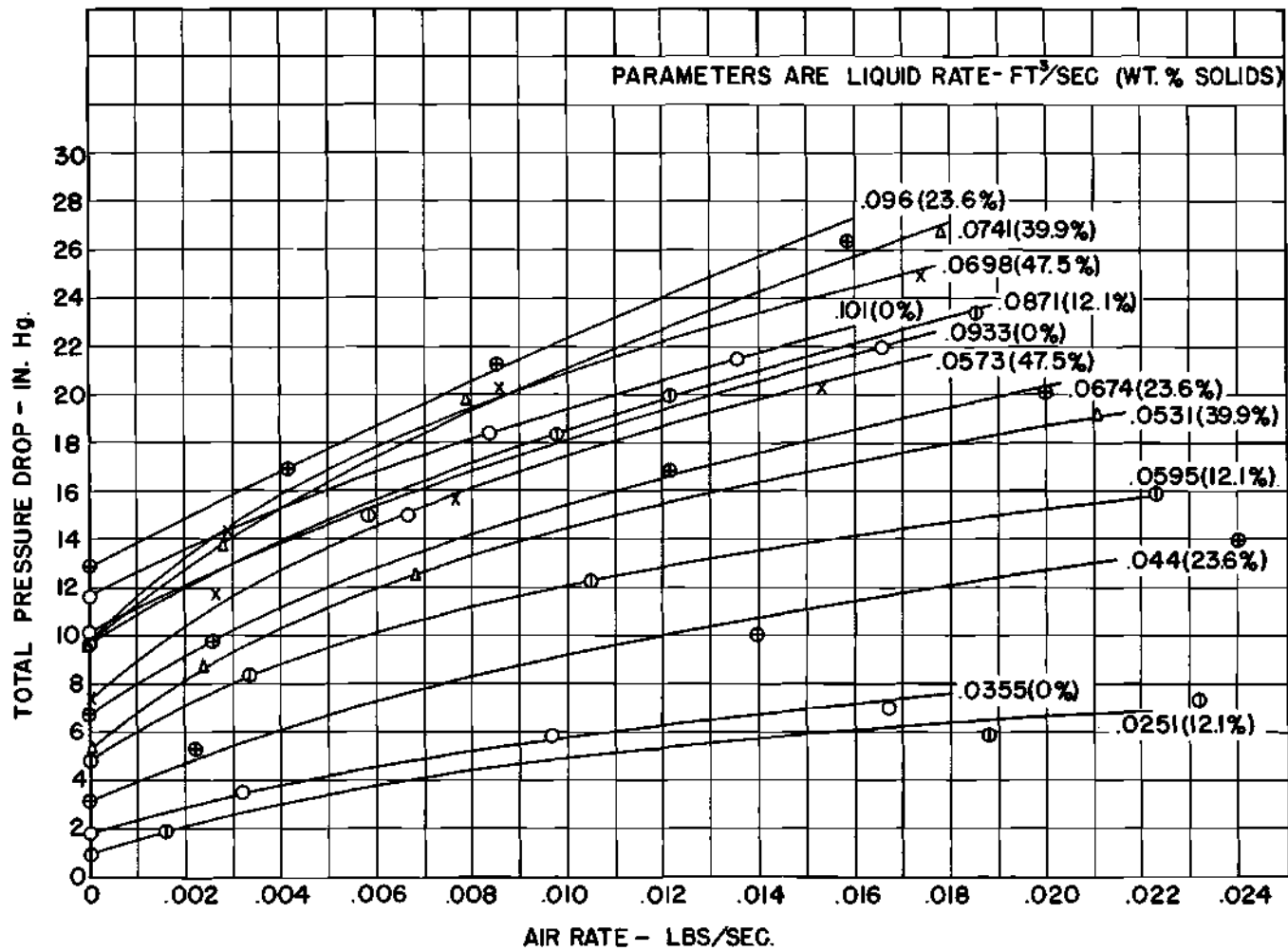


TURBULENT VISCOSITY VS. SHEARING STRESS AT PIPE WALL
 FIGURE 26



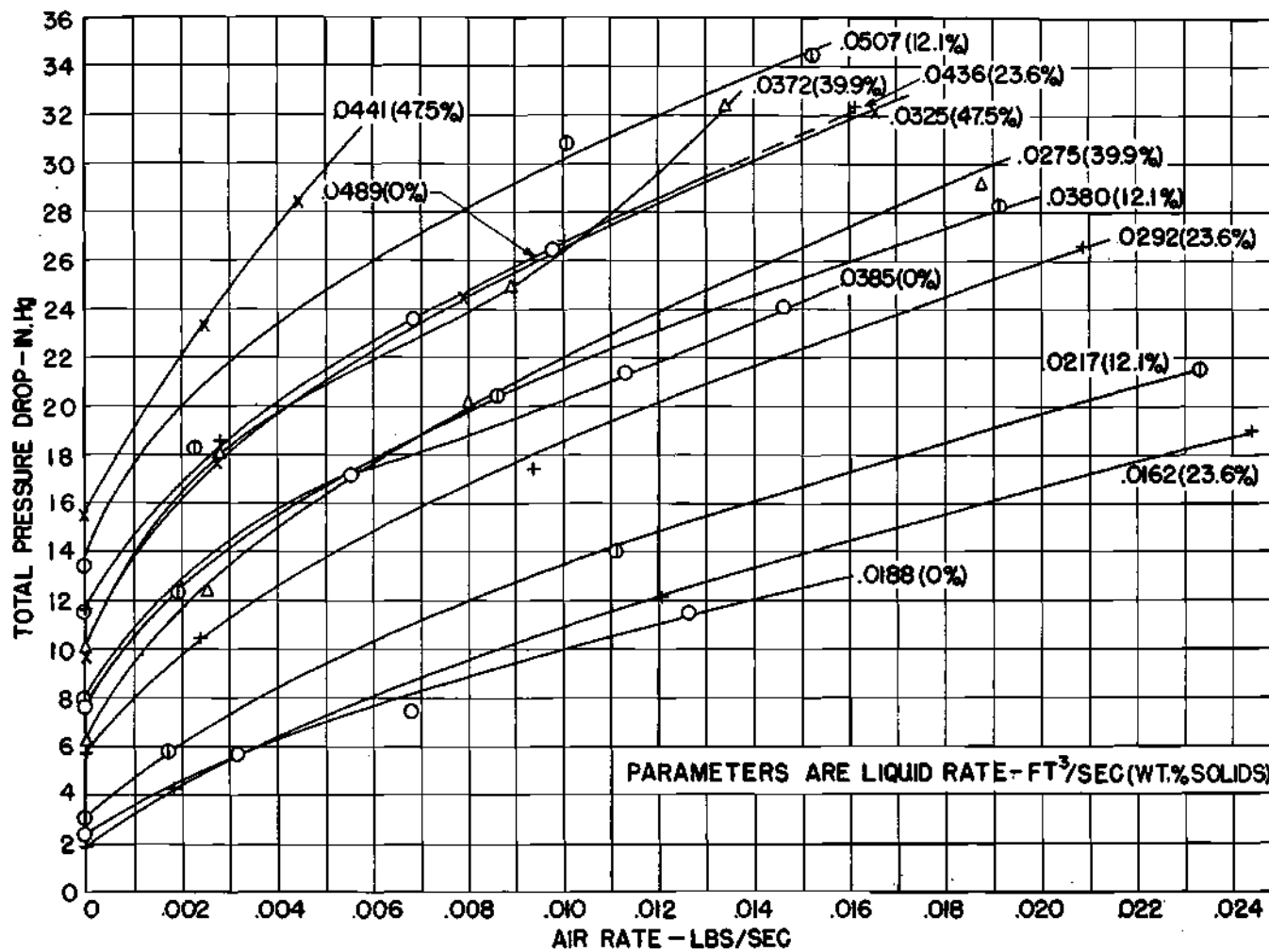
TOTAL PRESSURE DROP VS. AIR RATE CO-CURRENT TURBULENT-TURBULENT FLOW OF
AIR AND WATER-CLAY SUSPENSIONS IN A 1.60 IN. PIPE 15.0 FEET LONG

FIGURE 27



TOTAL PRESSURE DROP VS. AIR RATE CO-CURRENT TURBULENT-TURBULENT FLOW OF
AIR AND WATER-CLAY SUSPENSIONS IN A 1.06 IN. PIPE 16.55 FT. LONG

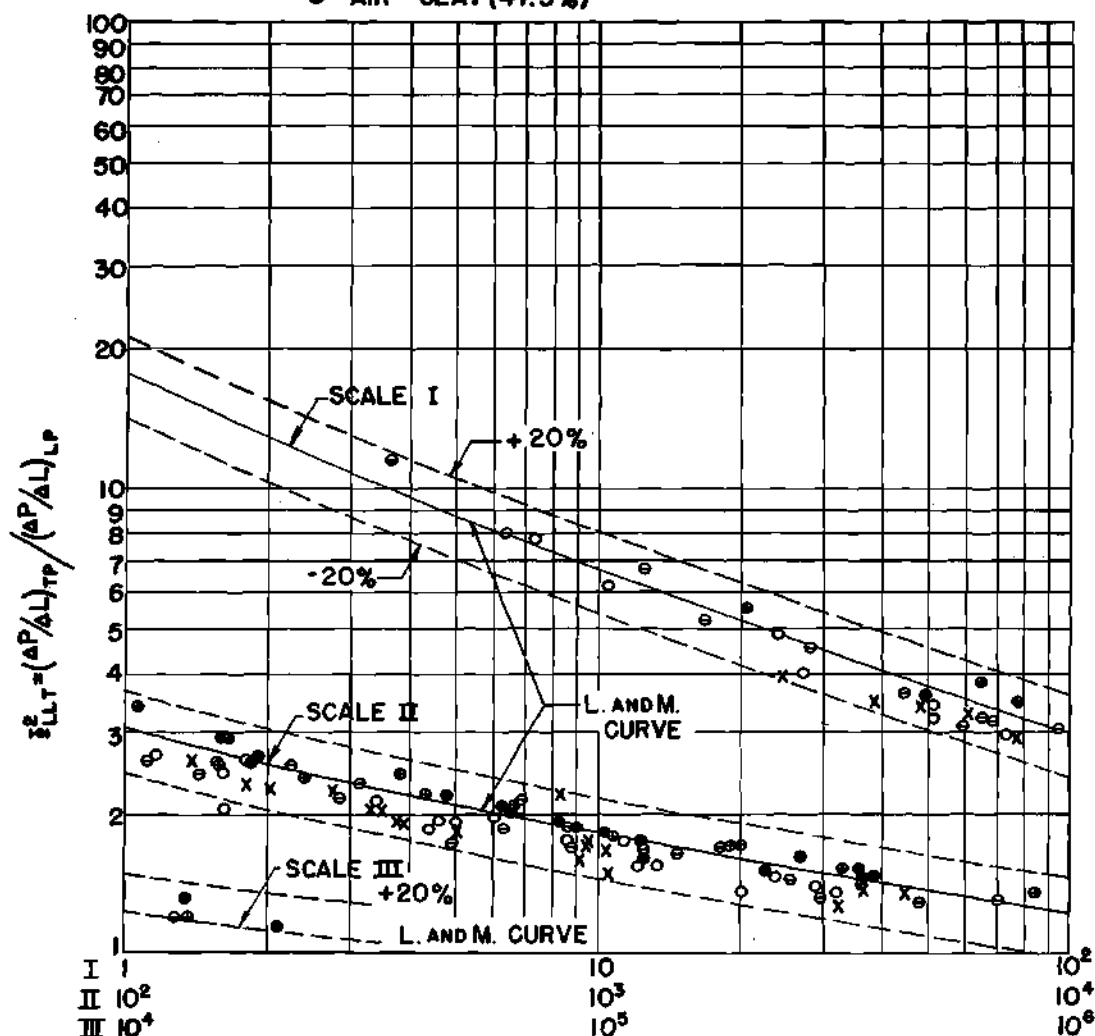
FIGURE 28



TOTAL PRESSURE DROP VS. AIR RATE CO-CURRENT TURBULENT-TURBULENT FLOW OF AIR AND WATER-CLAY SUSPENSIONS IN A 0.82 IN. PIPE 17.25 FT. LONG

FIGURE 29

- X AIR-WATER
- O AIR-CLAY (12.1%)
- ⊖ AIR-CLAY (23.6%)
- ⊕ AIR-CLAY (39.9%)
- AIR-CLAY (47.5%)

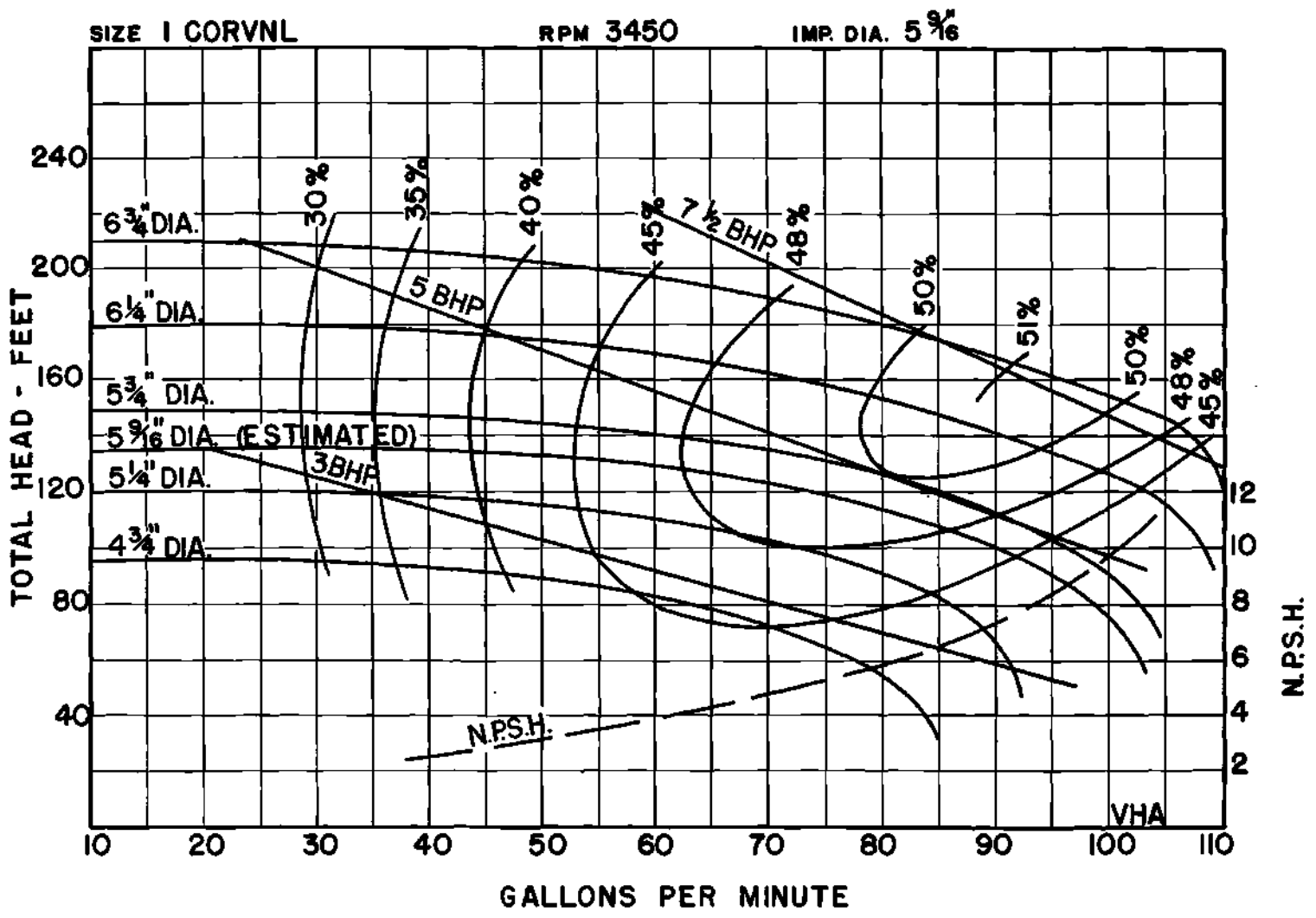


$$x^2 = \frac{\text{PRESSURE DROP PER UNIT LENGTH FOR LIQUID PHASE ALONE}}{\text{PRESSURE DROP PER UNIT LENGTH FOR GAS PHASE ALONE}}$$

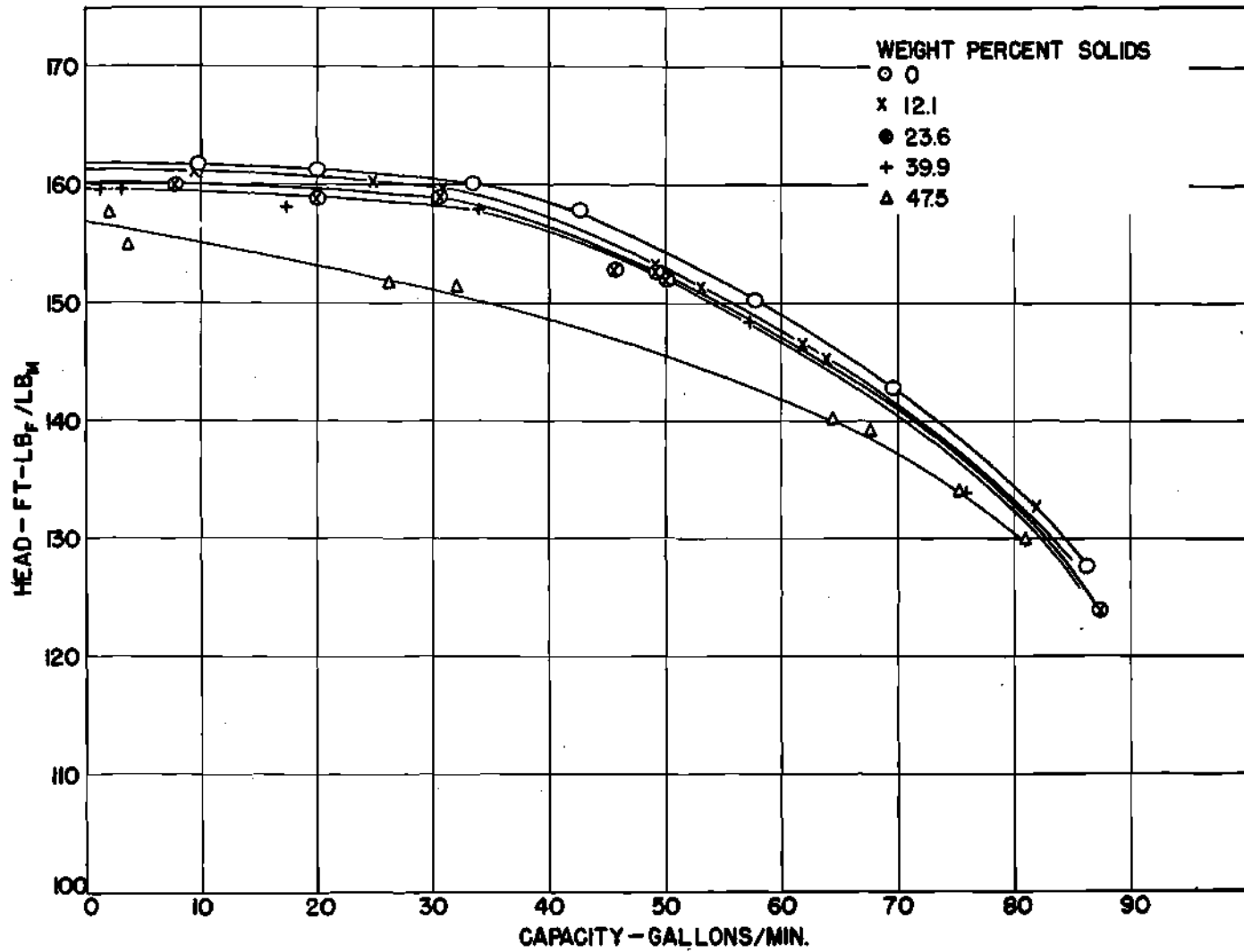
$$\frac{(\Delta P/\Delta L)_{LP}}{(\Delta P/\Delta L)_{GP}}$$

COMPARISON OF DATA FOR CO-CURRENT TURBULENT-TURBULENT FLOW OF AIR AND WATER-CLAY SUSPENSIONS IN 1.60, 1.06 AND 0.82 IN. PIPES WITH CORRELATION OF LOCKHART AND MARTINELLI (8)

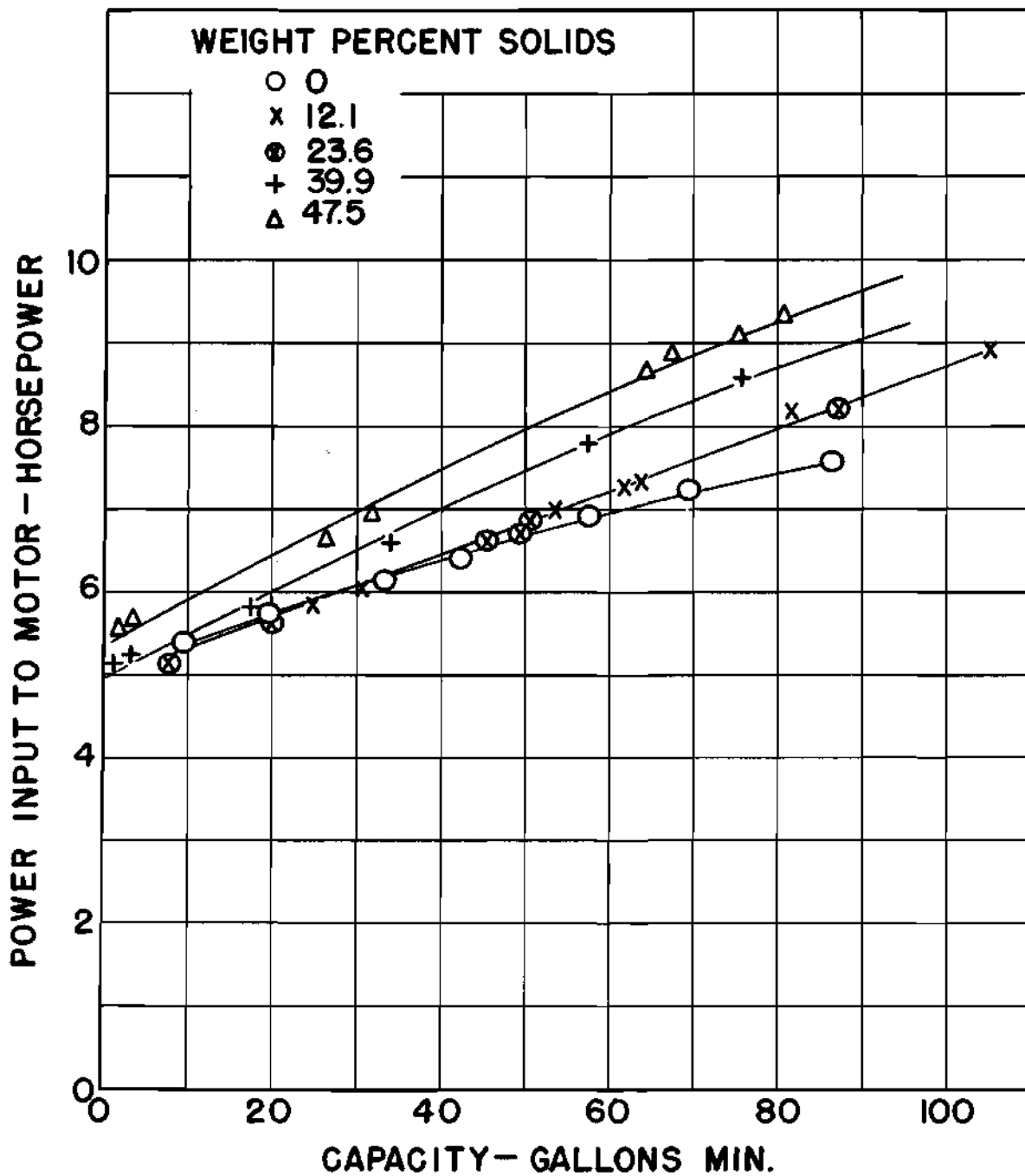
FIGURE 30



PREDICTED PUMP CHARACTERISTIC CURVES
FIGURE 31



HEAD vs. CAPACITY CURVES FOR CENTRIFUGAL
PUMP HANDLING WATER-CLAY SUSPENSIONS
FIGURE 32



POWER VS. CAPACITY CURVES FOR CENTRIFUGAL PUMP HANDLING WATER-CLAY SUSPENSIONS

FIGURE 33

APPENDICES

	Page
I Derivation of Lockhart and Martinelli's Correlation (8).	144
II Brookfield Synchro-lectric Viscometer.	150
III Comparison of Rotational and Cylindrical Tube Instrument Data (11).	152
IV Pressure Transmitter Calibration	158
V Rotameter Calibration.	160
VI Development of Equations for Determining Pump Characteristics.	162
VII Sample Calculations	
A. Curves Used in Calculations.	166
B. Flow of Water Alone in a 1.60 Inch Pipe.	174
C. Flow of a 23.6 Weight Percent (Sp. Gr. 1.164) Water-Clay Suspension in a 1.06 Inch Pipe	176
D. Co-Current Flow of Air and Water in a 0.82 Inch Pipe	179
E. Co-Current Flow of Air and a Water-Clay Suspension of Specific Gravity 1.313 Containing 39.9 Weight Percent Solids in a 1.60 Inch Pipe	182

APPENDIX I

DERIVATION OF LOCKHART AND MARTINELLI'S CORRELATION (8)

The basic assumptions upon which this correlation for the co-current flow of a gas and a liquid in cylindrical pipes is based are:

1. That the frictional pressure drop in the liquid phase is equal to the frictional pressure drop in the gas phase.
2. That the volume of the liquid plus the volume of the gas at any instant is equal to the volume of the pipe.

These assumptions require that the flow pattern is steady with respect to both time and distance.

Utilizing the first assumption and expressing the frictional pressure drops by the usual Fanning equation

$$\left(\frac{\Delta P}{\Delta L}\right)_{TP} = 2f_L \frac{\rho_L U_L^2}{D_L g_c} = 2f_G \frac{\rho_G U_G^2}{D_G g_c} \quad (I-1)$$

where D_L and D_G are the hydraulic diameters of the liquid and gas phases respectively. Since for a cylindrical flow area, the hydraulic diameter is given by

$$A = \frac{\pi}{4} D_H^2 \quad (I-2)$$

the respective flow areas of each phase may be written as

$$A_L = \alpha \left(\frac{\pi}{4} D_L^2 \right) \quad (I-3)$$

$$A_G = \beta \left(\frac{\pi}{4} D_G^2 \right) \quad (I-4)$$

where the parameters α and β are introduced to permit the hydraulic diameters D_L and D_G to be defined by the simple equations above. Using

these equations, the respective velocities of each phase are given by

$$U_L = \frac{W_L}{\alpha \left(\frac{\pi D_L^2}{4} \right) \rho_L} \cdot \frac{D_P^2}{D_P^2} = \left(\frac{W_L}{\pi D_P^2 \rho_L} \right) \left(\frac{1}{\alpha} \right) \left(\frac{D_P}{D_L} \right)^2 = \frac{U_{LP} \left(\frac{D_P}{D_L} \right)^2}{\alpha} \quad (I-5)$$

$$U_G = \frac{W_G}{\beta \left(\frac{\pi D_G^2}{4} \right) \rho_G} \cdot \frac{D_P^2}{D_P^2} = \frac{U_{GP} \left(\frac{D_P}{D_G} \right)^2}{\beta} \quad (I-6)$$

where D_P is the pipe diameter and U_{LP} and U_{GP} are the velocities of the liquid and gas phases respectively based on the cross-sectional area of the pipe. Expressing the friction factors in the generalized Blasius form, they become

$$f_L = \frac{C_L}{(Re_L)^n} = \frac{C_L}{\left(\frac{D_L U_L \rho_L}{\mu_L} \right)^n} = \frac{C_L \alpha^n \left(\frac{D_L}{D_P} \right)^n}{(Re_{LP})^n} = f_{LP} \alpha^n \left(\frac{D_L}{D_P} \right)^n \quad (I-7)$$

$$f_G = \frac{C_G}{(Re_G)^m} = f_{GP} \beta^m \left(\frac{D_G}{D_P} \right)^m \quad (I-8)$$

where the subscripts LP and GP denote superficial quantities, that is based on the cross-sectional area of the pipe. Before substituting these equations into equation (I-1) it should be pointed out that the velocities in the equation (I-1) involve the relative velocities between the fluids and the substitutions will not be exact. However, these investigators point out that since the quantities α and β are derived from experimental data, the error is not so serious as might first appear. Making these substitutions and simplifying, the result is

$$\left(\frac{\Delta P}{\Delta L} \right)_{TP} = \left(\frac{\Delta P}{\Delta L} \right)_{LP} \alpha^n - 2 \left(\frac{D_P}{D_L} \right)^{5-n} = \left(\frac{\Delta P}{\Delta L} \right)_{GP} \beta^m - 2 \left(\frac{D_P}{D_G} \right)^{5-m} \quad (I-9)$$

where $(\Delta P/\Delta L)_{LP}$ and $(\Delta P/\Delta L)_{GP}$ are the pressure drops for the flow of the liquid and gas phases respectively alone in the pipe. The three equations of (I-9) can be written as

$$\left[\frac{\left(\frac{\Delta P}{\Delta L} \right)_{TP}}{\left(\frac{\Delta P}{\Delta L} \right)_{LP}} \right]^{1/2} \equiv \Psi_L = \alpha \left(\frac{D_P}{D_L} \right)^{\frac{5-n}{2}} \quad (I-10)$$

$$\left[\frac{\left(\frac{\Delta P}{\Delta L} \right)_{TP}}{\left(\frac{\Delta P}{\Delta L} \right)_{GP}} \right]^{1/2} \equiv \Psi_L = \beta \left(\frac{D_P}{D_G} \right)^{\frac{5-m}{2}} \quad (I-11)$$

$$\left[\frac{\left(\frac{\Delta P}{\Delta L} \right)_{LP}}{\left(\frac{\Delta P}{\Delta L} \right)_{GP}} \right]^{1/2} \equiv X = \frac{\beta \left(\frac{D_P}{D_G} \right)^{\frac{5-m}{2}}}{\alpha \left(\frac{D_P}{D_L} \right)^{\frac{5-n}{2}}} \quad (I-12)$$

where the quantities Ψ_L , Ψ_G and X are introduced for simplicity.

Application of the second assumption, that the volume of the liquid plus the volume of the gas equals the volume of the pipe, gives

$$\alpha D_L^2 + \beta D_G^2 = D_P^2. \quad (I-13)$$

The fractions of the pipe, R_G and R_L , occupied by the gas and liquid respectively are

$$R_G = \frac{\beta D_G^2}{D_P^2} = 1 - \alpha \left(\frac{D_L}{D_P} \right)^2 \quad \text{or} \quad \alpha = R_L \left(\frac{D_P}{D_L} \right)^2 \quad (I-14)$$

and

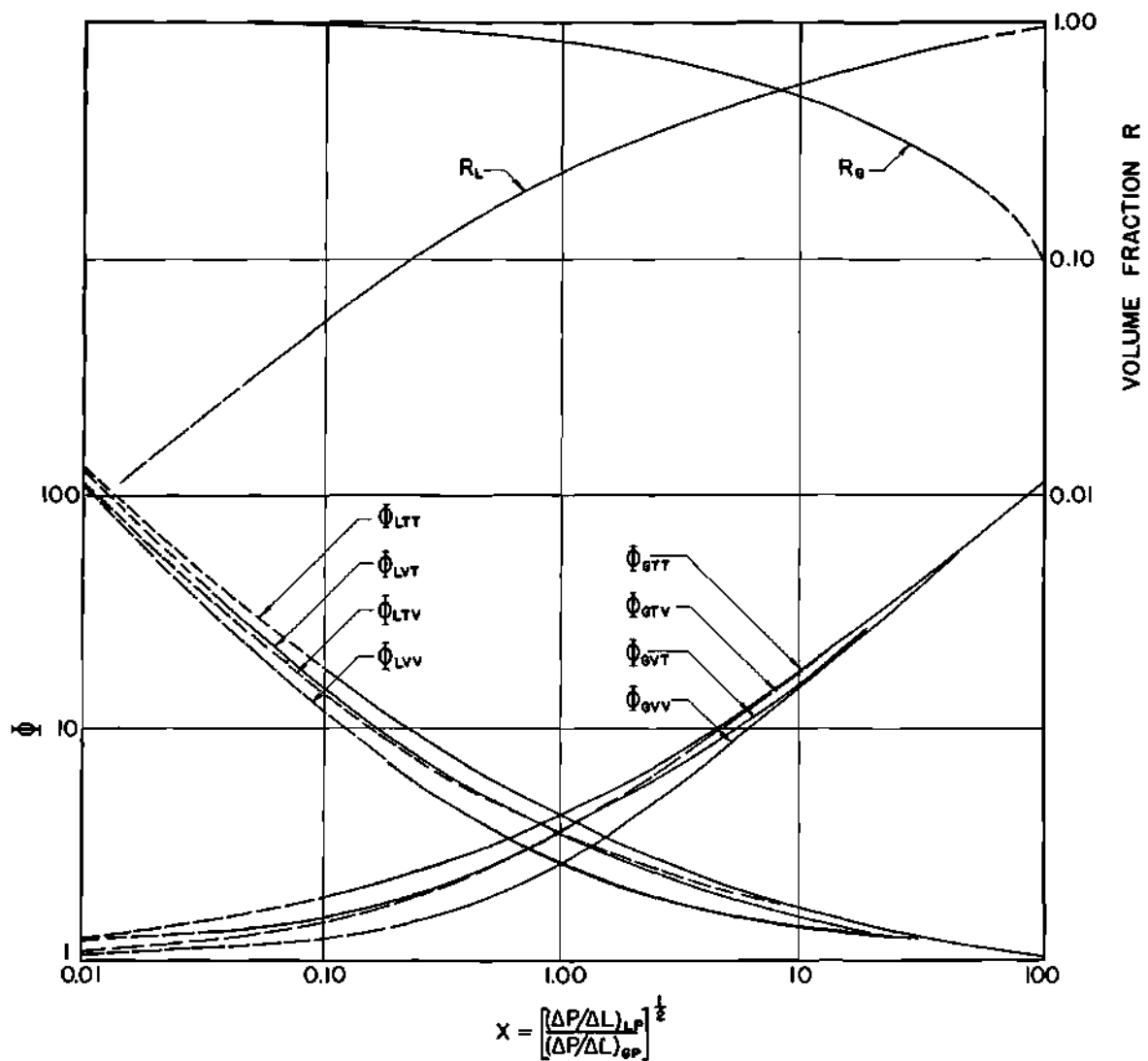
$$R_L = \frac{\alpha D_L^2}{D_P^2} = 1 - \beta \left(\frac{D_G}{D_P} \right)^2 \quad \text{or} \quad \beta = R_G \left(\frac{D_P}{D_G} \right)^2. \quad (I-15)$$

In all of the equations thus far, five variables have appeared

$$X, \frac{D_L}{D_P}, \frac{D_G}{D_P}, \alpha, \text{ and } \beta \quad (\text{I-16})$$

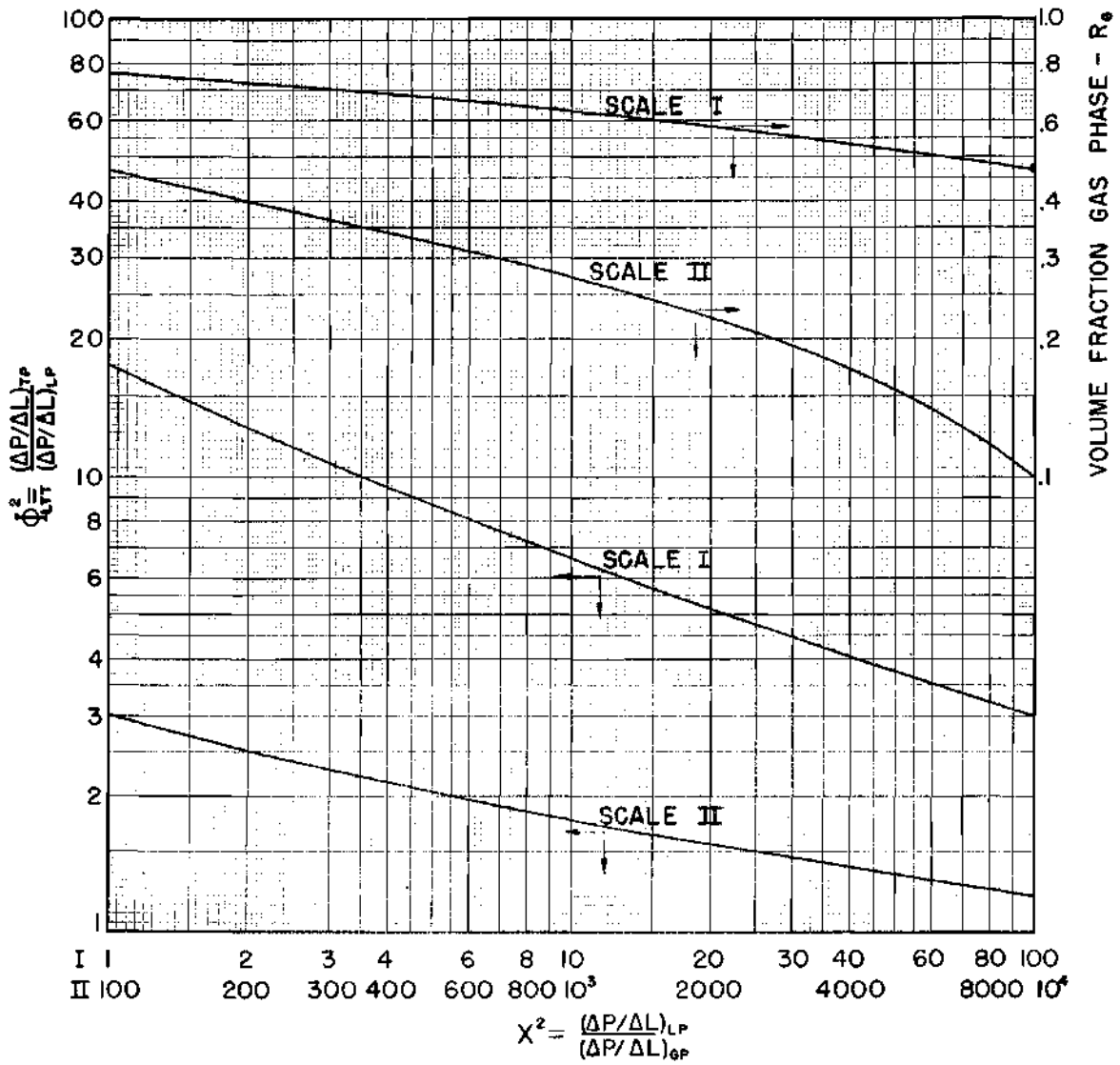
and the variables D_L/D_P , D_G/D_P , α , and β can be expressed in terms of the experimentally determined variables $\bar{\Phi}_L$, $\bar{\Phi}_G$, R_L , and R_G . These investigators then postulated that these four variables were functions of the variable X alone and verified this postulate by experimental data over a wide range of the variables involved and flow types. These flow types are classified as turbulent-turbulent (TT), turbulent-viscous (TV), viscous-turbulent (VT), and viscous-viscous (VV) where the liquid condition is given first.

The final correlation curves give $\bar{\Phi}_L$ or $\bar{\Phi}_G$ as a function of the variable X with the flow types as parameters, and the variables R_G and R_L as functions of X alone. These investigators proposed the following criteria, based on the superficial Reynolds number of each phase, to determine the flow type: the flow is considered to be turbulent if the Reynolds number is more than 2000 and viscous if less than 1000, with the intermediate zone being the transition region. All of these curves are reproduced in figure I-1 while figure I-2 gives the $\bar{\Phi}_{LTT}^2$ and R_G curves versus X^2 on a larger scale as these were used in the present investigation.



CORRELATION CURVES OF LOCKHART AND MARTINELLI (8)
FOR CO-CURRENT GAS-LIQUID FLOW IN CYLINDRICAL
TUBES.

FIGURE I-1



CORRELATION CURVES OF LOCKHART AND MARTINELLI (8)
 FOR CO-CURRENT GAS-LIQUID FLOW IN CYLINDRICAL TUBES

FIGURE I-2

APPENDIX II

BROOKFIELD SYNCHRO-ELECTRIC VISCOMETER

A model LVF four-speed, 60-30-12-6 RPM, instrument having four spindles giving a range of from 0-100,000 centipoises was used in this investigation. In this type of rotation viscometer, the spindle rotates and the cup is any container with a diameter greater than 2 3/4 inches. The instrument measures, by means of a beryllium copper spring, the torque required to rotate the spindle at a constant angular velocity and reads directly in centipoises on a calibrated scale. This scale reading is the viscosity that the material would have if it were a Newtonian liquid being sheared at the same speed.

To derive the equations for this instrument, in the basic viscosity equation

$$\dot{R}_s = \frac{g_c S}{\mu} \quad (\text{II-1})$$

the appropriate values of \dot{R}_s and S

$$\dot{R}_s = -r \frac{d\dot{\theta}}{dr} \quad (\text{II-2})$$

$$S = \frac{T_o}{2\pi r^2} \quad (\text{cylindrical spindle with no end effects}) \quad (\text{II-3})$$

are substituted giving

$$d\dot{\theta} = - \frac{g_c T_o}{2\pi r^3 \mu} dr \quad (\text{II-4})$$

Since in the case of the Brookfield instrument, the viscosity is that of

a Newtonian and therefore constant, designated μ_B , integration of (II-4) gives

$$\int_0^{\dot{\omega}_1} d\dot{\theta} = -\frac{g_c T_o}{2\pi h \mu_B} \int_{R_E}^{R_i} \frac{dr}{r^3} \quad (\text{II-5})$$

where, as the integration limits indicate, it has been assumed that no slippage occurs at either boundary. Integration of equation (II-5) and simplification gives

$$\dot{\omega}_1 = \frac{g_c T_o}{4\pi h \mu_B R_i^2} \left[1 - \left(\frac{R_i}{R_E} \right)^2 \right] \quad (\text{II-6})$$

which, by using equation (II-3), can be written

$$\dot{\omega}_1 = \frac{g_c S_1}{2 \mu_B} \left[1 - \left(\frac{R_i}{R_E} \right)^2 \right] \quad (\text{II-7})$$

Of the four spindles supplied with this instrument only numbers 1 and 4 have the required cylindrical shape and were therefore used. The dimensions of these spindles are

<u>Spindle Number</u>	<u>Diameter (inches)</u>	<u>Height (inches)</u>
1	0.7420	2.562
4	0.1254	1.203

In these investigations, a 600 ml. beaker, having an internal diameter of approximately 3.25 inches, was used as the cup. Therefore, since the term $\left(\frac{R_i}{R_E} \right)^2$ is very small in the case of the number 4 spindle it may be neglected in computations involving that spindle. However, in the case of the number 1 spindle it must be retained.

APPENDIX III

COMPARISON OF ROTATIONAL AND CYLINDRICAL TUBE INSTRUMENT DATA (11)

According to Alves, Boucher and Pigford (11), a comparison of rotational and cylindrical tube viscometer data can be made by comparing the rate of shear and shear stress at the tube wall with the rate of shear and shear stress at the inner cylinder wall of the rotational viscometer.

In the case of the tube instrument, the rate of shear at the tube wall can be obtained from the flow curve, plotted as $y/\phi/4$ versus x , by equation (37) derived by Mooney (30) and which is repeated here as

$$-\left(\frac{du}{dr}\right)_W = 3\left(\frac{8Q\phi}{\pi D^3}\right) + \left(\frac{DAP_F}{4L}\right) \frac{d\left(\frac{8Q\phi}{\pi D^3}\right)}{d\left(\frac{DAP_F}{4L}\right)} = 3\left(\frac{y\phi}{4}\right) + \frac{x}{4}\left(\frac{dy\phi}{dx}\right) \quad (\text{III-1})$$

where $-\left(\frac{du}{dr}\right)_W$ is the rate of shear and x is the shear stress, both at the tube wall.

In the case of the rotation instrument, the determination of these quantities is more difficult and involves several assumptions. Starting with the basic equation

$$\dot{R}_s = \frac{g_c S}{\mu} \quad (\text{III-2})$$

where for this type of instrument

$$\dot{R}_s = -r \frac{d\dot{\theta}}{dr} \quad (\text{III-3})$$

and

$$S = \frac{T_o}{2\pi hr^2} \quad (\text{III-4})$$

and assuming that the viscosity is a function of the shearing stress

$$\mu = F(S) \quad (\text{III-5})$$

equation (III-2) becomes by using (III-3) and (III-5)

$$-r \frac{d\dot{\theta}}{dr} = \frac{g_c S}{F(S)} \quad (\text{III-6})$$

Since the torque T_o is constant, differentiation of equation (III-4) gives

$$- \frac{dr}{r} = \frac{dS}{2S} \quad (\text{III-7})$$

and substitution of this result into (III-6) yields

$$2 \frac{d\dot{\theta}}{dS} = \frac{g_c}{F(S)} \quad (\text{III-8})$$

Assuming no slippage at either boundary, integration of (III-8) gives

$$2 \int_0^{\dot{\omega}_1} d\dot{\theta} = 2\dot{\omega}_1 = g_c \int_{S_E}^{S_1} \frac{dS}{F(S)} \quad (\text{III-9})$$

Differentiation of this equation with respect to S_1 produces

$$\frac{2d\dot{\omega}_1}{dS_1} = \frac{g_c}{F(S_1)} - \frac{g_c}{F(S_E)} \frac{dS_E}{dS_1} \quad (\text{III-10})$$

But since, by (III-4)

$$\frac{dS_E}{dS_i} = \left(\frac{R_i}{R_E} \right)^2 \quad (\text{III-11})$$

(III-10) becomes, using (III-5)

$$\frac{2d\dot{\omega}_i}{dS_i} = \frac{g_c}{\mu_i} \left[1 - \frac{\mu_i}{\mu_E} \left(\frac{R_i}{R_E} \right)^2 \right] \quad (\text{III-12})$$

This relationship Alves et.al. call the general equation for rotational viscometers. In order to obtain the rate of shear at the inner cylinder wall Alves et.al. assume that

$$\mu = K_1 S^{-n'} \quad (\text{III-13})$$

and by using (III-4) obtain

$$\frac{\mu_i}{\mu_E} = \left(\frac{S_E}{S_i} \right)^{n'} = \left(\frac{R_i}{R_E} \right)^{2n'} \quad (\text{III-14})$$

Now letting

$$n = n' + 1 \quad (\text{III-15})$$

and substituting into (III-12), the result is

$$\frac{2d\dot{\omega}_i}{dS_i} = \frac{g_c}{\mu_i} \left[1 - \left(\frac{R_i}{R_E} \right)^{2n} \right] \quad (\text{III-16})$$

Finally by substituting (III-2) into (III-16), the final result is obtained

$$\left(\dot{R}_s \right)_i = \frac{2S_i \left(\frac{d\dot{\omega}_i}{dS_i} \right)}{1 - \left(\frac{R_i}{R_E} \right)^{2n}} \quad (\text{III-17})$$

In order to obtain n , equation (III-13) is substituted into (III-9) and the integration carried out giving

$$2\dot{\omega}_1 = \frac{S_1^n g_c}{K_1 n} \left[1 - \left(\frac{S_E}{S_1} \right)^n \right] \quad (\text{III-18})$$

This becomes, using (III-14) and rearranging,

$$S_1 = \left[\frac{2 K_1 \frac{n}{g_c}}{1 - \left(\frac{R_1}{R_E} \right)^{2n}} \dot{\omega}_1 \right]^{1/n} \quad (\text{III-19})$$

Thus n is given by

$$n = \frac{d \log \dot{\omega}_1}{d \log S_1} \quad (\text{III-20})$$

which is the slope of the log-log plot of $\dot{\omega}_1$ versus S_1 .

Alves et.al. point out that n is constant for many materials and suggest that even if it is not, an approximation can be made by evaluating it at the point in question. How good such an approximation will be, though, is questionable.

In summary, then, to convert rotational viscometer data to the usual type of tube flow curve, a log-log plot of $\dot{\omega}_1$ versus S_1 is constructed from which $\dot{\omega}_1$ can be obtained as a function of S_1 and n determined. From this function, $\dot{\omega}_1 = f(S_1)$, and equation (III-17), $(\dot{R}_s)_1$ as a function of S_1 can be obtained, say $(\dot{R}_s)_1 = F(S_1)$. Then, since the rate of shear at the inner cylinder wall and at the tube wall are equivalent at equal shearing stresses,

$$(\dot{R}_s)_1 = - \left(\frac{du}{dr} \right)_W \quad (\text{III-21a})$$

$$S_1 = x \quad (\text{III-21b})$$

Substitution of these results into equation (III-1) gives

$$F(x) = \frac{3}{4} y_\phi + \frac{x}{4} \frac{dy_\phi}{dx} \quad (\text{III-22})$$

Integration of this equation gives y_ϕ as a function of x which is the desired result. Of course, the analytical methods described above may be replaced by graphical methods when more convenient.

Alves et.al. have obtained good correlations using this technique on data obtained on several different materials in different types of rotational viscometers and various sizes of cylindrical tubes.

However, it should be emphasized that equation (III-17) depends on the assumed viscosity function of equation (III-13) which is at best no more than an empirical relationship which, when applicable, often covers but a limited range of the data. For a more detailed discussion of the representation of viscosity by power functions, the reader is referred to the following references (16, 21).

In conclusion, then, it can be said, that while the method is sound, the equation for the determination of the rate of shear at the inner cylinder wall as a function of the shearing stress at that point, (III-17), is approximate and, in order to make it exact, the viscosity function must be known. This in turn leads to the big problem in rheology today and, as pointed out in the Theoretical Background Chapter, no exact solution is known. In many cases, better approximations to the viscosity function can be made as indicated there and the use of these would lead to better equations for $(R_s)_1$. However, these relationships

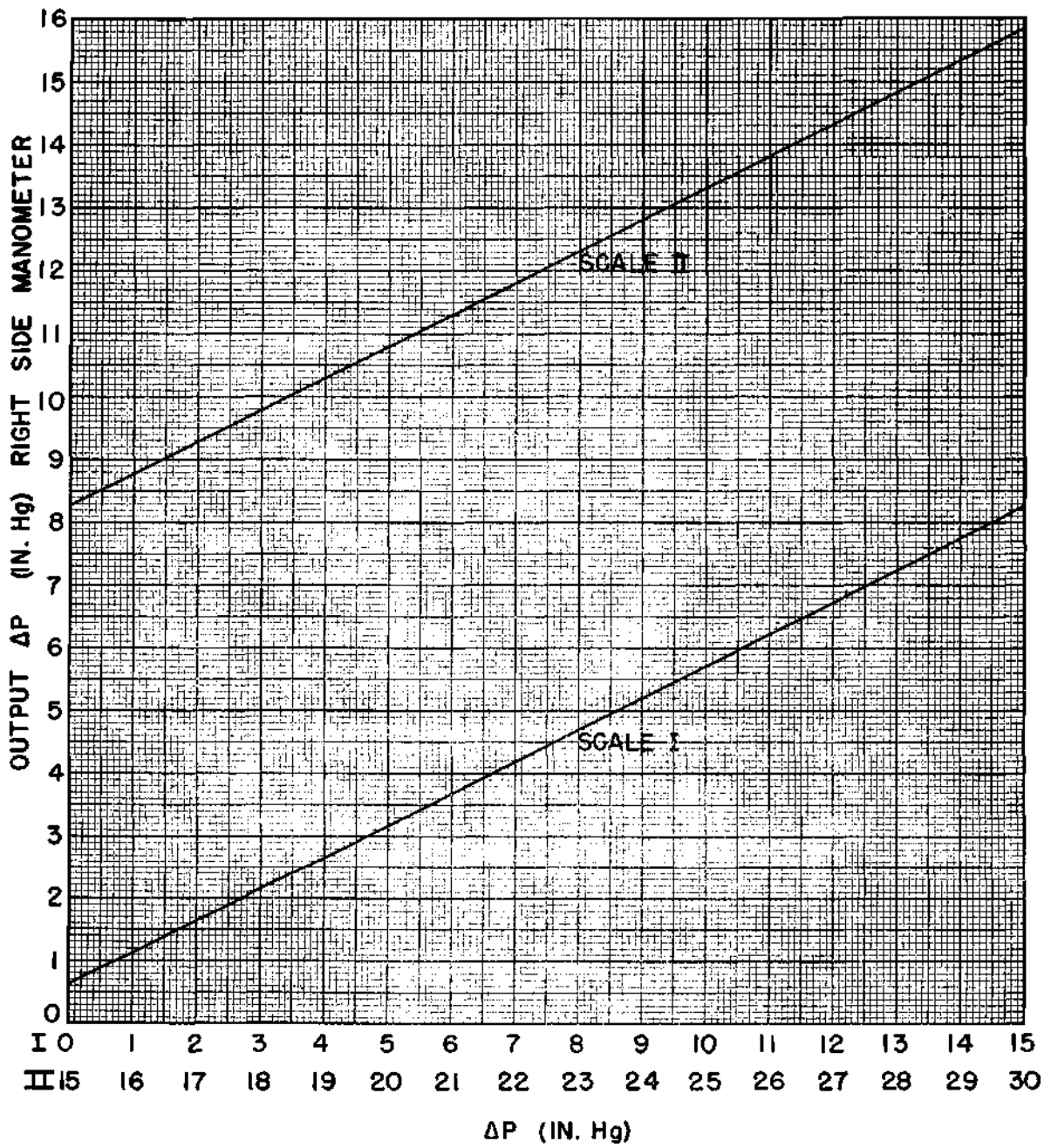
would no doubt be complicated and difficult to use. For these reasons, if equation (III-17) is found applicable, it should be used only in the range covered by the data since extrapolation outside of this range is not justified by present theory.

APPENDIX IV

PRESSURE TRANSMITTER CALIBRATION

A model PDP-12 Republic differential pressure transmitter, with a $3 \frac{1}{8}$ square-inch differential diaphragm and 1.25 square-inch reaction diaphragm, was used to measure the pressure drop across the test sections. Pressure lines were $\frac{3}{8}$ inch copper tubing and water was used as the transmitting agent. Suitable valving, $\frac{1}{4}$ inch needle valves being used for shut off purposes, permitted the transmitter to be connected across the desired test section.

The calibration of this instrument was made in these laboratories by applying known water pressures to the differential diaphragm and measuring the resulting output pressures as recorded on a 30-inch mercury filled U-tube manometer. The resulting calibration curve is presented in figure IV - 1.



TRANSMITTER CALIBRATION CURVE

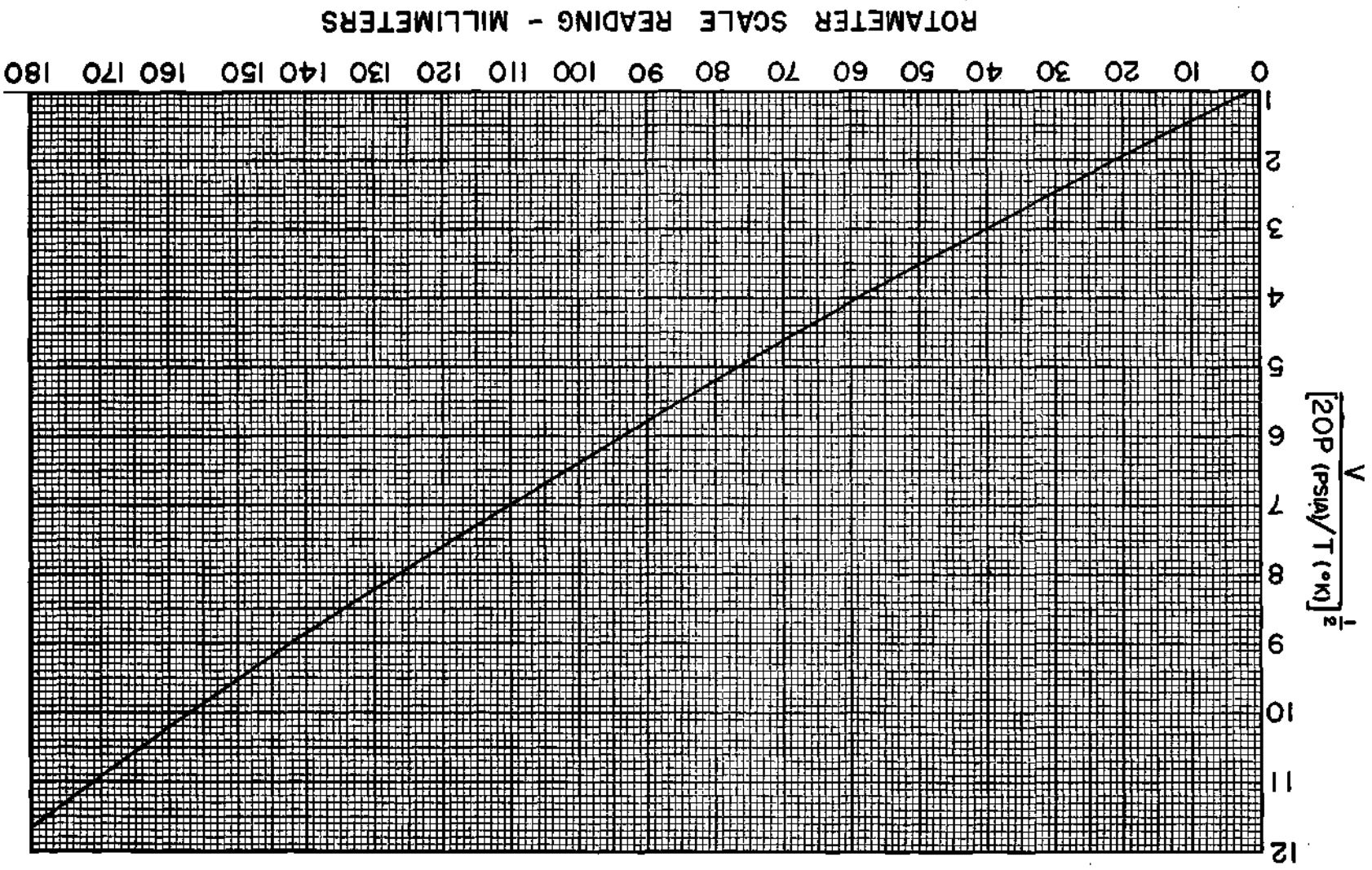
FIGURE IV-1

APPENDIX V

ROTAMETER CALIBRATION

A Schutte-Koerting number 6 rotameter equipped with an aluminum float was used to measure the air flow rate. The original calibration scale was furnished by the manufacturers and the curve presented in figure V - 1 was derived therefrom.

ROTAMETER CALIBRATION CURVE
FIGURE V-1



APPENDIX VI

DEVELOPMENT OF EQUATIONS FOR DETERMINING PUMP CHARACTERISTICS

Tests were conducted on an Ingersoll-Rand 1 CORVNL open-impeller centrifugal pump to determine its characteristics while handling various water-clay suspensions. This pump has a 2 inch suction and a 1 inch discharge and was driven by a 15 horsepower motor. Details of this pumping unit are shown in figure VI-1.

The net head delivered by the pump can be determined by applying the mechanical energy balance, equation (58), between Sections 1 and 2 of figure VI-1. Application of this equation yields, assuming incompressible flow and neglecting friction in the pipes

$$-W_S = H = \frac{P_2 - P_1}{\rho} + \frac{g}{g_c} (h_2 - h_1) + \frac{U_2^2 - U_1^2}{2g_c}$$

This equation becomes, for the arrangement under consideration

$$H = \frac{144 \left(P_D + \frac{g}{g_c} \frac{40}{12} \rho_W - P_S \right)}{\rho_L} + \frac{g}{g_c} \left(\frac{6.5 - 5.5}{12} \right) + \frac{W_L^2}{2g_c \rho_L^2} \left(\frac{1}{A_D^2} - \frac{1}{A_S^2} \right)$$

which simplifies to

$$H = \frac{2.31(P_D - P_S)}{\text{Sp. Gr.}} + 0.104 \left(\frac{W_L}{\text{Sp. Gr.}} \right)^2 + \frac{3.33}{\text{Sp. Gr.}} + 0.083$$

where H = net head delivered by the pump, ft. lb.(force)/lb.(mass)

P_D = discharge pressure, psig

P_S = suction pressure, psig

W_L = weight rate of flow, lb./sec.

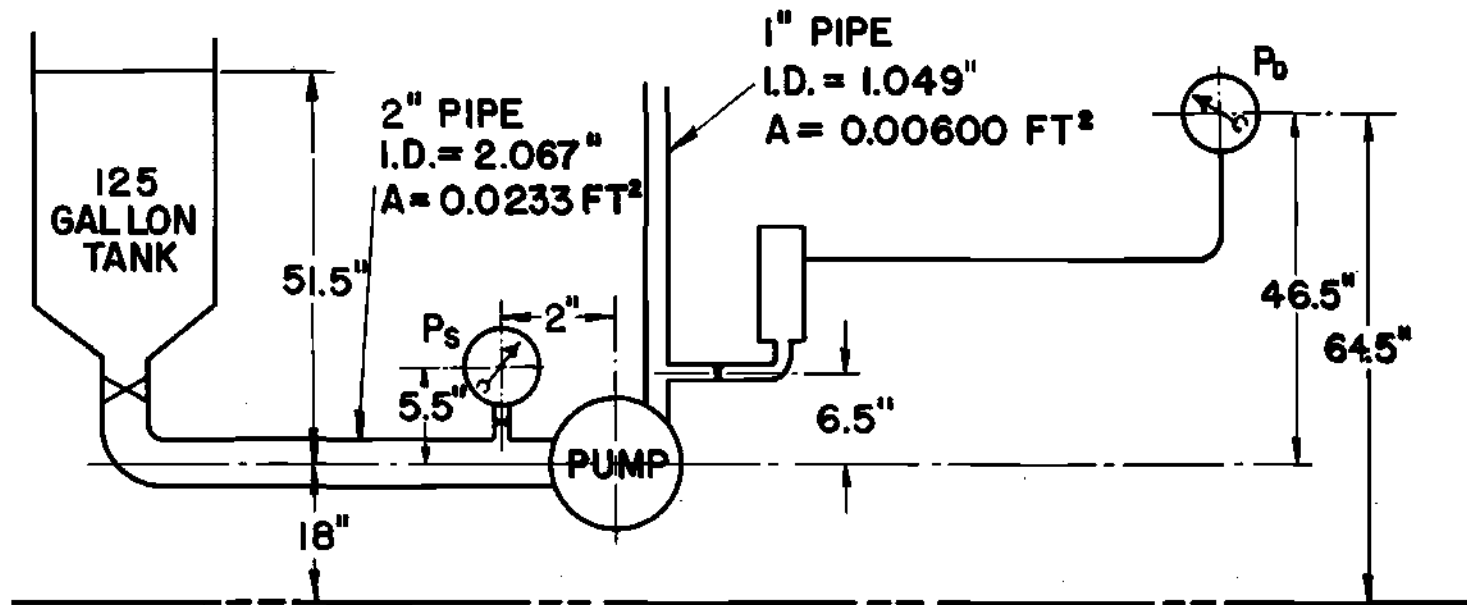
The volumetric rate of flow in gallons/min., V' , is

$$V' = 7.20 \left(\frac{W_L}{\text{Sp. Gr.}} \right)$$

and the overall efficiency is

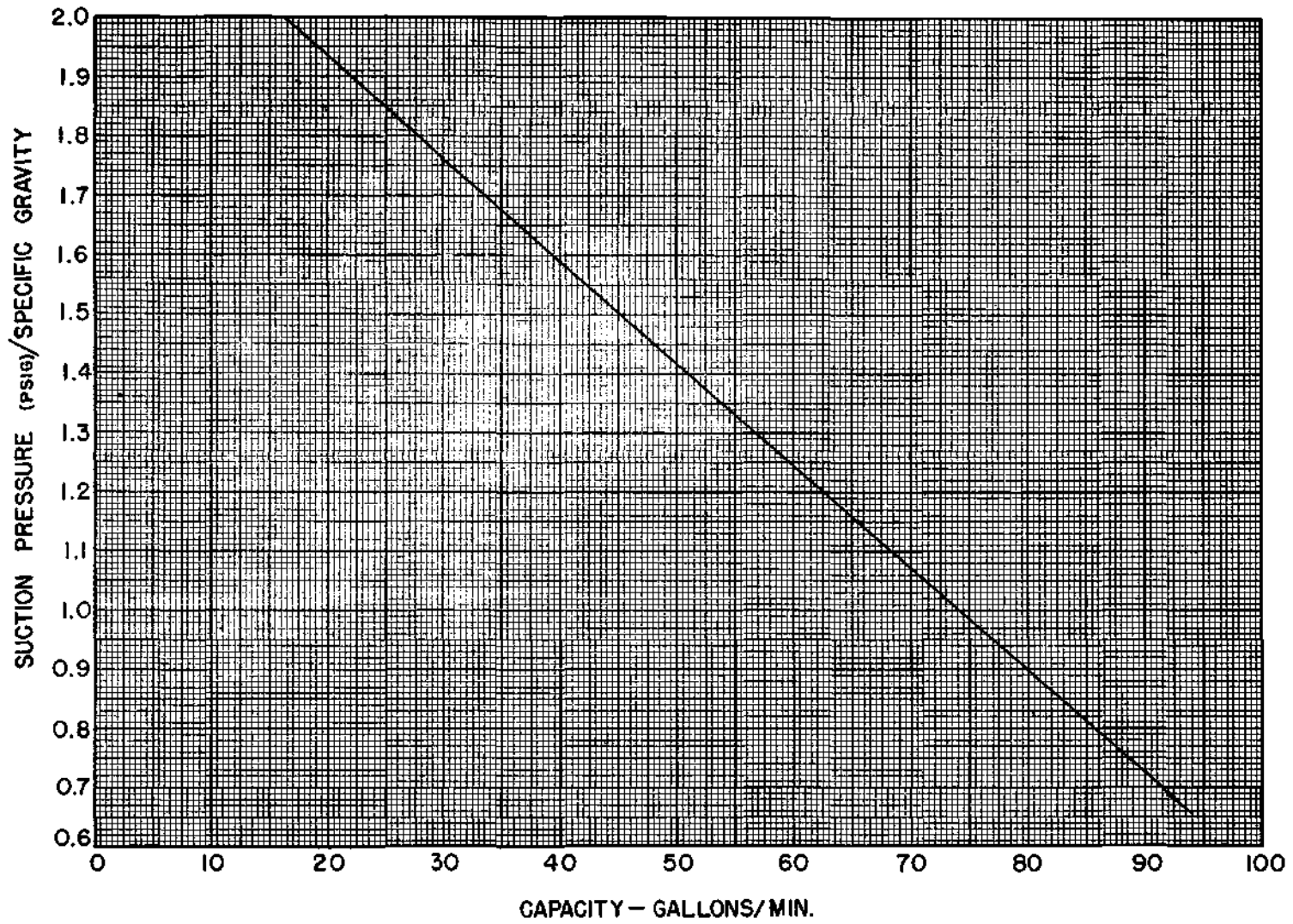
$$\text{overall eff.} = \frac{W_L H}{550 (\text{Horse Power Input to Motor})}$$

As the suction pressure gage became fouled during the water-clay runs, it was necessary to estimate the suction pressure from the measurements made during the water runs. Figure VI-2 was used for this purpose.



SCHEMATIC DIAGRAM OF PUMP ARRANGEMENT

FIGURE VI - 1



ESTIMATED SUCTION PRESSURE/SPECIFIC GRAVITY
VS. CAPACITY FOR CENTRIFUGAL PUMP

FIGURE VI-2

APPENDIX VII - A

CURVES USED IN CALCULATIONS

The various quantities used in the calculations of the present investigation are presented in figures VII - A1 through VII - A7 and are as follows:

- Figure VII - A1: Friction factor versus Reynolds Number for Newtonians (42)
- Figure VII - A2: Curve of Hedström (25) for laminar pressure drop of Bingham plastics: $F(G)$ versus G
- Figure VII - A3: Curve of Hedström (25) for transition point of Bingham plastics: Re_{crit} versus G
- Figure VII - A4: Viscosity of water versus temperature (39)
- Figure VII - A5: Density of water versus temperature (40)
- Figure VII - A6: Viscosity of air versus temperature (41)
- Figure VII - A7: Weight and volume percent solids versus specific gravity

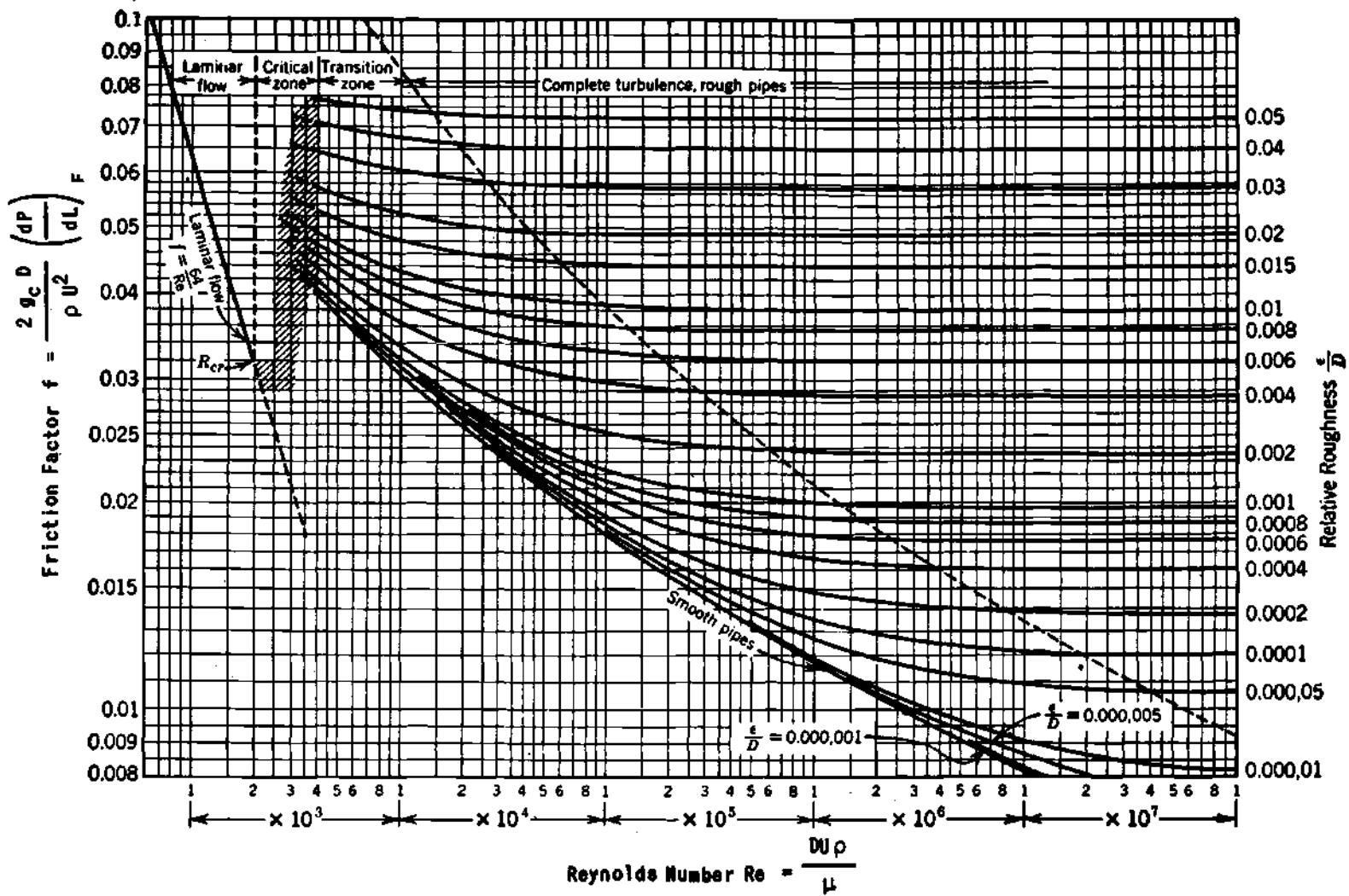
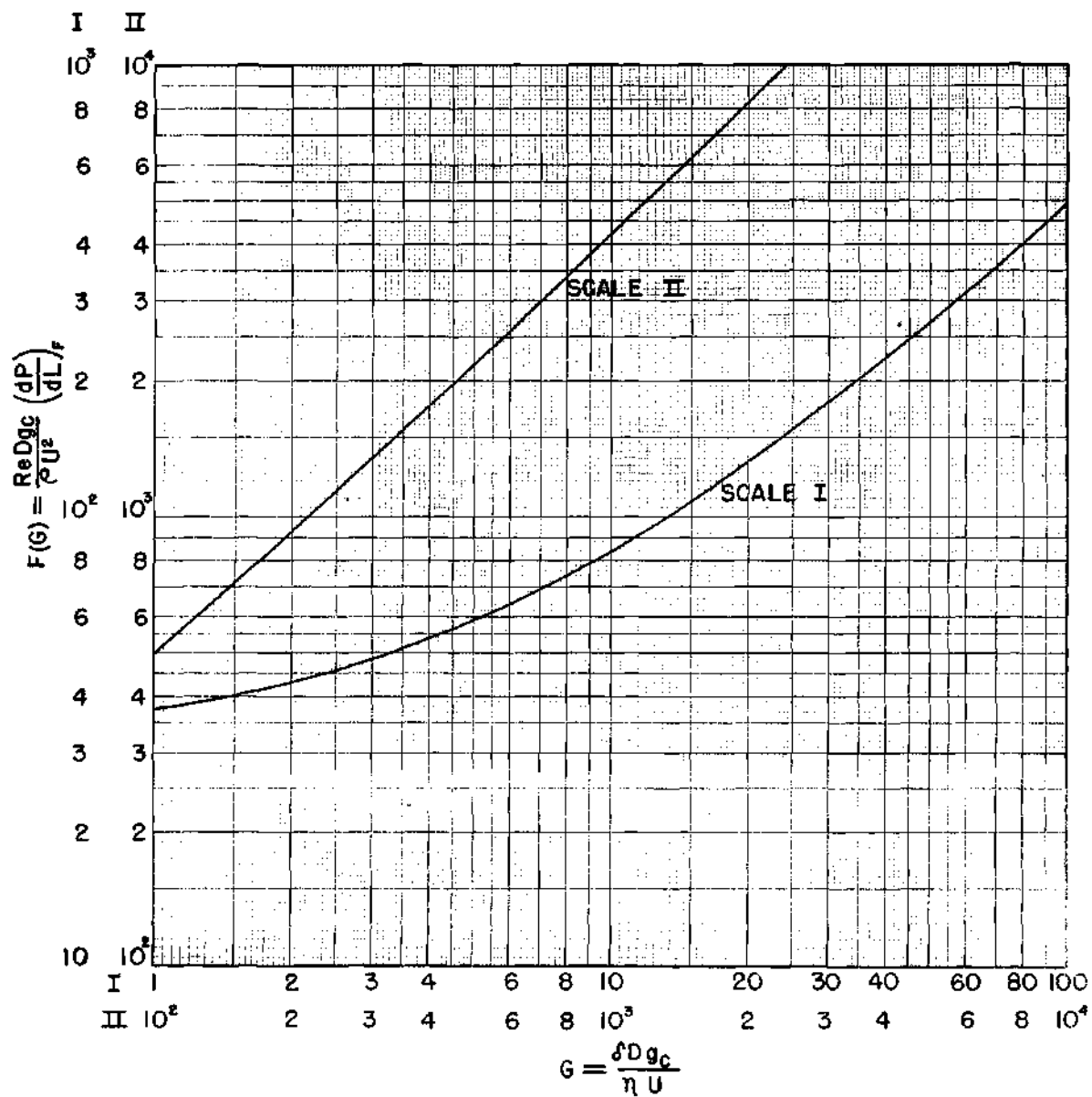
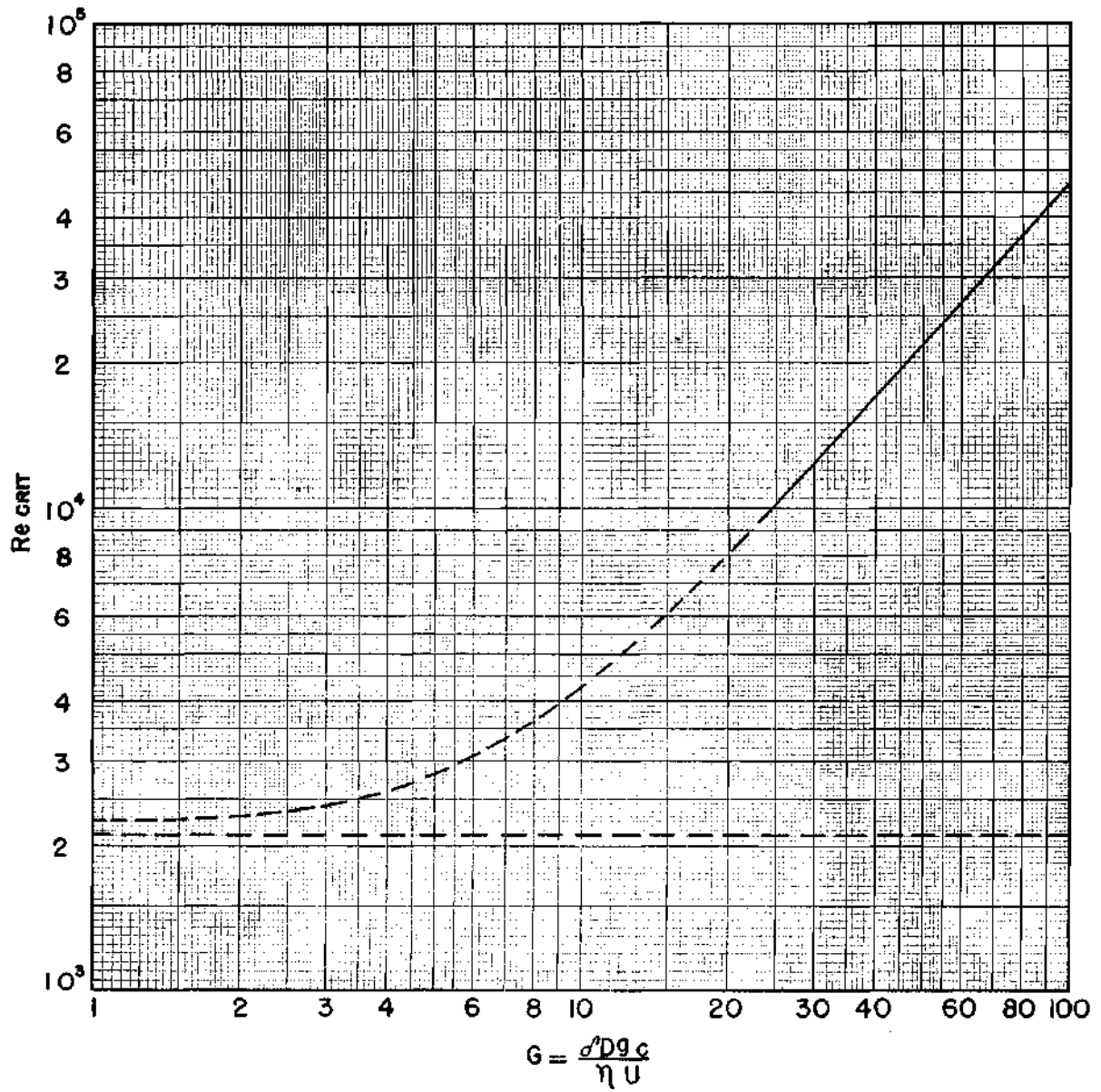


Figure VII A-1. Friction Factor vs. Reynolds No. (42).



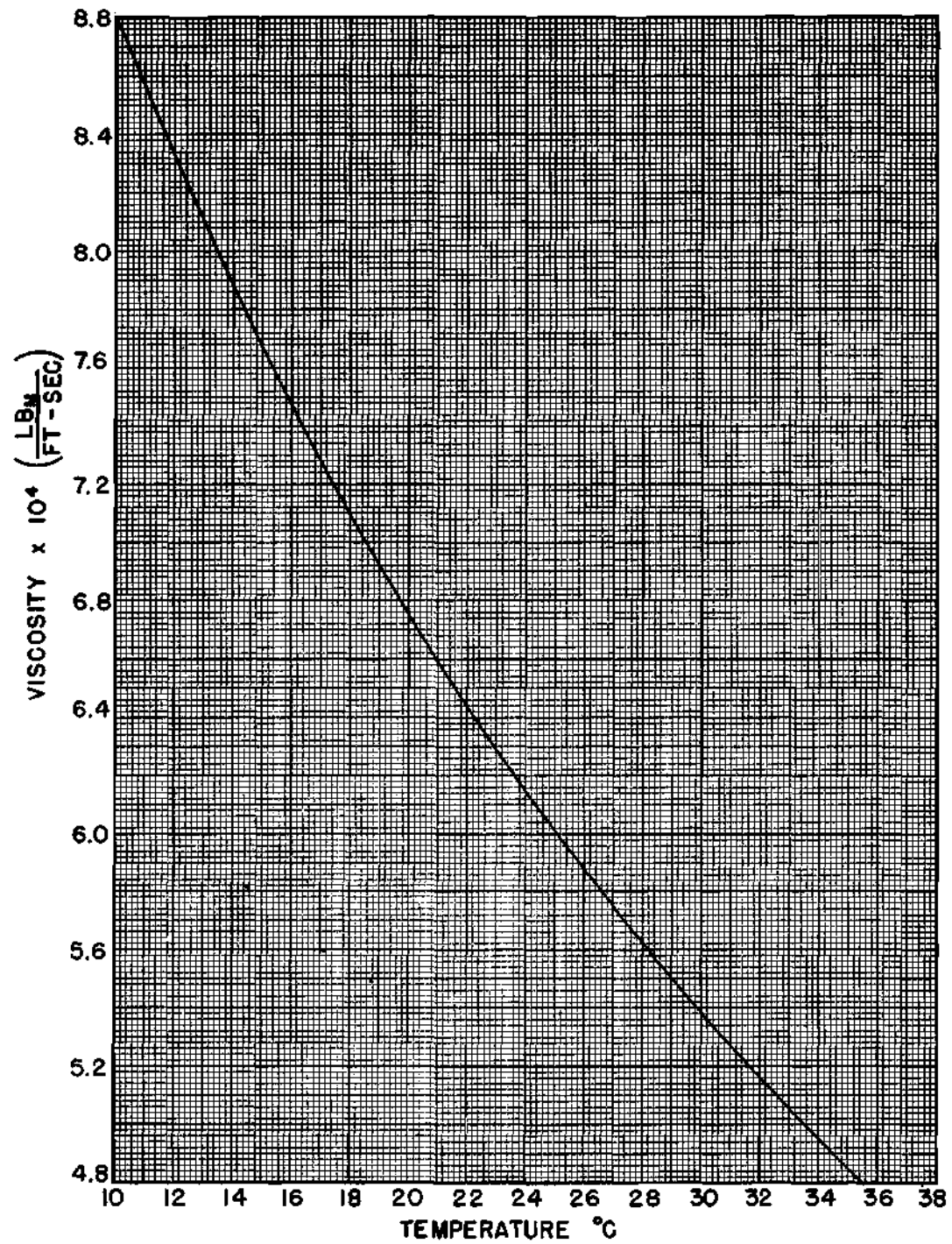
CURVE OF HEDSTRÖM (25) FOR PRESSURE DROP OF BINGHAM PLASTICS IN CYLINDRICAL TUBES
 F(G) vs. G

FIGURE VIIA-2



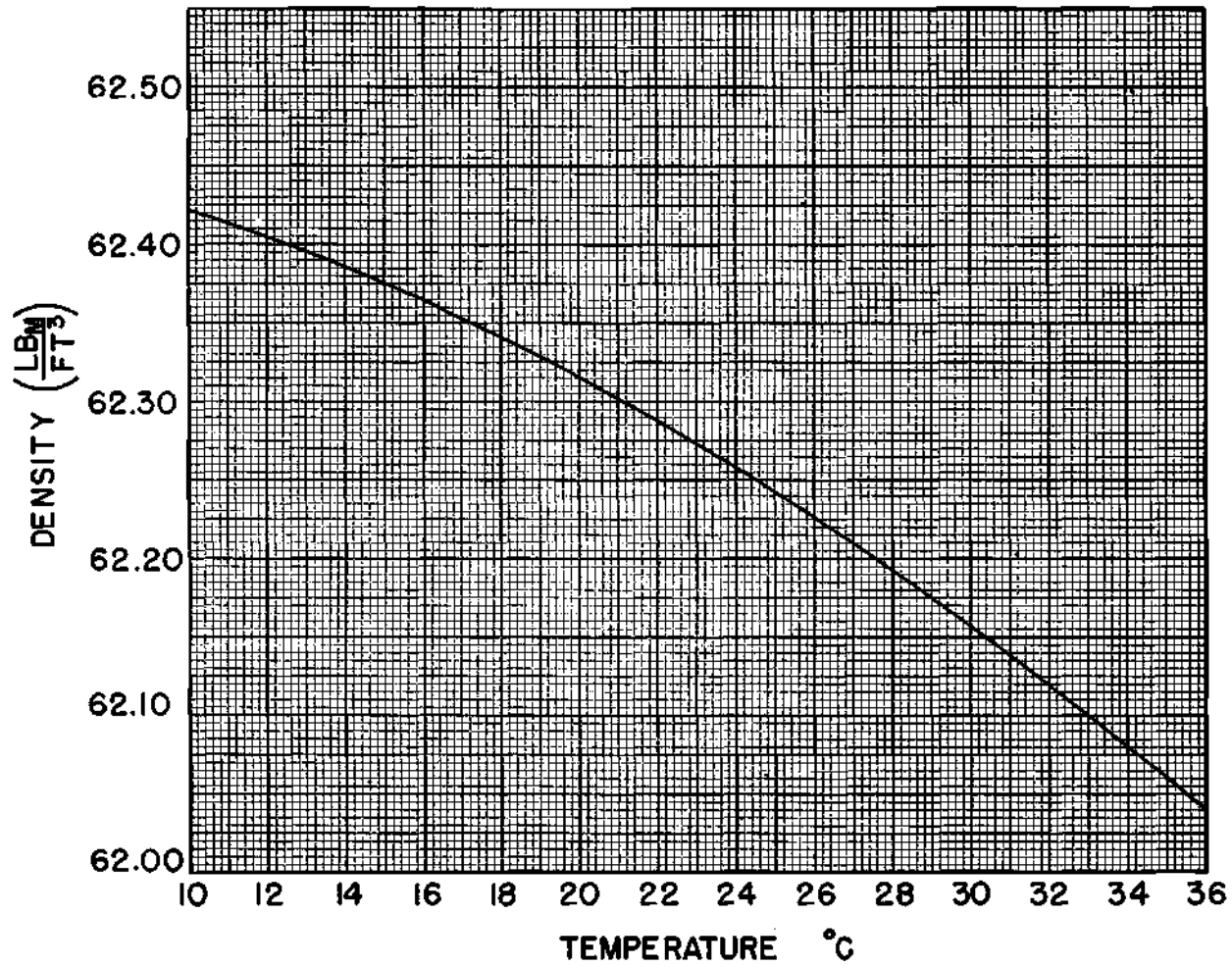
CURVE OF HEDSTRÖM (25) FOR CRITICAL REYNOLDS NUMBER OF BINGHAM PLASTICS AS A FUNCTION OF G

FIGURE VII A-3



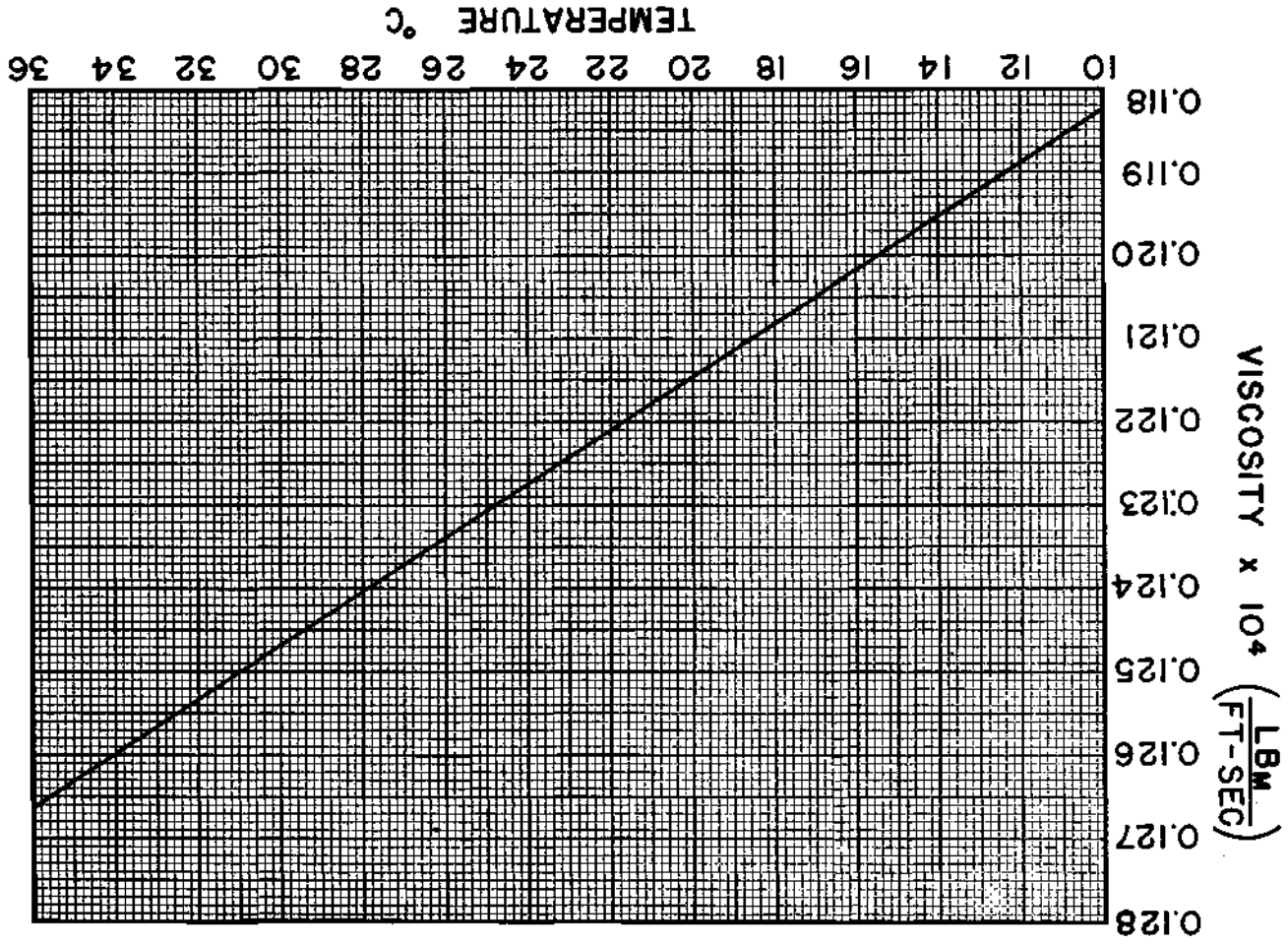
VISCOSITY OF WATER VS. TEMPERATURE (39)

FIGURE VII A-4



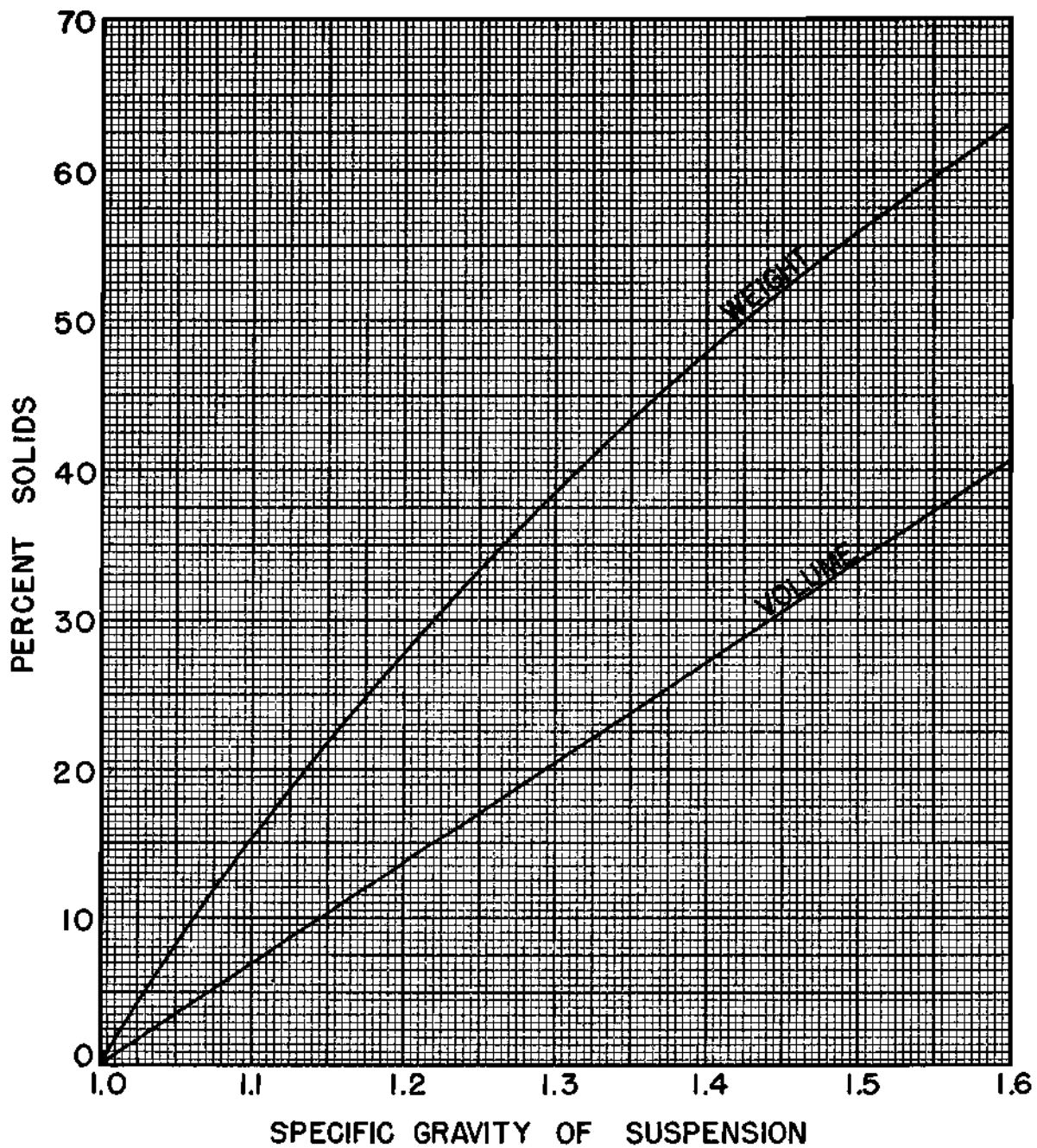
DENSITY OF WATER vs. TEMPERATURE (40)

FIGURE VII A-5



VISCOSITY OF AIR vs. TEMPERATURE (41)

FIGURE VII A-6



PERCENT SOLIDS vs. SPECIFIC GRAVITY

FIGURE VII A-7

APPENDIX VII - B

SAMPLE CALCULATION

Flow of water alone in a 1.60 inch pipe: Run 3 (Table I)

The pressure drop over the 15.0-foot length was read on the right side of the U tube manometer connected to the output side of the differential transmitter and was recorded as

$$\Delta P_{\text{OUTPUT}} = 1.52 \text{ in. Hg}$$

which, using the calibration curve for this instrument in figure IV - 1, corresponds to an observed pressure drop of

$$\Delta P_{\text{OBS}} = 1.85 \text{ in. Hg}$$

During this run, 297.1 pounds of water were collected in 41.4 seconds and the liquid rate was determined as

$$W_L = \frac{297.1}{41.4} = 7.18 \text{ lb./sec.}$$

The average liquid temperature was measured and found to be 18° C. and from figures VII - A4 and VII - A5 the viscosity and density were determined as

$$\begin{aligned}\mu_L &= 7.10 \times 10^{-4} \text{ lb. m./ft. sec.} \\ \rho_L &= 62.34 \text{ lb. m./ft.}^3\end{aligned}$$

Using these values the Reynolds number was computed as

$$Re_L = \frac{4W_L}{\pi D \rho_L} = \frac{4(7.18)}{\pi \left(\frac{1.60}{12}\right) (7.10 \times 10^{-4})} = 9.66 \times 10^4$$

and the corresponding friction factor was found from figure VII - A1 to be

$$f_{CALC} = 0.0181$$

The calculated pressure drop was determined to be

$$\Delta P_{CALC} = \frac{f_{CALC} W_L^2 L}{2g_c D A^2 \rho_L} = 2.037 f_{CALC} W_L^2 = 2.037(0.0181)(7.18)^2 = 1.90 \text{ in. Hg}$$

and the deviation between the observed and calculated pressure drops was computed as

$$\% \text{ Deviation} = \frac{\Delta P_{OBS} - \Delta P_{CALC}}{\Delta P_{CALC}} \times 100 = \frac{1.85 - 1.90}{1.90} \times 100 = -2.63$$

APPENDIX VII - C

SAMPLE CALCULATION

Flow of a 23.6 weight percent (Sp. Gr. = 1.164) water-clay suspension in a 1.06 inch tube: Run 123 (Table II - B)

The pressure drop over the 16.5-foot length was determined from the output pressure of the differential transmitter as in Appendix VII - B and found to be

$$\Delta P_{OBS} = 3.20 \text{ in. Hg}$$

The rate of flow was determined from the time-weight measurements as

$$W_L = \frac{193.0 \text{ lbs.}}{59.7 \text{ sec.}} = 3.23 \text{ lb./sec.}$$

and the temperature measured as 30.2° C. The specific gravity, referred to water at 25° C., was determined by a pycnometer as 1.164 and the concentration of the suspension determined as

$$\text{Wt. \%} = \frac{\text{Sp. Gr. Clay} \left(\frac{\text{Sp. Gr. Suspension} - 1}{\text{Sp. Gr. Suspension}} \right)}{\text{Sp. Gr. Clay} - 1} \times 100 =$$

$$\frac{2.48 \left(\frac{1.164 - 1}{1.164} \right)}{2.48 - 1} \times 100 = 23.6$$

$$\text{Vol. \%} = \left(\frac{\text{Sp. Gr. Suspension} - 1}{\text{Sp. Gr. Clay} - 1} \right) \times 100 =$$

$$\left(\frac{1.164 - 1}{2.48 - 1} \right) \times 100 = 11.1$$

The quantity $8Q/\pi D^3$ was computed as

$$\frac{8Q}{\pi D^3} = \frac{8W_L}{\pi \rho_L D^3} = \frac{8(3.23)}{\pi(1.164 \times 62.25) \left(\frac{1.06}{12}\right)^3} = \frac{164.9}{\text{sec.}}$$

and the shearing stress at the pipe wall was found to be

$$\frac{D \Delta P_F}{4L} = \frac{0.4895(1144) \left(\frac{1.06}{12}\right) (3.20)}{4(16.5)} = 0.302 \text{ lb. F./ft.}^2$$

In order to determine the turbulent viscosity, the friction factor was computed as

$$f_L = \frac{0.4895(1144)(2)g_c D A^2 \rho_L \Delta P_F}{W_L^2 L} =$$

$$\frac{0.4895(1144)(2)(32.17)(0.0883)(0.006125)^2(1.164)(62.25)(3.20)}{(3.23)^2(16.5)}$$

$$f_L = 0.0202$$

and the Reynolds number was determined from figure VII - A1 to be

$$Re_L = 5.80 \times 10^4$$

The turbulent viscosity was then found to be

$$\mu_T = \frac{\left(\frac{4W_L}{\pi D}\right)}{Re_L} = \frac{\left[\frac{4(3.23)}{\pi(0.0883)}\right]}{5.80 \times 10^4} = 8.03 \times 10^{-4} \text{ lb. m./ft. sec.}$$

From figure VII - A4 the viscosity of water at this temperature (30.2° C.) was determined as

$$\mu_{\text{H}_2\text{O}} = 5.36 \times 10^{-4} \text{ lb. m./ft. sec.}$$

and the ratio of the turbulent viscosity to the water viscosity was found to be

$$\frac{\mu_T}{\mu_{\text{H}_2\text{O}}} = \frac{8.03 \times 10^{-4}}{5.36 \times 10^{-4}} = 1.50$$

APPENDIX VII - D

SAMPLE CALCULATION

Co-current flow of air and water in a 0.82 inch pipe: Run 48 (Table V - C)

The pressure drop over the 17.25-foot length was determined from the output pressure of the differential transmitter as in Appendix VII - B and found to be

$$\Delta P_{OBS} = 7.22 \text{ in. Hg}$$

The rate of flow of the liquid was determined from the time-weight measurements as

$$W_L = \frac{139.5 \text{ lbs.}}{122.8 \text{ sec.}} = 1.137 \text{ lb./sec.}$$

and the temperature measured as 14° C.

The superficial pressure drop of the water, that is the pressure drop that would occur if the water were flowing alone in the pipe, was computed exactly as in Appendix VII - B, and found to be

$$\Delta P_{LP} = 2.06 \text{ in. Hg}$$

The air flow rate was determined from the measurements taken at the rotameter

Scale reading = 55 millimeters

Pressure = 28.4 psia

Temperature = 297° K.

and the rotameter calibration curve of figure V - 1 as

$$\frac{V}{\left[20\left(\frac{28.4}{297}\right)\right]^{1/2}} = 3.79 \text{ ft.}^3/\text{min. at } 14.7 \text{ psia and } 21.1^\circ \text{ C.}$$

The air flow rate in lbs./sec. was then determined by the perfect gas law as

$$W_G = \frac{MPV}{RT} = \frac{29(14.7)(3.79)}{(10.74)(1.8)(294.3)} \left[20\left(\frac{28.4}{297}\right)\right]^{1/2} \left(\frac{1}{60}\right) = 0.00654 \text{ lb./sec.}$$

The pressure at the downstream pressure tap was measured on a Bourdon gage and found to be 18.4 psia and the average pressure in the test section was approximated as

$$P_{AVG} = P_{DT} + \frac{0.4895\Delta P}{2} = 18.4 + \frac{0.4895}{2}(7.22) = 20.2 \text{ psia}$$

The viscosity of the air at the average temperature in the test section, 14° C., was evaluated as

$$\mu_G = 0.1195 \times 10^{-4} \text{ lb. m./ft. sec.}$$

from figure VII - A6 and the Reynolds number was then calculated as

$$Re_{GP} = \frac{4W_G}{\pi D \rho_G} = \frac{4(0.00654)}{\pi\left(\frac{0.82}{12}\right)(0.1195 \times 10^{-4})} = 10.2 \times 10^3$$

The corresponding friction factor was found to be

$$f_{GP} = 0.0302$$

from figure VII - A1.

The superficial pressure drop of the air was then calculated as

$$\Delta P_{GP} = \frac{f_{GP} U_{GP}^2 \rho_G L}{2g_c D (0.4895) (144)} = \frac{f_{GP} W_G^2 L}{2g_c D A^2 \rho_G (0.4895) (144)} =$$

$$1.468 \times 10^{-4} \left(\frac{L}{D} \right) \left(\frac{1}{A^2} \right) \frac{f_{GP} W_G^2 L}{P} =$$

$$1.468 \times 10^{-4} \left(\frac{17.25}{0.0683} \right) \left(\frac{1}{1.343 \times 10^{-5}} \right) \frac{(0.0302) (0.00654)^2 (287)}{20.2} =$$

$$0.0506 \text{ in. Hg}$$

Using the ratio of the superficial liquid pressure drop to the superficial air pressure drop

$$X^2 = \frac{\Delta P_{LP}}{\Delta P_{GP}} = \frac{2.06}{0.0506} = 40.7 ,$$

Φ_{LTT}^2 of Lockhart and Martinelli's correlation (8) was evaluated from figure I - 2 as

$$\Phi_{LTT \text{ MART}}^2 = 4.09$$

The predicted pressure drop was then calculated as

$$\Delta P_{TP \text{ MART}} = \Phi_{LTT}^2 \Delta P_{LP} = 4.09(2.06) = 8.43 \text{ in. Hg}$$

and the percent deviation from the actual pressure drop found to be

$$\% \text{ Dev.} = \frac{\Delta P_{OBS} - \Delta P_{TP \text{ MART}}}{\Delta P_{TP \text{ MART}}} \times 100 =$$

$$\frac{7.22 - 8.43}{8.43} \times 100 = -14.4$$

APPENDIX VII - E

SAMPLE CALCULATION

Co-current flow of air and a water-clay suspension of specific gravity 1.313 containing 39.9 weight percent (21.2 volume percent) solids in a 1.60 inch pipe: Run 160 (Table VI - C1)

The pressure drop over the 15.0-foot length, the suspension rate, the temperature, and physical properties of the suspension were determined as in Appendix VII - C

$$\Delta P_{OBS} = 9.60 \text{ in. Hg}$$

$$W_L = 12.84 \text{ lb./sec.}$$

$$T_{AVG} = 30.4^\circ \text{ C.}$$

$$\text{Sp. Gr.} = 1.313$$

$$\text{Wt. \%} = 39.9$$

$$\text{Vol. \%} = 21.2$$

In order to determine the superficial suspension pressure drop, $8Q/\pi D^3$ was determined as

$$\frac{8Q}{\pi D^3} = \frac{8W_L}{\pi D^3 \rho_L} = \frac{8(12.84)}{\pi \left(\frac{1.60}{12}\right)^3 (1.313)(62.2)} = 168.3/\text{sec.}$$

and the corresponding shearing stress at the pipe wall was evaluated from figure 22 as

$$\frac{D\Delta P_{LP}}{4L} = 0.690 \text{ lb. F./ft.}^2$$

from which

$$\Delta P_{LP} = \frac{4L}{D} \frac{(0.690)}{144(0.4895)} = \frac{4(15.0)}{\left(\frac{1.60}{12}\right)} \frac{(0.690)}{144(0.4895)} = 4.40 \text{ in. Hg}$$

The air rate, average pressure in the test section, superficial air pressure drop, X^2 , $\mathcal{E}_{LTT \text{ MART}}^2$, predicted pressure drop, and percent deviation were determined exactly as in Appendix VII - D

$$W_G = 0.0225 \text{ lb./sec.}$$

$$P_{AVG} = 34.6 \text{ psia}$$

$$Re_{GP} = 17.5 \times 10^3$$

$$f_{GP} = 0.0267$$

$$\Delta P_{GP} = 0.01002 \text{ in. Hg}$$

$$X^2 = \frac{4.40}{0.01002} = 439$$

$$\mathcal{E}_{LTT \text{ MART}}^2 = 2.15$$

$$\Delta P_{TP \text{ MART}} = 2.15(4.40) = 9.46 \text{ in. Hg}$$

$$\% \text{ Dev.} = \frac{9.60 - 9.46}{9.46} \times 100 = + 1.48$$